Application of the Surface Renewal technique for evapotranspiration estimates of field crops

M.Sc. Thesis submitted to the Robert H. Smith Faculty of Agriculture, Food and Environment of the Hebrew University of Jerusalem

Rafael Rosa

25th March, 2012

This research was carried out under the supervision of:

Dr. Josef Tanny

Institute of Soil, Water and Environmental Sciences, Agricultural research Organization, Volcani Center, Bet Dagan.

Acknowledgements

I would like to thank all the people I met during these two years of work. I am deeply thankful to my supervisor, Dr. Josef Tanny, whose dedication, guidance and support in every stage of this process encouraged me to carry out this research in a very enjoyable way. Thanks to Dr. Shabtai Cohen, Dr. Hugo Lemcoff and Dr. Uri Dicken for their academic support and field work assistance. I am very grateful to all the friends that I have met at our laboratory at the Volcani Center, Moran Pirkner, Yoni Mekhmandarov, Michael Bahar, Tal Kanety, Indira Paudel, Ori Ahiman, Shani Yanai, Itay Roei, Abraham Grawa and Victor Lukyanov. It has been a pleasure to spend time with them, both at the laboratory and during the long days of work at the field. Support by Dr. Moshe Meron, Dr. Joseph Tsipris and Rony Foyer is also acknowledged. Thanks to KANAT (קרן לביטוח נזקי טבע בחקלאות) and to Sam Hamburg Fund for supporting this research activity.

Special thanks to Dr. Gerald Stanhill, for all the good conversations we had about science and life, all of which have been moments of deep learning for me.

This thesis is dedicated to my father, Dr. Jorge Rosa (*z''l*), who taught me the meaning of being a curious person.

Abstract

With the aim of increasing the agricultural irrigation efficiency it is critical to correctly quantify crop water use. These estimations can be performed by either measuring evapotranspiration (ET) at agricultural stands or calculating ET using different models. Most of the current methods for ET measurements are either expensive or complicated to apply, or both. The Surface Renewal (SR) method, the topic of this thesis, may be a feasible, simple and low-cost alternative method for ET estimations.

This research examined the application of the SR technique for ET estimates of two different field crops, namely processing tomato and cotton, at the Hula Valley in Northern Israel. The SR method is based on the dynamics of sweeps and ejections of air parcels that occur near the canopy surface; it is assumed that this renewal mechanism is responsible for the exchange of sensible heat (and other constituents) between the crop and the atmosphere. Using high frequency air temperature measurements, the renewal of sweeps and ejections is modeled as temperature ramps through a Structure Function analysis. Ramps amplitude and frequency enable estimating the sensible heat (H) exchange between the canopy and the atmosphere. The specific goal was to calibrate the SR method, using eddy covariance (EC) data as a reference measurement and to optimize the calibration by adjusting three parameters: temperature measurement height, sampling frequency and sensor diameter.

SR and EC systems were deployed simultaneously in two different experimental seasons, denominated as S1 and S2, which correspond to 13 days in August 2010 and 96 days between June and September 2011 respectively. The crop under study was processing tomato for S1 and cotton for S2. S1 was divided into 7 days of calibration and 6 days of validation of the analyzed data while S2 was subdivided into different sub-periods for performing a variety of specific analyses depending on plant growth stage and sensor configuration. The temperature measurements for the SR were performed simultaneously at different heights with miniature (76 μm wire diameter) thermocouples (TC) at a sampling frequency f=20 Hz and data were analyzed at 1, 2, 5, 8 and 10 Hz frequencies. The maximum plant height was h=0.6 and 1.5 m for processing tomato (S1) and cotton (S2) respectively.

The obtained temperature signal was analyzed using Structure Functions. This mathematical tool decomposes the temperature signal into organized and turbulent contributions in order to fit the organized part into a deterministic ramp model, for each time interval (30 min in this study). Each interval is characterized with an average ramp amplitude *a* (°C) and an average inverse ramp frequency τ (s). These two parameters together with the measurement height *z* (m) and a calibration coefficient (α) are used to calculate H_{SR}. For a given temperature signal both a and τ depend on the time lag *r* (s) and *f* used in the Structure Functions analysis, therefore a set of parameters was defined as a combination of the three variable parameters in this study (z,f,r). For each couple of *a* and τ, associated with a set of parameters (z,f,r), half-hourly non-calibrated estimate of H with SR (H_{NC}) was calculated. The calibration was performed by regressing H_{NC} with H measurements with EC (H_{EC}) for stable and unstable conditions separately thus obtaining two α values (α_{st} and α_{uns}) the slopes of regressions, two R^2, two RMSE and two p-values. Finally the latent heat flux (LE) estimated with the SR (LE_{SR}) is calculated as the residual of the energy balance (EB) equation using additional measurements of net radiation (Rn) and soil heat flux (G).

Overall the SR technique was calibrated successfully (p-value<0.001) for most of the analyzed measurement heights and frequencies with clear variations of α and R^2 with *z* and *f*. A major innovation of this research is the variation of the α coefficient and R^2 with *f*. Comparison of the obtained results with those reported in the literature showed agreement in the trends of α in relation with *z*. For S1 (processing tomato) the optimal calibration among all the measurement sets was achieved measuring at zn=z/h=2 (where h is canopy height) at f=10 Hz, with α_{st}=2.44 and α_{uns}=1.48, R^2=0.47 and 0.71 and RMSE=25.06 and 23.37 W m^{-2} for stable and unstable conditions, respectively. For S2d (cotton), defined as the period between the 22th and 25th August 2011, the optimal calibration was achieved measuring at zn=1.6 at f=8 Hz, with α_{st}=1.14 and α_{uns}=0.8, R^2=0.83 and 0.33 and RMSE=20.38 and 12.56 W m^{-2} for stable and unstable conditions respectively. These calibrations resulted in an average 20% underestimation of H_{EC} by H_{SR} during the validation periods of S1 and S2d. LE_{SR} was used for ET estimates in S1 and S2d periods, applying the optimal calibrations for each tested frequency. The SR estimates of daily ET at sampling frequencies 1, 2, 5 and 10 Hz, were all within a small range of variability, being overestimated and underestimated in the validation periods of

S1 and S2d, respectively. However, except for f=1 Hz estimation in S2d, these deviations never exceeded 5%. These results are promising for the future development of a low-cost SR system which does not require high sampling rates and large data storage and thus may be attainable for growers for day-to-day irrigation management. Regarding TC diameter, this study poses the necessity of correctly assessing this parameter and the large influence that small changes (~0.05 mm) in sensor diameter can have on the results.

Among the results obtained in cotton it was found that for the TCs adjacent to the canopy top, and in certain days, H_{NC} had an opposite sign than H_{EC} during several hours of the day. The general pattern of this phenomenon was entitled here as a *time lag in stability change* because when this situation occurred, H_{EC} (measured at 3.35 m) turned negative (stable) some hours before H_{NC}. Different tests were performed to the available data in an attempt of explaining this phenomenon, which showed a relation between its length with high ET rates and wind speed. However it was not possible to identify a specific mechanism relating high ET rates and long *time lag in stability change.* Its occurrence may represent a limitation in the application of the SR in a cotton crop with temperature sensors in close proximity to the canopy top.

In summary, the SR technique was shown to be reliable in estimating whole canopy ET in processing tomato and cotton crops. The results of this study are presented for two given crops at a specific climatic region. Extending this approach to different crops at other regions and over a wider range of crop development stages is desirable with the aim of pursuing a practical application at the farm level.

Table of contents:

List of symbols and abbreviations

Symbol	Description
a	Ramp amplitude (°C)
b	Slope of the energy balance equation regression (-)
c_d	Leaf drag coefficient (-)
C_d	Dry soil heat capacity (J g^{-1} $°C^{-1}$)
C_p	Specific heat of air at constant pressure (J kg^{-1} $°K^{-1}$)
C_s	Specific heat values of each soil granular component (J g^{-1} $°C^{-1}$)
C_v	Volumetric heat capacity of the soil (J m^{-3} $°C^{-1}$)
C_w	Water heat capacity (J g^{-1} $°C^{-1}$)
d	Zero plane displacement (m)
d_{hf}	Depth of the installation of the soil heat flux plates (m)
dT/dt	Total derivative of T with respect to time (°C s^{-1})
$\partial T/\partial t$	Partial derivative of T with respect to time (°C s^{-1})
du_h/dz	Wind shear (s^{-1})
E	Evaporation (mmH_2O)
ET	Evapotranspiration (mmH_2O)
f	Measurement sampling frequency (Hz)
f_{clay}, f_{silt}, f_{sand}	Volumetric fractions of each of the soil granular components (-)
f_H	Sampling frequency f=10 (Hz)
f_M	Corresponding sampling frequency to each α_M (Hz)
Fc	Carbon dioxide flux (W m^{-2})
F_{dry}	Dry fraction of soil (-)
F_{wet}	Wet fraction of soil (-)
G	Soil heat flux (W m^{-2})
$G_{flux\text{-}reg}$	Average heat flux measured by the heat flux plates in region *reg,* either dry or wet (W m^{-2})
h	Canopy height (m)

H	Sensible heat (W m^{-2})
H_{NC}	Non-calibrated estimation of H with the SR method (W m^{-2})
H_{EC}	H estimated with the SR method (W m^{-2})
H_{SR}	H estimated with the SR method (W m^{-2})
l	Gradually increasing or decreasing temperature ramp period (s)
L_{AI}	Leaf area index (-)
LE	Latent heat flux (W m^{-2})
LE_{ECf}	Corrected latent heat flux using *residual LE closure* (W m^{-2})
LE_{SR}	LE obtained with the SR method (W m^{-2})
L_v	Latent heat of vaporization (J g^{-1})
PAR	Photosynthetically active radiation (J)
q	Air vapor density (g m^{-3})
q_m	Soil water content (g g^{-1})
r	Time lag used in Structure Functions analysis (s)
r_d	Soil bulk density (g cm^{-3})
R^2	Coefficient of determination of a linear regression (-)
Rn	Net radiation flux (W m^{-2})
s	Quiescent ramp period (s)
Sc	Rate of change of heat storage (air and biomass) between the ground and the canopy top (W m^{-2})
S^n	Structure functions of order *n*
S_{reg}	Energy stored in the layer above heat flux plates in region *reg,* either dry or wet (W m^{-2})
T	Temperature (°C or °K)
Ts	Sonic temperature (°K)
u	Horizontal wind speed in x direction (m s^{-1})
u_*	Friction velocity (m s^{-1})
u_h	Horizontal wind speed (m s^{-1})

U_i=(U_1, U_2 and U_3)	Air velocity components in the longitudinal, lateral and vertical directions (x_1, x_2 and x_3 respectively) (m s^{-1})
v	Horizontal wind speed in y direction (m s^{-1})
V	Volume of an air parcel of height z (m^3)
V_h/A	Volume of air per unit area under the canopy height (m)
w	Vertical wind speed (m s^{-1})
|X|	Absolute value of magnitude X
$\overline{X}$	Average of X over a measurement period (30 min in this study)
z	Measurement height (m)
z*	Roughness sublayer depth (m)
z_m	Roughness length (canopy) (m)

Greek letters

α	Coefficient of calibration of the SR (-)
α_{st}	Coefficient of calibration of the SR (stable conditions) (-)
α_{uns}	Coefficient of calibration of the SR (unstable conditions) (-)
α_H	α obtained sampling at f=10 Hz (-)
α_M	α obtained sampling at different frequencies (-)
β	Bowen ratio (-)
ΔC	Change in heat content of an air parcel (J $°K^{-1}$)
ϑ	Stability parameter (-)
ρ	Air density (kg m^{-3})
τ	Inverse ramp frequency (s)

Abbreviations

DOY	Day of the year
EB	Energy balance
EC	Eddy covariance method

IRGA	Infrared gas analyzer
RMSE	Root mean square error (units depend on the parameter)
S1	Experimental season number 1 (summer 2010)
S2	Experimental season number 2 (summer 2011)
S1a	Sub-period of S2 between DOY 153 and 166
S1b	Sub-period of S2 between DOY 208 and 224
S1c	Sub-period of S2 between DOY 220 and 229
S1d	Sub-period of S2 between DOY 234 and 237
SR	Surface Renewal method
SR1	Classic method of SR
SR2	Similarity method of SR
TC	Thermocouples
TDR	Time domain reflectometry

1. Introduction

1.1. Preface

As the world population increases, agriculture practices encounter new challenges in order to meet the ever increasing world food demand. In this context, increasing productivity appears to be a key objective for allowing sustainable agriculture from the environmental point of view. Water is one of the main natural resources needed for any agricultural practice. In Israel agricultural water consumption has multiplied by four from 1964, as irrigated crop production extended to the whole country, when the National Water Carrier linked the north of the country with the arid south (Stanhill and Rosa, 2011). With the aim of increasing the agricultural irrigation efficiency it is critical to correctly quantify crop water use. These estimations can be performed by either measuring evapotranspiration (ET) at agricultural stands or calculating ET using different models.

Stand ET is composed of three components namely, plant transpiration, soil evaporation and plant water interception (Wilson et al., 2001). A wide range of techniques have been developed for measuring either ET or its components. Among them the eddy covariance (EC) method is considered the most reliable real time measurement of ET (Anandakumar, 1999; Simmons et al., 2007), using direct measurement of water vapor exchange between the canopy and the atmosphere. Depending on the sensors used, in addition to latent heat flux (LE), the EC method can measure sensible heat (H) and carbon dioxide (Fc) fluxes. EC systems are becoming relatively widely used for ET measurement because of ease of set up, reduced costs for sensors, and the ability to co-measure directly the three aforementioned fluxes (Allen et al., 2011a).

In spite of its remarkable advantages, the EC technique is not available for day-to-day use by growers due to its operational and data analysis complexity; hence simpler and cheaper methods for ET estimation are desirable so as to provide growers with reliable real time estimations of ET. The Surface Renewal (SR) method may be a feasible alternative for achieving the goals of simple and cheap method for ET estimations. This method is based on the dynamics of the turbulent boundary layer above the canopy which was modeled by the mixing layer analogy by Raupach et al. (1996). Among other

characteristics of this layer, sweeps and ejections of air parcels from the canopy, driven by wind shear and/or temperature changes, have been identified. The SR technique is based on modeling these ejections and sweeps through simple temperature measurements as a way of estimating the sensible heat exchange between the canopy and the atmosphere (Castellvi, 2012). Two methods for applying the SR have been proposed. The first approach, applied by Snyder et al. (1996) among others, will be named hereafter as *classic method* (SR1) and needs calibration (see section 2.4.3). Castellvi (2004) proposed a new method, which combines SR analysis with similarity theory (see section 2.4.4) and does not need calibration. This latter approach will be referred to as *similarity method* (SR2) and requires high frequency temperature and 2-D (horizontal) wind measurements. The main advantage of the SR1 method is its simple application: it only requires high frequency temperature measurements which are performed with miniature thermocouples (TC) and measurements of other two energy balance (EB) components, namely net radiation (Rn) and soil heat flux (G). The latent heat flux is then extracted as a residual of the energy balance equation (Eq. 2.1). Aiming to keep the simplicity in measurement techniques and devices with the objective of developing an available tool for practical applications, the SR1 method was applied in this study.

1.2. The research goal

The major goal of this study is to examine the applicability of the SR technique in two different field crops at the Hula Valley of Northern Israel: processing tomato and cotton.

The specific goal is to calibrate the SR method, using the EC data as a reference, for the above crops, and to optimize the calibration by adjusting the following system parameters:

a. Temperature measurement height.
b. Temperature measurement sampling frequency.
c. Temperature measurement sensor (thermocouple) diameter.

2. Literature survey

2.1. Evapotranspiration measurement methods

Several ET measurement techniques have been developed, some of them directly measuring ET and some measuring one of the ET components. All of them are representative within a spatial and temporal scale, being necessary to extrapolate the results for characterizing ET rates outside these scales. In the following some of the major methods are presented following Allen et al. (2011a).

2.1.1. Methods related to the energy balance

Both transpiration and evaporation require energy for the conversion of liquid water to vapor (Allen et al., 2011a). This energy is provided by the solar radiation, as part of the global energy income to the Earth, or by the air internal energy. On a smaller scale, an energy budget can be posed to a control volume defined between the ground and the canopy top. The EB states that the sum of consumed energy, LE and H, should equal all other energy sources and sinks, namely Rn, G, the rate of change of heat storage (air and biomass) between the ground and the canopy top (Sc) and a residual small neglected term which represents the sum of all additional sources and sinks. The EB closure can be assessed by a linear regression through the origin given as:

$$LE + H = b(Rn - G) \qquad (2.1)$$

where *b* represents the slope of the regression. An ideal 100% EB closure prevails when *b*=1. Sc is usually neglected for agricultural plant canopies; for forest stands it represents an average increase of 7% in the slope of the regression (Wilson et al., 2002).

From the energy fluxes involved in this energy budget; LE is the transport mechanism for water exchange between the atmosphere and the canopy.

2.1.1.1. Bowen ratio energy balance method

This method solves the EB equation based on relative simple measurements as air temperature and vapor pressure gradients, Rn and G. The Bowen ratio (β) is defined as the ratio between H and LE, which are separately calculated with the help of certain

humid air characteristics data as temperature and vapor pressure, among others. Once β is obtained, LE is recalculated as follows:

$$LE = \frac{Rn-G}{1+\beta} \qquad (2.2)$$

Therefore periods of β near to -1 may affect the validity of Eq. 2.2. This is one of the main problems of the method.

2.1.1.2. Scintillometry

The principle lying behind a scintillometer is the measurement by optical means of the variations of refractive index of air, caused by temperature, humidity and pressure variations. H is derived from these measurements. Together with additional input of Rn and G, LE is resolved as the residual of the EB equation (Eq. 2.1). The main drawback of this technique is its relatively high cost of sensors.

2.1.1.3. Surface renewal method

The Surface Renewal method is discussed thoroughly in section 2.4.

2.1.2. Methods related to mass balance

2.1.2.1. Soil water budgets

This technique estimates ET by considering the change in soil water content within the root zone and all other water outputs and inputs like runoff or rain that may occur in an area of interest. There is a wide variety of measurement techniques including time domain reflectometry (TDR), neutron probes or soil water potential. Among the sources of error for this approach it is possible to identify uncertainty in drainage, unaccounted elevation of underground water table and spatial variability in soil properties and water content.

2.1.2.2. Mass balance in large areas

This estimation is based on considering the inflow and outflow of a large area (e.g. catchment), with an appropriate morphology so as to eliminate any other losses or gains. Measurements can be carried out with weirs in streams or with rainfall measurement techniques. This approach can be useful for calibrating hydrodynamic models or assessing whole seasonal or annual ET rates.

2.1.2.3. Lysimetry

Lysimetry is based on measuring the weight variation of a given soil portion loaded on a lysimeter, considering percolation and thus estimating the rate of water loss to the atmosphere. Lysimeters are devices capable of holding potted plants; they can have varied shapes, size and operational designs. The error sources of this technique are mainly caused by the isolation of the plant from its natural environment and the limited area that the lysimeter represents namely different vegetation density and development on them, poor representation of field soil profile within the lysimeter or non representative water movement through it.

2.1.3. Independent methods

2.1.3.1. Eddy covariance

The eddy covariance method is discussed thoroughly in section 2.3.

2.1.3.2. Sap flow methods

These methods measure the water (sap) flow through the stem or branches of plants and trees using heat as a tracer and can be divided into heat pulse and steady state heat methods. These methods only measure one of the ET components (i.e. transpiration) thus providing information about plant water use. Estimates of the other ET components: soil evaporation and plant water interception, should be accomplished by other methods. Hence, these methods are mostly useful for ET estimation in dense canopies on dry seasons where soil evaporation and plant interception are negligible. The sources of errors for final estimations are wounds caused by sensors, sensor misplacement, uncertainty of plant conductive cross section and the need of scaling transpiration from one plant to a whole stand.

2.2. Turbulence in plant canopies

The SR method is based on the turbulent heat flow that is interchanged between the canopy and the atmosphere. It models the ejections and sweeps of air parcels that occur in the canopy and that are characteristic of the turbulent layer which develops over the canopy. Therefore, understanding the characteristics of this turbulence is essential for a proper comprehension and interpretation of the method.

2.2.1. The mixing layer analogy

Turbulent canopy flows drive the scalar exchange of water, carbon dioxide and heat between vegetation and the atmosphere. A scalar is a magnitude or quantity which has no given direction. Three decades ago, Raupach and Thom (1981) showed that turbulent flows in canopies are dominated by large coherent structures of whole canopy scale. Following this observation, Raupach et al. (1996) suggested an analogy between canopy flows and a plane mixing layer in order to characterize these turbulent structures. The plane mixing layer is the free shear layer that forms when two airstreams of different velocity, initially separated by a splitter plate, merge downstream of the trailing edge of the plate (Finnigan, 2000). This analogy replaces (under certain conditions) the classical view of canopy flows where a thick porous layer (the canopy) is immersed within the lower section of an overlying turbulent boundary layer. In the latter, turbulence is characterized by the small scale flow patterns induced by drag elements of the canopy. In canopy flows the mixing layer coincides with the so-called roughness sublayer which is the region within the atmospheric boundary layer located just above the canopy, and directly affected by the canopy elements.

Large coherent structures, associated with mixing layer characteristics, control canopy turbulence dynamics. This coherence can be visualized and compared to turbulence structure above the canopy by modeling averaged eddies. The process responsible for momentum and scalar transfer is composed of sweeps and ejections, which represent the penetration (exit) into (from) the canopy of fast downward (upward) air gusts (Harman and Finnigan, 2008).

2.3. Eddy covariance method

2.3.1. Historical development

The theoretical framework for the EC technique was established by Sir Osborne Reynolds who first derived the foundations of turbulent flows in 1895 (Baldocchi, 2003). The next step for applying the technique was the development of the first instruments, which occurred around thirty years later. During the twentieth century the instrumentation continued developing but it was not until the early 1970s that the first carbon dioxide measurements using a propeller anemometer and a closed-path infrared gas analyzer (IRGA) were performed. The next wave of technical improvements was

during the late 1980s with the availability of commercial sonic anemometers and open-path IRGAs. Nevertheless, the last step for wide implementation of the technique was taken by the development of data acquisition systems capable of storing large amounts of data thus allowing long-term EC measurements. By the year 1997 regional networks of flux measurements were established in Europe and North America. Currently the EC method is used worldwide.

2.3.2. Theory

The principle of the EC technique is to sample the upward and downward turbulent motion of air parcels that transport scalars between the canopy and the atmospheric boundary layer. For achieving this it is necessary to perform high frequency measurements of wind velocity and scalar concentration. Fluxes that are generally (but not only) measured are LE, H, Fc and friction velocity or momentum flux (u_*). The mean flux density (averaged over some time period, usually 30 min) of a scalar is expressed as the covariance between the fluctuations in vertical wind velocity (w) and the scalar concentration or mixing ratio (see equations in Appendix VIII). Since the measurement is based on the constant flux layer assumption (i.e. the flux emanating or absorbed at the canopy is the same as that measured several meters above), the EC method requires some conditions to be accomplished. The EC sensors should be installed within a fully developed turbulent surface boundary layer on a flat homogeneous terrain, which presents a logarithmic wind profile under steady state conditions. The above terrain characteristics would avoid advection conditions and associated horizontal flux divergence. To meet the above requirements the field under study must be large enough, providing sufficient fetch for the development of the required turbulence conditions. Due to the co-spectral density (i.e. amount of flux associated with a given frequency) that each covariance presents, it is necessary to apply relatively high sampling rate; a sampling frequency of 10 Hz was found to be enough for the high frequency portion of the flux co-spectrum (Baldocchi, 2003).

2.3.3. Current application

A large scale application of the EC technique is carried out by the FLUXNET global network (*http://fluxnet.ornl.gov*) coordinated by NASA. It provides an integrated global carbon dioxide and energy fluxes database, which is essential for the estimation of the

terrestrial water, energy and carbon balances (Hendricks et al., 2010). It is comprised by more than 500 long-term and continuous flux measuring towers, distributed on the five continents and has a latitudinal distribution range between 70 degrees north and 30 degrees south, hence covering a wide range of climates and vegetations.

In Israel, EC has been applied successfully for assessing ET rates in screenhouses (Möller et al., 2004; Tanny et al., 2006, 2010) and for evaporation (E) rates measurements in water reservoirs (Assouline and Mahrer, 1993 (WRR); Assouline et al., 2007 (AWR); Tanny et al., 2008, 2011). Tanny et al. (2006) performed their measurements in a banana screenhouse during 14 days in mid-June with a one-dimensional sonic anemometer, a fine wire thermocouple and a Krypton hygrometer, obtaining a mean ET rate of 5.6 $mmH_2O\ day^{-1}$ and an EB closure (Eq. 2.1) of 94%. After two additional field campaigns carried out on a nearby location, Tanny et al. (2010) concluded that in a screenhouse the turbulence development allows for EC measurements and that the conditions are favorable for a reasonable EB closure. The water reservoir application (using a sonic anemometer and a Krypton hygrometer, Tanny et al., 2008) in northern Israel yielded a mean E rate of 5.81 $mmH_2O\ day^{-1}$ based on measurements performed during 14 days in the first half of September and an EB closure of 80% when deviations in the water heat flux measurements were eliminated.

2.3.4. Limitations and energy balance closure

EC instrumentation and installation limitations influence the ability of measuring the whole flux co-spectrum by introducing high and low pass filtering (attenuation of low and high frequency contributions to the flux respectively). It is necessary to consider these filters during data analysis by applying corrections to the raw measurements (see Appendix IX). Examples of high and low pass filtering are the average period for defining mean fluxes (most severe under convective conditions) and the effect of sensor separation, respectively (Baldocchi, 2003).

EC flux measurements are made at some height above the surface; therefore the flux measurement represents a surface upwind from the sensor location that is quantified by the flux footprint (Horst and Weil, 1994). This footprint when considered in all directions defines the total surface which the flux is accounted for. Certain EC applications are limited by this footprint definition since the measurement surface may not be exactly the

desired one or may include flux inhomogeneities which do not allow quantifying a flux within a specific area. As a rule of thumb, the required fetch should be between 50 and 100 times the height of the EC sensors above the plant zero plane displacement (d) height. Footprints models were derived in the literature (e.g. Hsieh et al., 2000 ; Schmid, 1997; Horst and Weil, 1992) which quantify the actual footprint under given airflow and surface conditions. For example, Horst and Weil (1994) found that under moderately stable conditions the fetch requirement is considerably larger than 100 times sensor's height.

The EB budget is an important test for EC data and it is done as a standard procedure in most applications. The lack of EB closure that EC systems systematically show is a matter of concern among researchers (Foken, 2008). Wilson et al. (2002) hypothesized five main causes to account for the lack of closure, namely sampling errors (including not sufficient measuring fetch), systematic bias in instrumentation, neglected energy sinks, high and low pass filters and neglected advection of scalars. They performed a study considering twenty-two FLUXNET sites and found a mean imbalance in the EB equation (Eq. 2.1) of 20% caused by an underestimation of the LE+H term. None of the causes mentioned above could be identified as the governing reason and the problem cause was settled as a combination of small but multiple issues.

The difficulty in assessing factors that prevent a complete closure of the EB with EC measurements made it reasonable to assume that the EB should be forced. Twine et al. (2000) justified forcing the EB closure with the EC fluxes by proving that the measurement of the remaining fluxes of the balance (i.e. Rn and G) is more reliable and representative of the flux footprint. This conclusion is based on the fact that Rn is the most accurate measurement (5% accuracy) and that G errors arise from spatial sampling thus obtaining an overall error from both fluxes that, even considering all random contributions to it, is still half of the shortfall in LE and H. Two EB closure forcing methods are proposed by Twine (2000); the first one is to discard measured LE and calculate it as the residual of the energy balance budget and is named as *residual LE closure* while the second one, named as *Bowen ratio closure*, assumes that although LE and H measurements by the EC system include some error, the ratio between them, the Bowen ratio (i.e. β=H/LE) is accurately estimated. Hence LE is estimated by preserving this ratio and conserving energy (Twine et al., 2000). The

authors did not find significant reasons for discarding LE; therefore they recommend the second method for forcing EB closure. Nevertheless, they found that there was no statistical difference in the bias between LE obtained by applying either of the two forcing methods and a reference LE measurement. Moreover, they state that increased EB closure at very dry sites may imply accurate H measurements while LE may be erroneous given its small magnitude. Although they highlight their preference for applying the second forcing method (*Bowen ratio*), they advice that assuring that EC measurements are consistent with the conservation of energy is much more important than the method chosen for obtaining the closure.

2.4. Surface renewal method

2.4.1. Historical development

The first SR theory was developed by Higbie in 1935 to investigate heat transfer between a liquid and a gas that change phases (Katul et al., 1996); his theory was based on the concept of a fresh fluid element arriving from an outer region to a heated surface, having a residence time which allows a diffusive scalar interchange and the eventual replacement (i.e. renewal) of this mass of fluid by another fresh element from outside. This theory was later refined between the 1950s and the beginning of the 1990s by adapting it to eddy turbulent motion. Considering the specific case of canopy, for example, it was shown that the duration of contact between the arriving fluid and the heated surface (i.e. canopy), and the renewal frequency are variable. Paw U and Brunet (1991) proposed the first SR scheme applied to canopies by combining Higbie's reasoning with the observed ramp patterns of high frequency temperature signals observed over a canopy. Paw U et al. (1995) justified the need of a scalar (i.e. without using high frequency wind velocity signals) method for estimating H considering the limitations that the latter methods have (low winds or fetch requirements) and the cost of measuring devices and general installation. In their study they proved that SR was more accurate than other scalar methods, which have many limitations (e.g. for stable conditions) and they propose the basic equation (Eq. 2.3) for estimating H obtaining the scalar ramps characteristics with a low pass filter. Snyder et al. (1996) applied for the first time the Structure Functions (Van Atta, 1977) approach for characterizing the scalar ramps and applied the *classic method* (SR1) (see section 2.4.3). Later, Castellvi (2004) proposed the *similarity method* (SR2) method (see section 2.4.4). A broad literature

dealing with the SR method has been accumulated during the past twenty years, being the main common research objective developing a cheap and simple technique for estimating H as an intermediate step for estimating LE in plant or forest canopies.

2.4.2. Theory

2.4.2.1. Mechanism, ramps and equation

The SR application for canopies is based on the ejections and sweeps mechanism (see section 2.2) and is explained, among others, by Castellvi (2012) by considering an air parcel and its movement to and away of the canopy surface. This air parcel has some scalar concentration (e.g. temperature, although the theory is valid for any scalar) and travels above the canopy. Suddenly this parcel moves down approaching the canopy top layer (i.e. a sweep) being connected to scalar sources (sinks) of the surface (i.e. vegetation) during a certain period of time. This parcel is subsequently ejected upwards (i.e. an ejection) and substituted by another parcel sweeping from above. During the time that the parcel was in contact with the canopy scalars were exchanged between air and canopy, hence when the parcel is ejected it has been enriched or depleted with the scalar.

When high frequency temperature measurements are taken at a point at or above the canopy top, ramps are observed in the signal because the fluctuations are created by coherent large-scale eddies (Snyder et al., 1996; Castellvi, 2004). A ramp is characterized by an amplitude *a* (°C) and inverse ramp frequency τ (s). When conditions are unstable (stable), the canopy is warmer (cooler) than the air. After the sweep, the temperature signal shows a sharp drop (rise) because of the invasion of a cooler (warmer) air parcel from above. This is followed by a quiescent (i.e. no temperature change) period *s* (s) and then a period *l* (s) with gradually increasing (decreasing) temperature as the air parcel is heated (cooled) by the vegetation (i.e. $l+s=\tau$). This heating (cooling) is observed as positive (negative) temperature ramp amplitude *a* (°C). Afterwards this air parcel is ejected upwards and is replaced by an incoming parcel from above. A scheme of the mechanism and the ideal ramp for unstable conditions is shown in Fig. 2.1.

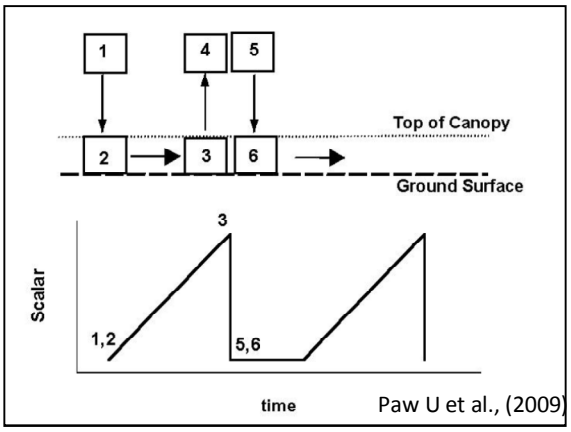

Figure 2.1 *– Cartoon of surface renewal process. Parcel instant drops from position 1 to position 2 in the canopy (upper cartoon). Scalar starts increasing in the parcel because of a source in the canopy, shown in the scalar T versus time plot (lower graph). After horizontally advecting some distance, the parcel instantly rises from position 3 to position 4 (upper cartoon). The scalar has continued to increase to a peak corresponding to position 3, in the scalar versus time plot (lower graph). Simultaneously, from position 5, a new parcel instantly replaces the old parcel's location in the canopy, shown as position 6 (offset horizontally in the upper cartoon for clarity). This results in an instant drop in the scalar value (lower graph), terminating the previous gradual scalar increase and forming the ramp pattern (Paw U et al., 2009).*

In reality the temperature ramp signal is more complex due to superposition of eddies of different sizes. According to Katul et al. (1996) the difference between the ideal ramp and the real signal is caused by high frequency eddies attached to the larger-scale coherent motion; Finnigan (2000) agrees with this approach, when describing the characteristic eddy in the roughness sublayer. The high frequency eddies appear in the signal because the measurement is done with an Eulerian approach (i.e. a fixed point) rather than with a Lagrangian one (i.e. following the motion).

The first expression for H was given by Paw U et al. (1995) as follows:

$$H = \rho C_p \frac{dT}{dt} \frac{V_h}{A} \qquad (2.3)$$

where ρ (kg m^{-3}) is the air density, C_p (J kg^{-1} °K^{-1}) is the specific heat of air at constant pressure and V_h/A (m) is the volume of air per unit area under the canopy height. It assumes that the air parcel height equals the canopy height (h), V_h/A = h, given that the direct heat exchange occurs where the canopy exists. The term dT/dt accounts for the total derivative (i.e. following the motion) of the temperature (T) of the air parcel.

By assuming that dT/dt=$\partial T/\partial t$ (partial time derivative of T; see section 2.4.2.2) the total derivative in Eq. 2.3 can be substituted by *a/l*. In addition, the process should consider the relative time of heating (i.e. the residence time of the air parcel within the canopy) with the term l/τ. Accounting for the vertical temperature gradient of the air parcel from the bottom to the top during the scalar exchange, this gradient is averaged by adding the term α (see section 2.4.6.1 for a further interpretation of α). Therefore Eq. 2.3 turns into:

$$H = \alpha \rho C_p \frac{a}{\tau} h \qquad (2.4)$$

The flux of sensible heat is assumed to consist of a series of instantaneous events that occurs when air parcels sweep to, or eject from, the canopy (Snyder et al., 1996). During the scalar exchange time within the canopy (i.e. between the sweep and ejections phase), the change in heat content ΔC of an air parcel of volume V (of height *z*) can be expressed as:

$$\Delta C = \rho C_p \frac{\partial T}{\partial t} V = \rho C_p \frac{a}{l} V \qquad (2.5)$$

Applying the conservation of energy under the assumptions that the heat exchange occurs only within the canopy height (h) and vertical flux of heat occurs instantaneously and adiabatically (i.e. no heat loss from the air parcel) by the aerodynamic transport (Snyder et al., 1996; Spano et al., 1997), Eq. 2.4 can be adapted into:

$$H_{SR} = \alpha H_{NC} = \alpha \rho C_p \frac{a}{\tau} z \qquad (2.6)$$

where H_{SR} is H estimated with the SR method, H_{NC} is a non-calibrated estimation of H with the SR method and z (m) is the measurement height.

2.4.2.2. Derivative simplification

The SR reasoning is based on the scalar variation of an air parcel during its sweep and ejection from the canopy. As expressed in Eq. 2.3 this variation is assessed with a total time derivative of the scalar (dT/dt). However, the practical application of the SR technique is done with stationary scalar sensors (e.g. a fix TC for the case of temperature) which measure the partial time derivative of the scalar ($\partial T/\partial t$). These two derivatives are related between them as follows:

$$\frac{\partial T}{\partial t} = \frac{dT}{dt} - U_i \frac{\partial T}{\partial x_i} \qquad (2.7)$$

where U_i (U_1, U_2 and U_3) are the air velocity components (transport terms) in the longitudinal, lateral and vertical directions (x_1, x_2 and x_3 respectively). Therefore the stationary sensor measures the total time derivative of the scalar plus the fluctuations resulting from transported eddies. Considering the difference between modeled ramp and real signal (see section 2.4.2.1) the coherent structure can be associated with the dT/dt term while the remaining concentration fluctuations are associated with the transport terms. Paw U et al. (1995) proposed the need of low pass filtering the signal for high frequency trace in the scalar signal. They argued that this is based on the fact that these components do not contribute to the flux, the kinematic nature of them results in higher frequencies than that of the total derivative and that they occur at the boundaries of the larger, coherent structures. Thus the energy is mostly exchanged by eddies of intermediate frequencies while low and high frequencies are thought to have a negligible contribution. Spano et al. (2000) stated that the transport term represents a local advection term and it can be neglected in the absence of advection (Paw U and Brunet, 1991). This local advection term (e.g. under high wind shear on the canopy top) should not be associated with other higher scale scalar advection (i.e. regional advection) that may add noise to the signal (e.g. lack of sufficient fetch) (Castellvi et al., 2008).

2.4.2.3. Measurement height and fetch

One of the main limitations of the EC method is its fetch requirement. This is directly related to the need of performing measurements at a minimum height above the canopy, i.e. within the inertial sublayer. By testing the roughness sublayer depth half-hourly and noting that, although the top of the sublayer oscillated above and below the measurement height the H estimates were acceptable, Castellvi and Snyder (2009b) concluded that the SR method is applicable at any height close to the canopy top. This directly influences the fetch requirements for flux measurements with the SR method. Castellvi (2012) tested the need of developing a footprint model for the SR method, and proved that the fetch requirements are in practice the same as for the EC method. Combining these two results Castellvi (2012) concluded that given that the SR sensors

can be positioned at any height above the canopy, the SR fetch requirement is significantly relaxed than that for EC.

2.4.2.4. TC diameter and measurement sampling frequency

As previously mentioned, a measurement sampling rate of 10 Hz is considered acceptable for the EC technique for most agricultural applications. The good performance of the SR method when comparing its H estimations (H_{SR}) with the EC method estimations (H_{EC}) suggests that a frequency of 10 Hz is also suitable for the SR method (Castellvi and Snyder, 2009b). Defining the sensor time constant as the time it takes for the sensor to respond to 63.2% of a step change in temperature, for the case of a 75 μm sensor this time constant is 50 ms < 100 ms which corresponds to a 10 Hz sampling rate. Therefore the use of 75 μm sensors is widely acceptable for air temperature measurements using the SR method (Mengitsu and Savage, 2010; Castellvi and Snyder, 2009b).

2.4.2.5. Structure functions for ramp analysis

Van Atta (1977) based his structure functions analysis on a statistically independent decomposition of a temperature field (signal) into organized (coherent) and turbulent contributions and modeled the organized part into a deterministic ramp structure. See *Appendix I* for a further explanation of the Structure Functions theory.

2.4.2.6. Wind influence on ramps formation and stability

Frequency of occurrence and clarity of ramp shapes appeared to be closely related to the mean wind shear (Snyder et al., 1996). Wind shear is understood as the vertical variation of horizontal wind speed. Its influence was observed for grass, where high wind shear did not allow clear ramp formation at the canopy top but at higher levels. These results were confirmed by Spano et al. (1997) who reported improvement in calibration associated with less wind shear thus better defined ramps. By comparing the results between three canopies, the best results (on different measurement heights) were coincident with similar wind shear ranges.

Castellvi and Snyder (2010) define regional advection as air movement from large non irrigated areas towards the irrigated areas under study. If the externally advected air is

warmer than that in the irrigated field, the boundary layer under study would be stabilized (Castellvi and Snyder, 2009a).

2.4.3. Classic method (SR1)

The classic method for applying the SR technique is based on estimating the ramp mean characteristics (*a* and τ) by applying Structure Function analysis to a temperature signal for a given time averaging period (usually 30 min). Once these characteristics are obtained, H_{NC} is calculated using Eq. 2.6. Finally the half-hourly estimations of H_{NC} are linearly regressed with reference H values (e.g. EC measurements - H_{EC}) and the coefficient α is obtained as the slope of that linear regression (with or without intercept) thus obtaining the H_{SR} calibration.

The regressions can be performed considering all the obtained data, i.e. one α value regardless of the stability conditions (Spano et al., 1997), or by splitting the data into stable and unstable cases thus obtaining two α values (i.e. α_{st} and α_{uns})(Paw U et al., 1995). Regardless of the chosen approach, α will be constant during the calibration period and should be tested subsequently during a validation period. The validation may be done for either estimated H_{SR} or LE_{SR} (i.e. LE obtained with the SR method) with EC (Simmons et al., 2007), Lysimetry (Zapata and Martinez-Cob, 2002) or Scintillometry (Anandakumar, 1999) measurements.

2.4.4. Similarity method (SR2)

This method combines the SR with the similarity theories. The similarity theory is based on flux-gradient relations that depend on stability conditions. Rearranging Eq. 2.6, Castellvi (2004) interpreted the term *αz* as the mean eddy size responsible for renewal and proposed an alternative method (SR2) for calculating α; turning this term into a variable, dependant of stability conditions, related to the variation of the roughness sublayer depth and not needing calibration. The SR2 method requires high frequency temperature and 2-D (horizontal) wind measurements.

2.4.5. Comparing SR1 with SR2

Castellvi et al. (2012) performed a comparison between the SR1 and SR2 methods motivated by the observation that SR1 was recommended because of its good

correlation with EC, although these recommendations were mainly obtained for unstable conditions and without testing the SR2 method. The comparison was done by estimating H for both methods over a mature orange orchard, which has constant canopy morphology throughout the year thus making calibration and validation only dependent on climatic conditions.

The results obtained by Castellvi et al. (2012) showed that there is a basic problem in α parameter estimated by SR1 (using the α_{st} and α_{uns} approach) and it is the fact that α proved not being constant for different periods of calibration (change ±15% for α_{uns} and more than ±20% for α_{st}). However, Mengitsu and Savage (2010) assured that α is stable for a given canopy and does not change from site to site, regardless of climatic conditions. Moreover, Snyder et al. (2008) states that changes in α should not occur over different calibration periods, as long as canopy height and density remain relatively unchanged. In addition, for an irrigated pasture Snyder et al. (2008) observed a 12% difference in α (single value) between two different years on the same location and applied the first year calibration for the second year temperature measurements. The acceptable results they obtained for the verification period suggest that deviations of such magnitude in α may not influence significantly the validation results.

Estimating with SR2, α parameter needs the estimation of the roughness sublayer depth, z* (m), which needs the estimation of the leaf drag coefficient (c_d). Estimating this drag coefficient may be complex, hence Castellvi et al. (2012) considered a constant c_d which they obtained during the calibrating period by iterations until minimizing the root mean square error (RMSE) of H. On the contrary to the result of SR1, in Castellvi et al. (2012), c_d proved to be robust and did not depend on the calibration periods thus making the SR2 method operational after a few days of calibration.

Considering a validation done with H_{EC} estimations, SR1 RMSE was in the range between 56 and 77 W m^{-2} whereas SR2 RMSE ranged between 39 and 52 W m^{-2}. Analyzing the linear regressions of both methods with the reference H_{EC}, SR1 showed underestimations for stable conditions while SR2 performed poorly around neutral cases (-40 W m^{-2}<H_{EC}<40 W m^{-2}). For all data the coefficient of determination of these linear regressions was higher for SR2 than for SR1.

Castellvi et al. (2012) highlighted the implications of a non constant α (e.g. changing from year to year because of inter annual climate variability) and concluded that SR2 is recommended. Nevertheless, SR1 does not require high frequency wind measurements, which makes it a simpler and cheaper method for field applications and hence an appealing technique for day-to-day use in the farm level.

2.4.6. α coefficient

2.4.6.1. Coefficient interpretation

The knowledge about α is limited, particularly under stable conditions, therefore it is difficult to provide general rules about it such as variability of its averaged or calibrated values, its dependence on measurement height, canopy architecture, time lag and frequency used in the Structure Functions application (see section 3.6.3.1 and *Appendix I*) and its dependence on stability conditions (Castellvi, 2004).

Considering the α parameter obtained with SR1 method, Spano et al. (2000) stated that α is a weighting factor accounting for the uneven cooling or heating of the air parcel below the measurement level and other factors, given that Eq. 2.6 assumes a uniformly heated air parcel, and depends on the measurement height. Non uniform heating of the parcel with height is expressed by $\alpha \neq 1$. According to Spano et al. (2000) a value $\alpha > 1$ means that the measurement level was lower than the mean height of the air volume being heated or cooled, whereas $\alpha < 1$ means a measuring level higher than the mean height of the air volume being heated or cooled, which would allow entrainment with air aloft, causing an overestimation of H. For example, Spano et al. (1997) explained their $\alpha = 0.5$ result with the change in heating with height from the ground to the top of the canopy which is assumed to be linear, and therefore heating of the parcel volume is only about half of the heating measured at the canopy top (heating of the air mass at the ground is assumed to be negligible). This value was found for canopies taller than 2.5 m (Paw U and Brunet, 1991; Paw U et al., 1995). Spano et al. (1997) analyzed data obtained by Paw U et al. (1995) for maize crop, a walnut orchard and a forest, and compared them to their own data for grass, wheat and sorghum. They concluded that α value closer to 1 was obtained for shorter canopies or measuring well above them, because of a more uniform heating of the air volume above the canopies. This effect was associated with small-scale turbulence superimposed on larger air parcels.

The derivation of α by Castellvi (2004) for the SR2 method allows a further interpretation of the parameter by an analysis of the equations. In this approach the principal meaning of α is scaling the mean eddy size responsible for renewal (i.e. αz). This formulation also states that α is dependent on measurement height and stability conditions which differs from the SR1 method which is partially based on a constant α for a given measurement height.

2.4.6.2. Coefficient dependence

The dependence of α obtained with SR1 has been discussed by many authors. Snyder et al. (2008) stated that α value depends on TC diameter, sampling frequency, measurement height above the ground and underlying vegetation. Mengitsu and Savage (2010) reinforce this statement by adding that α increases with temperature-sensor size. Regarding calibration time, according to Snyder et al. (2008) α can be obtained and considered unchanged after one or two campaigns of 1 or 2 weeks each during a season, and remains unchanged if vegetation architecture, measurement height and temperature sensors are constant. This statement was questioned by Castellvi et al. (2012) (see section 2.4.5). With respect to wind speed, given that the assumed heat exchange in the SR theory is between the air parcel and the vegetation, α depends more on the vegetation characteristics than on the air temperature in or above the canopy; therefore wind has little effect on α (Snyder and O'Connell, 2007).

The dependence of α on measurement height can be associated with the position of the sensor with respect to the sublayer it is placed within. After reviewing several studies performed with sensors placed both within the roughness and the inertial sublayers, Castellvi (2004) suggested that the pattern for both positions is similar, i.e. α tends to decrease with increasing measuring height.

Using the α_{st} and α_{uns} approach with intercept and measuring at the canopy top, Paw U et al. (1995) obtained α_{st} and α_{uns} values of 0.99 and 2.51 (maize crop), 0.66 and 1.42 (walnut) and 0.64 and 1.06 (forest) respectively; suggesting that α_{st} tends to be around half the magnitude of α_{uns}, thus raising the question of the dependence of α on stability conditions.

By relating a stability parameter (ϑ) with α for SR2, Castellvi (2004) managed to confirm the dependence of α on stability conditions, in agreement with the results obtained by Paw U et al. (1995). Increasing values of α with increasing instability was linked to the initial (Spano et al., 2000) interpretation of α accounting for uneven heating while a reduction of α was observed for very stable conditions. These results were interpreted by Castellvi (2004) as increases and decreases of mean vertical eddy size responsible for renewal as surface layer become more unstable or stable, respectively. This result is in accordance with the height dependence analysis for the SR1 and fits the discussion of α for SR1 being larger or smaller than 1 depending on the measuring height (Spano et al., 1997); leaving the case of α=1 (uniform heating) as a particular case.

2.4.7. Application of the SR method

2.4.7.1. LE_{SR} estimation

The final aim of the application of the SR technique is the estimation of LE_{SR} for quantifying ET over an agricultural stand. This estimation is performed by calculating LE_{SR} as the residual of the EB equation (Eq. 2.1) using H_{SR} (Spano et al., 2000). Thus a cheap, simple and real-time method for ET estimation would be achieved.

Spano et al. (2000) obtained LE_{SR} values that differed less than 12% from LE estimations obtained as the residual of the EB equation using H_{EC} in a grape canopy. Zapata and Martinez-Cob (2002) suggested that their study was the first to compare LE_{SR} with LE obtained with an independent method, namely lysimetry for a wheat crop. They concluded that the accuracy of H_{SR} estimation does not influence significantly LE_{SR} estimation accuracy when most of the available energy is utilized for water vaporization. Simmons et al. (2007) compared LE_{SR} estimations with LE_{EC} (i.e. LE obtained with the EC method) measurements of pecan crop, and obtained an average error of 10% using a linear regression forced through the origin.

Castellvi et al. (2008) tested for the first time the ability of the SR method of directly estimating H, LE and Fc and the associated EB closure using the SR2 technique for temperature, water vapor and carbon dioxide concentration time series, respectively, over rangeland grass. The obtained SR fluxes were about 4%, 18% and 10% higher than EC fluxes measurements for H, LE and Fc, respectively. With respect to the EB, they obtained similar EB closures with SR as EC, 90% and 95%, and 88% and 91%,

respectively for dry and wet periods, respectively, under unstable conditions. Katul et al. (1996) tested the application of SR using wavelet and Fourier filtering for characterizing the turbulent signal applied for temperature and water vapor concentration scalar on a pine forest. They obtained an overestimation of around 5% for H and an underestimation of around 10% for LE, using EC measurements as a reference. They concluded that turbulence is more efficient for removing heat than water vapor for values of H>30 W m^{-2}. This deviation was attributed to the different sources of both scalars; water vapor is controlled by stomatal activity (i.e. fixed points in the vegetation) whereas heat sources are more abundant, widespread and occupy a larger surface area.

A problem may arise when trying to compare LE_{SR} estimates obtained by the residual of the EB equation (Eq. 2.1) with LE estimates measured with a reference method, if those reference measurements were not associated with a 100% EB closure. Such a comparison would be arithmetically biased and meaningless. Therefore forcing EB closure for correcting LE reference measurements is a widespread approach. This forcing can be performed following the suggestions by Twine et al. (2000). Castellvi and Snyder (2010) highlight that forcing using the *Bowen ratio closure* is not an adequate approach for sites influenced by regional advection and suggest that forcing by applying the simpler *residual LE closure* approach is a valid alternative if sensible heat flux measurements are reliable.

2.4.7.2. Table of applications

See *Appendix II* for a table presenting a summary of reviewed agricultural and forest applications of the SR method (Table II.1).

3. Materials and methods

3.1. Field campaigns – two seasons

The measurements were carried out during two experimental seasons, summer 2010 (S1) and summer 2011 (S2), at neighboring plots. Although essentially similar experimental setups were installed for both seasons, in S1 the studied crop was processing tomato whereas S2 crop was cotton. Data processing and analysis was done separately for each season. The dates are referred to the Julian calendar which numerates the days with their correspondent day of the year (DOY). See *Appendix III* for a detail of the Julian calendar (Table III.1).

The S1 experiment was installed on DOY 146 and the obtained data corresponds to the period of time between DOYs 225 and 237 (a day before dismantling the station) only. This limited amount of data retrieval was caused by several technical problems encountered during the first field campaign. The S2 experiment was installed on DOY 152 and yielded more data, which corresponds to the periods of time between DOYs 153 and 166, and between DOYs 192 to 249 (a day before dismantling the station). The lost of data between both periods was caused by a small accident with a tractor which run over the electric installation, causing a blackout to the measuring station which took several days to repair and recover.

3.2. Experimental site

3.2.1. Location

The experiments were located at the Hula Valley (33°11'N; 35°35'E; Elevation 72m AMSL) of northern Israel. The Hula Valley is delimited by the Golan Heights to the east, the slopes leading to Lake Kineret to the south, the Naftali Mountains to the west and the hills of Metulla to the north. See *Appendix IV* for a brief historical background of the Zionist agricultural settlement at the Hula Valley.

3.2.2. Climate

The local summer climate is rainless and predominantly sunny with little variation from day to day. Considering the rain years between 1970/1971 and 1999/2000, the annual average of rainy days (i.e. rainfall>=1 mm) was 52 days with an annual average rainfall of 509.4 mm. For the same period, there was no rainfall during summer considered as

the three-month period between June and August. In the period comprised between the years 1981 and 2000, the average annual and summer relative humidity at 12 h GMT was 42.83% and 38.3% respectively. The mean minimum air temperature for the same period was 12.29 °C and 18.2 °C on an annual and summer basis respectively; while the mean maximum temperature was 26.79 °C and 33.9 °C for the same averaging periods of time. These data are provided by the Israel Meteorological Service (*http://www.ims.gov.il*) and correspond to the meteorological station situated in Kfar Blum (2 Km far from the experiment location).

3.2.3. Soil

According to the map of soil type distribution in Israel presented by Singer (2007), the predominant soils in the area can be classified as alluvial soils or brown alluvial soils (Vertisols). The most frequent (but not only) parent material for Vertisols is alluvium; which is easily weatherable and capable of yielding a large amount of clay material. This soil group is usually found in valleys since leveled or only slightly sloping land surface appear to encourage its formation (Singer, 2007).

Soil tests were performed at the experimental farm area and determined the composition of its soil as shown in the following table:

Table 3.1 *– Composition of soils in the experimental area*

Season	Plot number	Depth (cm)	Sand (%)	Silt (%)	Clay (%)
S1	20	0 - 30	12	42	46
		30 - 60	20	41	39
		60 - 90	8	40	52
		90 - 120	4	26	70
S2	40	0 - 30	4	33	63
		30 - 60	6	35	59
		60 - 90	2	34	64
		90 - 120	2	38	60

3.3. Crop

3.3.1. Season 1 –Processing tomato

Processing tomato (variety Heinz 8892) was planted in East-West rows with a density of 25000 plants ha^{-1}. Total plantation area was about 15 ha (for a map of the plot see Fig. 4.3). The tomatoes were planted on May 15th 2010 (DOY 135), and harvested on

August 28th, 2010 (DOY 240). Irrigation was applied with sprinklers in the first two weeks and continued with drip irrigation throughout the rest of the growing period. Crop height was measured weekly and reached a maximum of 0.6 m. Leaf area index (L_{AI}) of the mature plants was determined on August 17th (DOY 229) by measuring the leaf area of one representative tomato plant using a DELTA T Devices area measuring system. The obtained leaf area for one plant was 0.9664 m^2 yielding a leaf area index of 2.42.

3.3.2. Season 2 – Cotton

Cotton (variety Akalpi) was planted in East-West rows with a density of 90000 plants ha^{-1}. Total plantation area was about 18 ha (for a map of the plot see Fig. 4.3). The cotton was planted on April 1st 2011(DOY 91), and harvested on mid-September 2011. Irrigation was applied with sprinklers in the first two weeks and continued with drip irrigation throughout the rest of the growing period. Crop height was measured with a frequency between one and two weeks and reached a maximum of 1.5 m (Fig 3.1). Leaf area index (L_{AI}) was measured as often as crop height and determined in the same way as was done for tomatoes (S1). The L_{AI} reached its maximum value on DOY 207, when the plant reached its maximum height and the canopy was fully covering the field (L_{AI}=9.8).

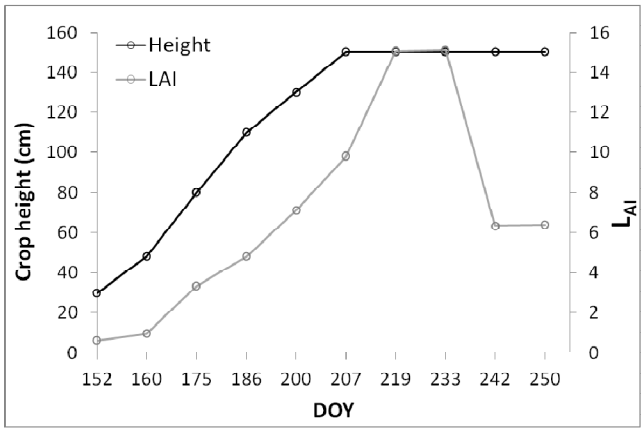

Figure 3.1 *– Cotton crop height (left vertical axis) and L_{AI} (right vertical axis) estimated during the growth season of S2. Canopy full coverage was reached on DOY 207 (LAI=9.8).*

3.4. Measurement devices calibration

See *Appendix V* for a description of the measurement devices calibration test performed before S2.

3.5. Experimental setup and procedure

3.5.1. EC system installation

The EC system is constituted by a sonic anemometer and an infra red gas analyzer (IRGA), for water vapor and carbon dioxide concentrations measurement (Fig. 3.2). In S1 the EC system together with the additional measurements (i.e. radiation, humid air and TCs) were installed on a metal tripod which has a maximal height of 2.0 m (Fig. 3.2). In S2 the same tripod was used but it was necessary to extend its height by adding a metal pole on its top. Another difference of the installation for S2 was the fact that the net radiometer and the TCs for SR were installed on a separate pole, 8 m south of the main EC tripod.

All the equipment was powered by car batteries charged during the day by solar panels that were deployed on poles about 5 and 10 m away from the measuring region for S1 and S2 respectively. The batteries provide an average of 13 mV continuous current and their charge is monitored on a half hourly basis. During both measurement seasons the power provision worked correctly with the exception of the period of time after the tractor accident in S2.

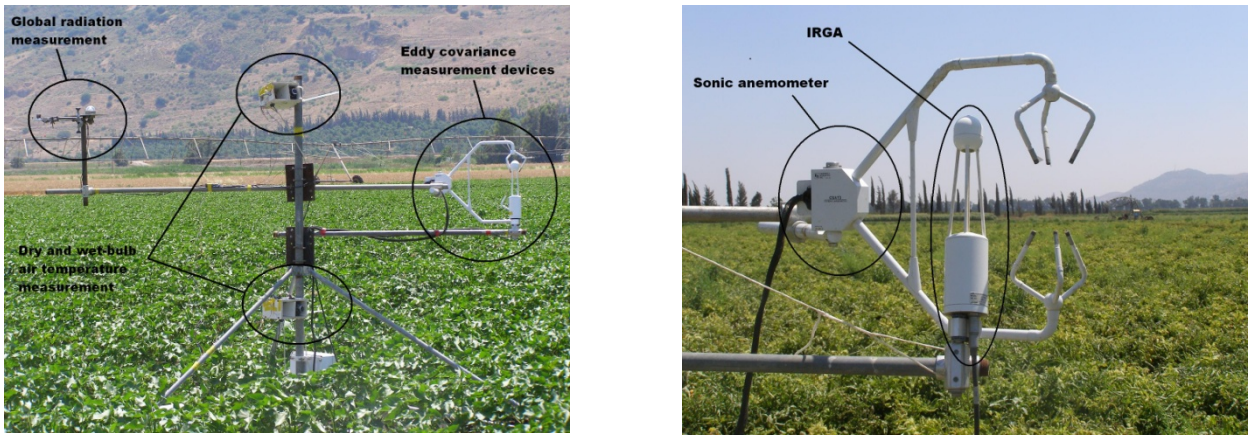

Figure 3.2 *– Left: Field installation showing the tripod and some measurement devices (i.e. EC devices, dry and wet-bulb air temperature and global radiation). Right: Approach to the EC devices, IRGA and sonic anemometer.*

3.5.1.1. EC system position and maintenance

See *Appendix VI* for a description of the measurement devices calibration test performed before S2.

3.5.2. Net radiation flux

Net radiation was measured by a net radiometer (Q*7.1, REBS, Seattle, WA, USA). In S1 experiment the device was installed at 1.75 m height on the same tower of the EC

system. For the S2 experiment the device was installed at 2 m height on an additional column, 8 m southward from the EC tower.

3.5.2.1. Net radiometer position

The source area for a net radiometer has a radius depending on its height (Wilson et al., 2002). The height/radius ratio as provided by the manufacturer is about 1:3. Considering this source radius is important since any external element or particular area of the vegetation beneath or above the device within this radius will influence the net radiation measurements. The net radiometer should always be directed to the south to avoid shading.

3.5.3. Soil heat flux

Soil heat flux was measured by four soil heat flux plates (HFT-3.1, REBS, Seattle, WA, USA) installed at a depth of 0.08 m. Two heat flux plates were installed in a region of wet soil (along hedgerow, between plants) and two in a region of dry soil (along the pathway). Observation showed that only the soil near the drip irrigation pipeline was wet. The area of wet soil surface was estimated by direct measurement and the fraction of wet soil to total soil area was estimated to be 0.4 and 0.5 in the S1 and S2 experiments respectively. To calculate the change in soil heat storage, two TCs were installed in the soil layer above each plate at depths of 0.02 m and 0.06 m. The installation for soil heat flux and storage measurements followed the recommendation by Campbell Scientific, Inc (1998).

3.5.3.1. Soil heat flux plates position

The soil heat flux plates were placed horizontally and care was taken for good contact between plate and soil.

3.5.4. Air temperature and humidity measurements

Dry and wet-bulb air temperatures were measured on the EC tower by two aspirated psychrometers, shielded against direct solar radiation, and positioned at heights of 1.0 and 2.0 m and 0.9 and 1.9 m above ground for S1 and S2 respectively. Since the EC height during the S2 experiment changed as plants grew taller, the psychrometers were

also moved to heights of 1.6 and 2.7 m in order to maintain an acceptable position correspondence between the covariance and the humid air measurements.

During S1, aspiration fans of the psychrometers were operated for the last 5 minutes of every 30 minute interval and dry and wet bulb temperatures were measured and averaged during the last minute of every 30 minute interval; whereas on S2 aspiration fans worked continuously, temperatures were sampled every 1 s and averages were calculated and recorded every 30 min. This data was also recorded on the CR23X data logger.

3.5.4.1. Psychrometers position

Regarding the psychrometers it is desirable to install at least one psychrometer at a height as nearer as possible to the EC system since psychrometer's data is used for part of the EC raw data corrections.

3.5.5. Additional measurements

Global radiation was measured by a pyranometer (CM5, Kipp and Zonen, Delft, NL) and PAR was measured by a quantum sensor (Licor LI-190 Quantumsensor, Lincoln, NE, USA). These measurements were used as an additional check of the radiation conditions. For example, global radiation measurements were useful in verifying net radiation measurements in case particular data points show irregular results (i.e. cloudy hours of the day or specially low or high radiation days).

3.5.6. Surface renewal

For a summary of the sensors positioning see *Appendix XI.* Some of the TCs used for the measurements are shown in Fig. 3.3.

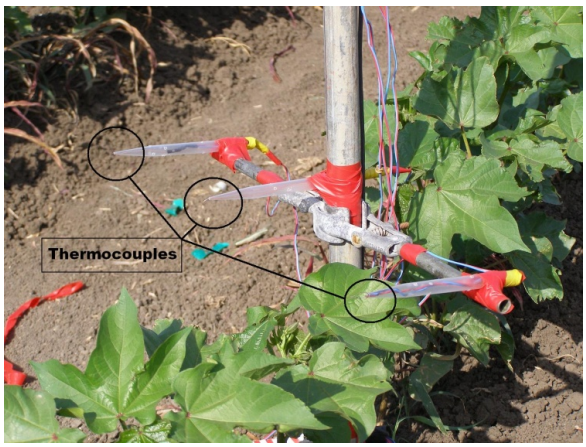

Figure 3.3 *– Three temperature sensors (thermocouples) as installed in the field for high frequency air temperature sampling.*

3.5.6.1. Season 1

The SR system consisted of exposed miniature TCs type T, made of single copper and constantan wires 76 µm in diameter. Five TCs were installed on the same pole as the EC system at heights of 0.3, 0.6, 0.9, 1.2 and 1.5 m above the ground which correspond to normalized measurement heights zn=z/h=0.5, 1, 1.5, 2 and 2.5 when the plants reached their maximum height. The five TCs worked properly and continuously during all the measurement period.

3.5.6.2. Season 2

Although the same type of measuring sensors (type T TCs) was used, the SR installation on S2 was different from S1. The main difference was the fact that the TCs were placed on a pole standing 8 m southwards from the EC system main tower. Seven TCs were installed, which did not stand on fixed heights during the experiment. In addition, two TCs with different diameters were installed; one for the whole measurement season (511 µm wire diameter) and another for three weeks (127 µm wire diameter). Considering the TC junction as approximately spherical, the diameter of the used TC junctions built with 76 µm wire diameter was between 0.10 and 0.25 mm. For the 511 and 127 µm wire diameter TCs, the diameters of the junctions were 0.92 and 0.20 mm respectively. The fact that the 127 µm wire diameter TC resulted in a thinner junction that some of the TCs built from a 76 µm wire diameter is discussed in section 4.3.5. During S2, only one of the seven TCs worked properly throughput the whole measurement period of 72 days; being necessary to replace the others regularly for obtaining continuous data. For a summary of the sensors performance days see *Appendix XI*.

3.5.6.3. Sensors building procedure

The TCs were self-built in the laboratory at the Volcani Center. The junction between the two wires is welded by an electric pulse which is transferred by a graphite conductor to a previously arranged joining between wires at the edge of the thermocouple cable. After this pulse is applied, the welded junction is observed through a microscope for checking its shape (spherical is the desirable) and that the only contact point between the two wires is indeed the junction.

3.5.7. Data Storage

For both measuring seasons, raw signals of EC and SR systems were sampled at 20 Hz. Signals were recorded and processed continuously on line, with averages and covariances stored every 30 min on a CR3000 data logger (Campbell Sci., Logan, UT, USA). All 20 Hz raw data was recorded on an external memory card (2 Gb) connected to the data logger for subsequent processing. Thirty minutes averages of other measured variables (net radiation, soil heat flux and temperatures, global radiation and PAR) were recorded on a CR23X data logger (Campbell Sci., Logan, UT, USA).

3.6. Data processing

All data processing was done using Matlab (The Mathworks, Inc.) with a code specifically written for this project. See Appendix VII for the part of the Matlab code related to the Structure Functions analysis. For a summary of all the devices involved in the measurements and their positioning see *Appendix XI*. In each season, all collected data was divided arbitrarily into two periods: calibration and validation. For S1 experiment the duration of each period was chosen to be 7 days of calibration (DOY 225-231, August 13 – 18, 2010) and 6 days of verification (DOY 232-237, August 21 – 25, 2010). For S2 more than one calibration and verification periods were analyzed: different periods were chosen by different criteria as denoted in Table 3.2. For the SR, only data at 10 Hz or lower frequencies were analyzed because the 20 Hz sampling rate was faster than thermocouples' response time.

3.6.1. Eddy covariance

During the calibration period, the eddy covariance LE_{EC} and H_{EC}, along with measurements of Rn and G were used to derive an energy balance equation (Eq. 2.1).

The results showed (see section 4.1.2) that the energy balance was not completely closed (i.e. b≠1in Eq. 2.1) therefore, following the *residual LE closure* suggested by Twine et al. (2000), a corrected latent heat flux (LE_{ECf}) was calculated a*s:*

$$LE_{ECf} = Rn - G - H_{EC} \qquad (3.1)$$

3.6.1.1. EC fluxes calculation and validation of the measurements

See *Appendix IX* for a description of the equations involved in the EC fluxes calculation and the validation methods for those measurements.

3.6.2. Soil heat flux

The calculation of soil heat flux and storage (denoted as soil heat flux and designated as G) was done using soil properties (soil heat capacity, water content and bulk density) extracted from local soil samples and other parameters extracted from the literature. See *Appendix X* for a description of the equations and data involved in G calculation.

3.6.3. Surface renewal

3.6.3.1. Surface renewal calculation procedure

In order to perform the SR analysis it is necessary to measure a high frequency turbulent signal of temperature. This signal is subsequently treated with the aim of modeling it by a ramp-like structure assuming that this is a good model of the turbulent dynamics of ejections and sweeps that occurs between the canopy and the atmosphere. The modeled ramps are calculated by a mathematical analysis called Structure Functions (Van Atta, 1977; see Appendix I for a further explanation of the Structure Functions theory) as follows:

$$S^n(r) = \frac{1}{m-j}\sum_{i=1+j}^{m}\left(T_i - T_{i-j}\right)^n \qquad (3.2)$$

Where *m* is the number of data points in the desired interval of time (30 min in this study), *n* is the power, *j* is a sample lag between data points corresponding to a time lag $r = j/f$ (s) and T_i is the i^{th} temperature sample. According to the structure functions theory, *r* should be smaller than τ (Spano et al., 1997), thus in this study a criterion was imposed to filter those points where τ is less than 5 times *r*. The filtered points were discarded and not included in the calibration described later; this resulted in removal of about 2% of all half-hourly periods analyzed.

The average amplitude *a* is estimated by solving the following polynomial:

$$a^3 + pa + q = 0 \qquad (3.3)$$

where

$$p = 10S^2(r) - \frac{S^5(r)}{S^3(r)} \quad (3.4)$$

$$q = 10S^3(r) \quad (3.5)$$

Equation (3.3) has three roots which can be either a set of two complex and one real or three real roots. In the first case, the real root is chosen as *a*. For the second case it was found that two of the roots had a common sign (plus or minus) while the third root had the opposite sign. In such cases *a* was associated with the root of the opposite sign. The inverse frequency τ is then estimated as:

$$\tau = -\frac{a^3 r}{S^3(r)} \quad (3.6)$$

Finally an estimation of H_{SR} (W m^{-2}) is obtained applying Eq. 2.6:

$$H_{SR} = \alpha H_{NC} = \alpha \rho C_p \frac{dT}{dt} z \cong \alpha \rho C_p \frac{a}{\tau} z \quad (2.6)$$

The numeric value of α is obtained as the slope of a linear regression through the origin between H_{NC} (independent variable) and the reference H_{EC} calculated with the eddy covariance (dependent variable).

3.6.3.1.1. Wind influence on Structure functions

The application of the Structure Function analysis is affected by wind because for lower wind shear τ is longer thus allowing application of longer time lags. Longer time lags may affect negatively the results by violating the structure functions assumption of $r<<\tau$. Although theoretically τ should be equal for all heights, since it is associated with the coherent structures, in practice it is influenced by wind action (Snyder et al., 1996).

3.6.3.2. Calibration of the SR method

Calibration of the estimations obtained with the SR technique (see section 2.4.6.2) is dependent on four main parameters. They are TC diameter, measurement height (z), sampling frequency (f) and time lag (r) used for Structure Functions application. These four parameters are controllable in the experimental design and will determine the calibration results (i.e. α_{st} and α_{uns}) and statistics in this study. In the Results chapter (Ch. 4) TC diameter will be considered as within the range obtained with a TC wire diameter of 76 μm (see section 3.5.7.2) unless this is specified (see section 4.3.5). The

measurement height (i.e. at which height the temperature signal is sampled with the TCs) was variable between and within seasons (see sections 3.7.1 and 3.7.2). For analyzing at the 1, 2, 5, 8 and 10 Hz frequencies, the required data points of the full time series (recorded at 20 Hz) were skipped. Regarding the time lag, this magnitude is related to the average time detected by the structure functions between ramp events in the temperature signal (see *Appendix I*) and considering the general values observed in the reported previous SR analysis the used time lags were 0.25, 0.5, 0.75, 1.0, 1.25, 3 and 5 s. A set of parameters is defined as a combination of the three variable parameters in this study (z,f,r). For each couple of *a* and τ, associated with a set of parameters (z,f,r), half-hourly H_{NC} (Eq. 2.6) was calculated.

The linear regressions through the origin applied for calibrating between H_{NC} and H_{EC} for stable and unstable conditions yield a slope (i.e. α value), an adjusted coefficient of determination (R^2), a root mean square error (RMSE) and a statistical significance analysis (p-value). RMSE is calculated as follows:

$$RMSE = \left[\frac{\sum_{i=1}^{n}(y_i - x_i)^2}{n_o}\right]^{0.5} \qquad (3.7)$$

where y_i and x_i are the time averaged (i.e. 30-min) reference and estimated data and n_o is the number of time averaged points in the studied period.

The procedure for calibrating is described in sections 2.4.3 and 3.6.3.1, however this calibration leads to a big amount of combinations from which only the best should be selected. Therefore some criteria are used in order to choose the best calibration. Data obtained with all the possible combinations (sets) are linearly regressed against the reference measurement. Given that in this study the α_{st} and α_{uns} calibration approach is applied, for each set there will be two α values, two R^2, two RMSE and two p-values, one for stable and another one for unstable conditions (i.e. both H_{EC} and H_{NC} showing negative or positive values respectively).

In S1 the calibration was done during 7 days, from DOY 225 to 231, when plant height was 0.6 m. The obtained data in S2 differed significantly from that in S1. Therefore rather than one calibration and validation period, different periods were defined and analyzed depending on the available data and desired tests. These periods were called *S2a, S2b, S2c* and *S2d* and defined as presented in Table 3.2:

Period	From DOY	To DOY	Plant height (m)	Type of test
S2a	153	166	Variable	Measurement height
S2b	208	224	1.50	Alpha stationarity
S2c	220	229	1.50	TC diameter
S2d	234	237	1.50	ET estimation

Table 3.2 *– Different periods defined for S2 showing the objective of the calibration for each one.*

3.6.3.3. Optimization – practical application

For each sampling rate, a set of (z,r) values is obtained as optimal considering as a criterion to choose the best (highest) R^2 of all the tested calibrations (including stable and unstable conditions). Once f and z are fixed, a (z,f,r) set is chosen for each stability condition according to the best obtained R^2 and allowing these two sets to have different *r* between them. In case that the best R^2 is similar between two different *z* for a given *f* (case of Fig. 4.8) the total RMSE, obtained as the addition of RMSE for stable and unstable conditions, is considered and the calibration that returns the lower deviation is chosen. For example, in S1 the total RMSE obtained for f=10 Hz at z=0.6 and z=1.2 m was 65.43 and 48.43 W m^{-2} respectively, thus z=1.2 m was chosen as the optimal measurement height. This procedure for establishing the best calibration is intended to real applications of the method which may require a specific positioning of the TCs (here it is assumed that only one sensor is used) and a fixed sampling rate.

3.6.3.4. Validation

Validation is an essential step in any calibration process. The aim of validating is to apply the obtained parameters during the calibration, α_{st} and α_{uns} in the case of this study, with independent data so as to test if they correctly estimate or predict the desired parameter (H in this case). The independent data in this case were different days than the ones used during the calibration period and the validation was tested with a linear regression through the origin between half-hourly averages of H_{EC} and H_{SR} including both stable and unstable conditions.

3.6.3.5. Obtaining LE_{SR}

H_{SR}, along with the other energy balance components, was used to extract the latent heat flux as residual:

$$LE_{SR} = Rn - G - H_{SR} \quad (3.8)$$

The regression between LE_{SR} and the deduced LE_{ECf} during the validation period (data not shown) resulted with values of slope, intercept, R^2 (and their corresponding statistical significance) and RMSE which indicated the performance of the SR method for estimating LE in a given period.

3.7. Summary of devices configuration

See *Appendix XI* for details of the instruments deployment during the two field campaigns.

4. Results

4.1. Eddy covariance

4.1.1. Fluxes

Fig. 4.1 shows measured half-hourly energy fluxes on three selected days: LE, H, G and Rn, corresponding to the first and second experimental seasons, S1 (left) and S2 (right).

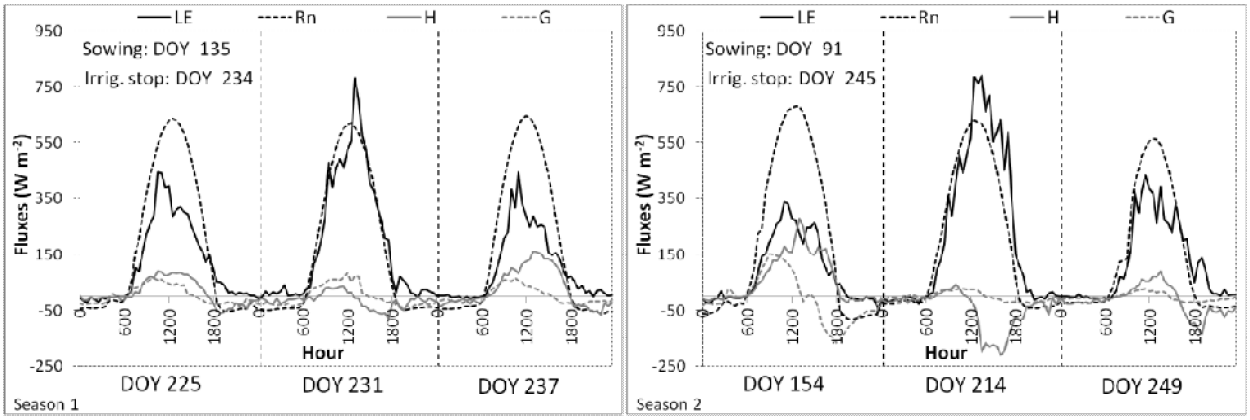

Figure 4.1 *– LE, H, G and Rn fluxes corresponding to three different growing and irrigation states of the crop and showing sowing and irrigation stop date for each crop.*

It is possible to appreciate the different ET rates, represented by the LE flux. DOYs 231 and 214 represent ET peaks for S1 and S2 respectively. When these high LE values are achieved, the available energy (i.e. Rn-G term in Eq. 2.1) may not be sufficient, therefore the additional energy required by the plant is obtained from the heat available in the surrounding air. This energy transfer from the air to the plant is associated with a more negative H flux. This process is most clear in DOY 214 of S2, when H turned negative (i.e. stable conditions, warm air above cooler plants) around midday. It continued this way during all the afternoon, which is the period of the day with stronger winds hence higher ET rates. A difference can be observed between DOYs 154 and 249 of S2. In these cases LE exceeded the available energy only during a short period of the day (i.e. after 18 h) and therefore H was positive during most of the day. These two DOYs differ in that DOY 154 corresponds to an early growth stage of the cotton crop while DOY 249 corresponds to a fully developed canopy but already in a senescence stage and with less irrigation thus less available water for transpiration.

This difference is also reflected by the different G, which may be explained mainly by the different covering of the soil by the plants.

4.1.2. Energy balance

Fig. 4.2 shows the EB closure analysis for the two seasons. In S2 the EB is presented only for the second period of measurements (see section 3.1). The regression was performed using Eq. 2.1. The obtained EB closure slopes (85% and 87% for S1 and S2, respectively) are within the range reported for FLUXNET sites and other EC applications in the literature (see section 2.3.4). These closures may vary depending on the number of days chosen. For example, the EB closure for the period between DOYs 210 and 218 in S2 is 98%, while a closure of 97% is achieved between DOYs 229 and 232 in S1; these better closures were associated with high ET rates.

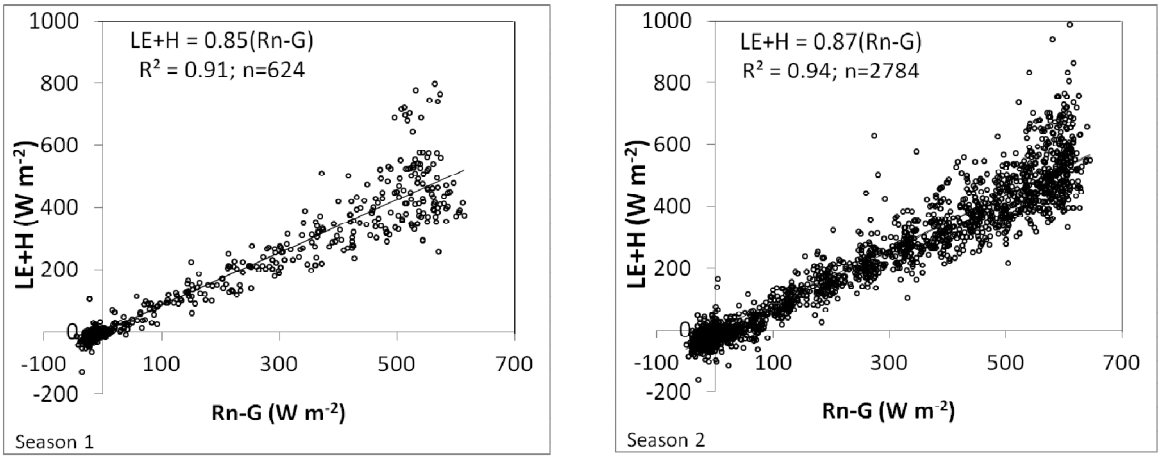

Figure 4.2 *– Energy balance closure for both experimental seasons, showing slope of the regression, coefficient of determination (R^2) and number of points (n).*

The procedure of this study is to use the EC estimations as a reference for calibrating and validating the SR technique. Although the lack of EB closure is within the accepted range, the estimation of LE using the SR technique is based on the EB equation assuming a 100% closure. Considering this assumption and in order to perform the final comparison between SR and EC estimations of LE, a correspondence is needed between the EB closures of both techniques. Therefore the *residual LE closure* technique (Eq. 3.1) was applied for the LE flux estimation in both seasons.

4.1.3. Footprint

To test the reliability of the EC measurements, the footprint model by Hsieh et al. (2000) was applied to the same periods when the EB closure was assessed for both seasons. In this study the model was used to estimate how often 90% of the flux measured by the EC system originated from within the available fetch of the crop field. The points in Fig. 4.3 show the distribution of these locations inside and outside the fields for each season. The model results showed that between 8:00 h and 18:00 h, i.e. the period which accounts for an average of 94% and 97% of water loss to the atmosphere each day for S1 and S2 respectively, 76% and 73% of the half-hourly data points were measured from within the field for S1 and S2 respectively. These results support the validity of the fluxes measured by the EC system.

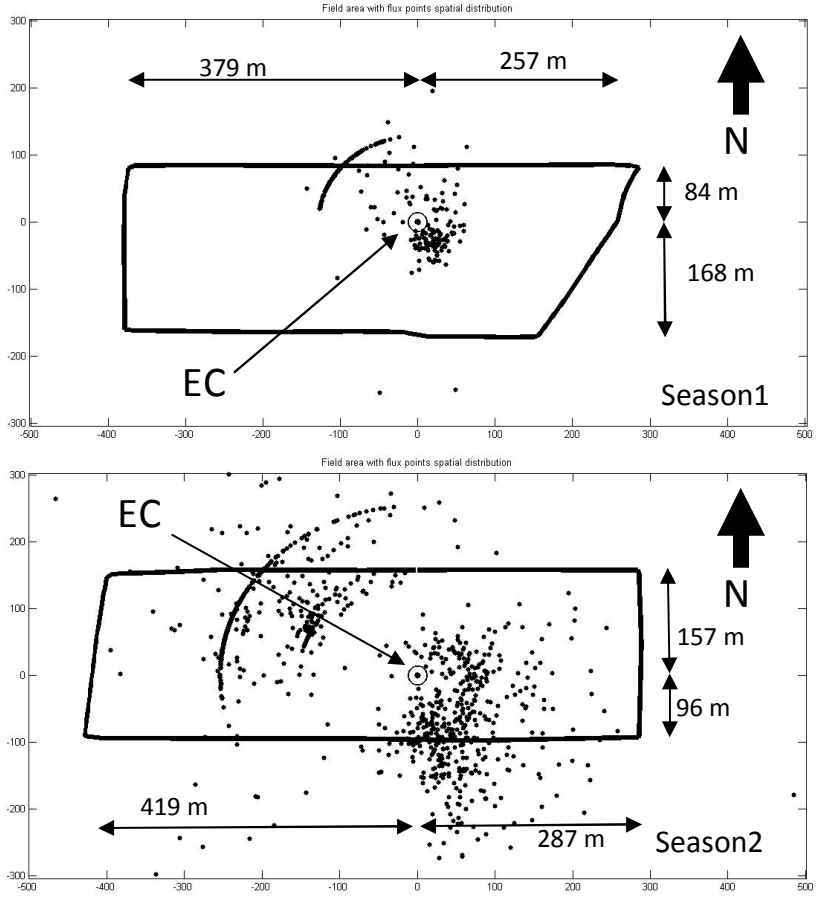

Figure 4.3 *– Points showing the origin of 90% of the flux measured with the EC system. The location of the EC system is the origin of the Cartesian axes (0,0). The distances from the EC system to the edges of the fields in the four directions are also shown. Dimensions are in meters.*

Fig. 4.3 also shows that the points had a similar distribution in the two seasons (i.e. two different years). This distribution is directly related to the prevailing wind direction and intensity at the experimental site. This is further visualized in Fig. 4.4 where the distribution of horizontal winds between DOYs 201 and 249, S2, is presented by relating their velocity with azimuth (i.e. the direction where the wind comes from) and with time of the day. Both plots show that when wind speed is over 2 m s^{-1} the wind azimuth is

mostly between 270 and 315 degrees (i.e. north western wind) and also that these strong winds occur in the afternoon, reaching their maximum speed (>2 m s^{-1}) between 14:30 and 17:30 h. These results suggest that the north western front of points (Fig. 4.3) is associated with strong winds which, in turn, are associated with relatively high ET rates. A final EC validation obtained with the footprint model is the calculation of the percentage of flux originated within the field, F_{IN}. This analysis showed that for data points associated with wind speeds larger than 2 m s^{-1} F_{IN} was always > 90% during the afternoons.

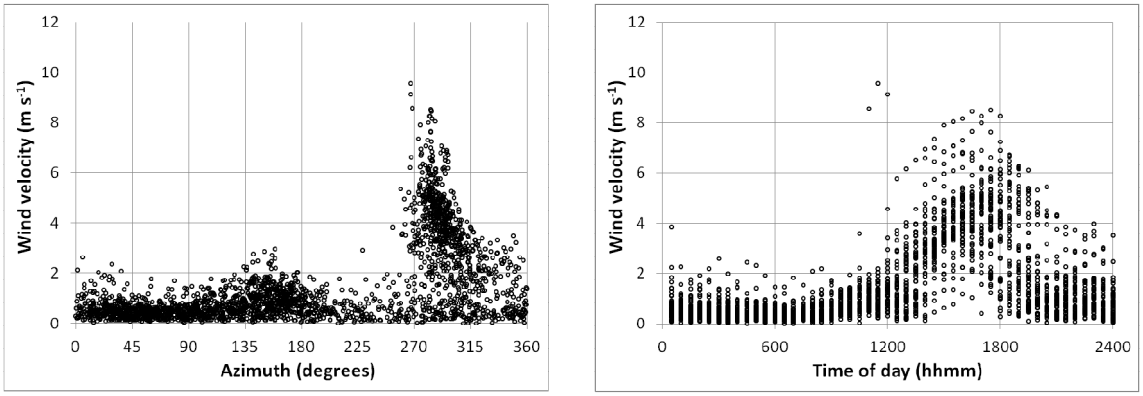

Figure 4.4 *– Plots relating wind velocity during the time period between DOYs 201 and 249 in S2 with azimuth and time of the day.*

4.2. Application of Structure Functions

Applying Structure Functions (see section 2.4.2.5) to the temperature signal allows obtaining an average estimation of the amplitude *a* (°C) and the inverse frequency τ (s) for a selected time interval, 30 min in this study. Fig. 4.5 shows one minute of the temperature signal obtained with a TC placed at z=0.6 m between 12:29 h and 12:30 h on DOY 226, S1. During the half-an-hour interval to which Fig. 4.5 corresponds (i.e. between 12:00 h and 12:30 h) the obtained values for *a* and τ were 0.50 °C and 9.59 s respectively. In the figure, the modeled ramps are schematically illustrated; with *a* = 0.5 °C and τ = 10 s, which would correspond to six ramp events in one minute.

The diurnal course of half hourly ramp *a*, obtained using a time lag r=0.25 s and frequency f=10 Hz, for DOY 226, S1, can be seen in Fig. 4.6. The sign of *a* determines the sign of H_{SR} (Eq. 2.6); therefore positive *a* corresponds to a positive (upwards) H_{SR} associated with unstable conditions (warmer soil/plants below cooler air); and vice

versa. The drop around 10:00 h and 10:30 h is not necessarily associated with a drop in H_{SR} since the latter depends on a/τ.

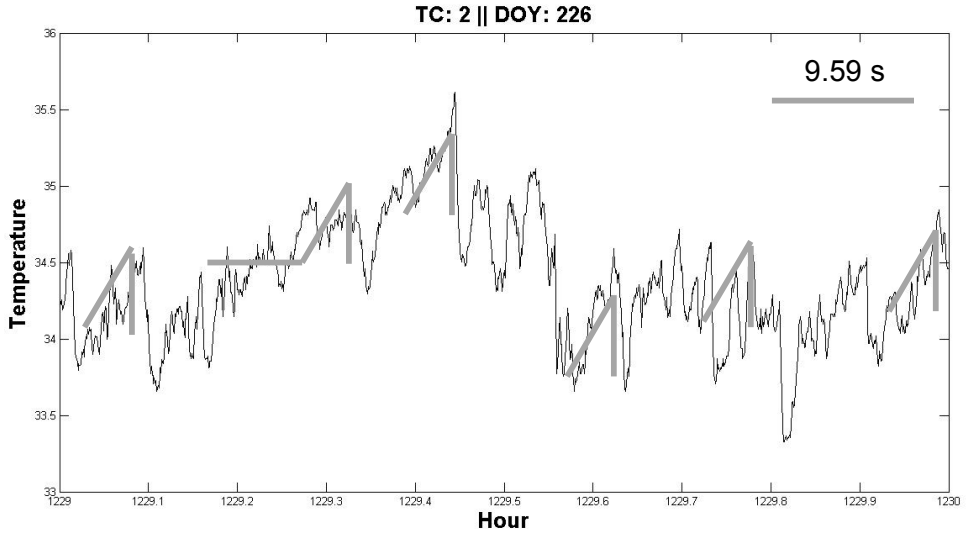

Figure 4.5 *– One minute of the temperature signal obtained with TC 2 (z=0.6 m) in DOY 226, S1. Over the signal the amplitude and inverse frequency obtained for this half-an-hour period (with time lag r=0.25 s) is schematically drawn respecting the correspondent obtained values of a=0.5* °C *and* τ *=9.59 s. Temperature is in units of* °C *while Hour is presented as HourHourMinMin and the figure after the comma is Min/60.*

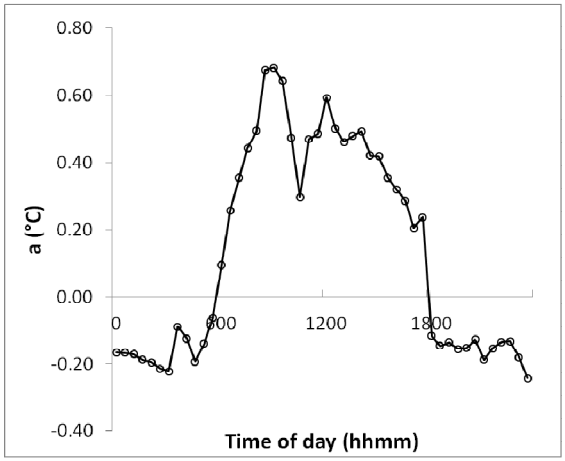

Figure 4.6 *– Daily curve of the amplitudes estimated by applying structure functions (r=0.25 s and f=10 Hz) to the temperature signal obtained with TC 2 (z=0.6 m) during DOY 226.*

4.3. Calibration of Surface Renewal technique

4.3.1. Time lag in stability change

For calibration two linear regressions are applied, one for each stability condition, and this requires splitting the available data (points with half hourly averages) accordingly. The criterion of splitting is to discard those points where H_{NC} and H_{EC} stability conditions are opposite: either stable (negative and downwards) or unstable (positive and

upwards). Therefore in the two linear regressions used for calibration only data that coincide in their stability are included.

Among the results obtained in S2 it was found that for some of the TCs in certain days H_{NC} had an opposite sign than H_{EC} during several hours of the day. The general pattern of this phenomenon is entitled here as a *time lag in stability change* because when this situation occurs, H_{EC} (measured at 3.35 m) turns negative (stable) some hours before H_{NC}. Fig. 4.7 shows this process for DOY 236 of S2, between 12:00 and 17:00 h. It can be seen that this does not happen for all the TCs, but only for the lower ones. H_{NC} estimated with a TC at z=2.4 m perfectly coincides with H_{EC} and does not present any lag whereas H_{NC} estimated with TCs at z=1.5 and 1.7 m do present the time lag. (see section 5.5 for a discussion on the characteristics of this process and possible reasons for its occurrence).

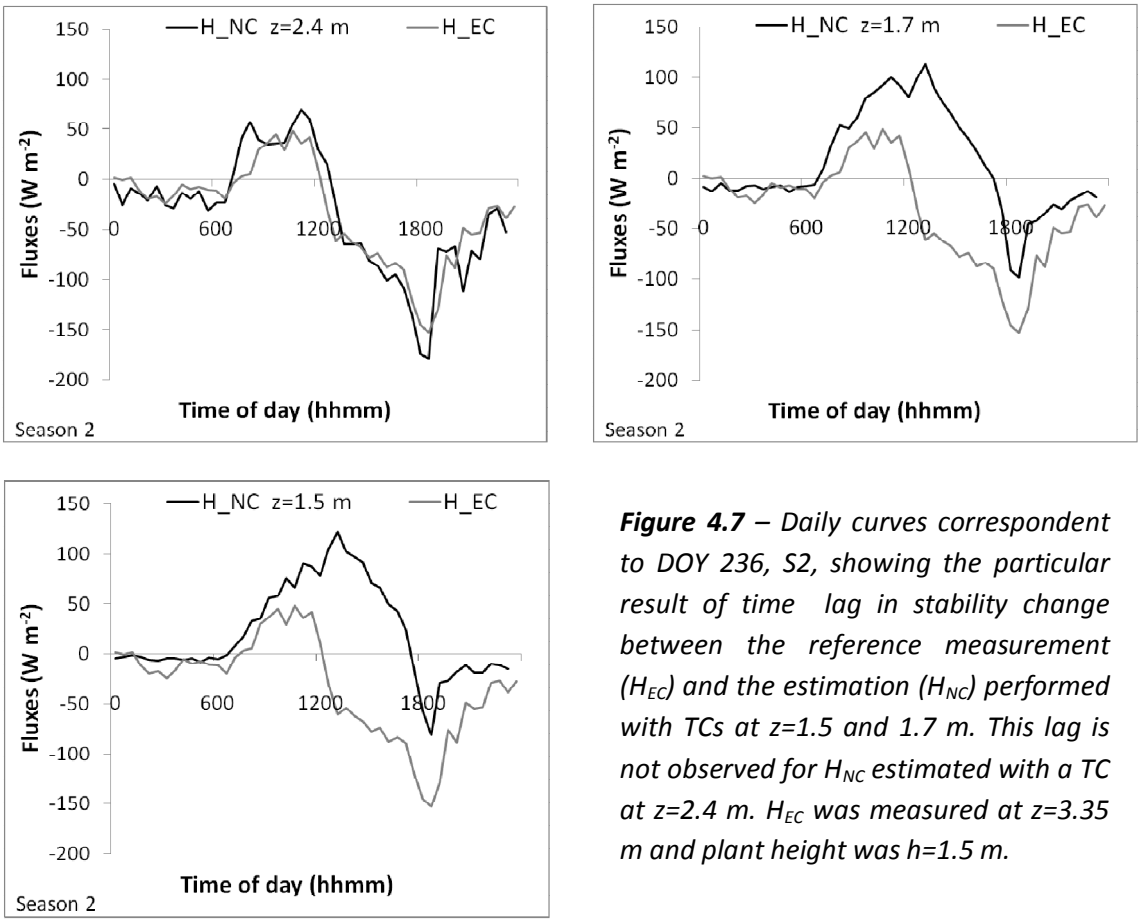

Figure 4.7 *– Daily curves correspondent to DOY 236, S2, showing the particular result of time lag in stability change between the reference measurement (H_{EC}) and the estimation (H_{NC}) performed with TCs at z=1.5 and 1.7 m. This lag is not observed for H_{NC} estimated with a TC at z=2.4 m. H_{EC} was measured at z=3.35 m and plant height was h=1.5 m.*

Fig. 4.7 suggests that this result is related to the measurement height since it was observed near the canopy top (z=1.5 to 1.7 m). Nevertheless, in the calibration process

only those points whose stability coincides were included. Considering the observations of Fig. 4.7, data points associated with the *time lag of stability change* (i.e. with opposite sign of H) were discarded from the calibration. During S2a the *time lag in stability change* was not observed. This period is associated with an early growth stage of the plants (not yet arriving to growth peak of h=1.5 m) and lower ET rates. During S1 the *lag in stability change* was not observed either.

4.3.2. General calibration – α_{st} and α_{uns} approach

4.3.2.1. Examples of regressions

Fig. 4.8 shows the regressions for stable and unstable conditions for two different (z,f) sets in S1. These two different calibrations (four regressions) returned the best R^2 (=0.71) from all the possible combinations in S1. R^2=0.71 was obtained for two different (z,f) sets but in different stability conditions. The selected optimal (z,f) set was (1.2,10) (Table 4.1; see section 3.6.3.3 for the criterion used in this selection). The four plots were statistically significant at a 0.01% level. The (0.6,10) set returned a maximal R^2 for stable conditions whereas the (1.2,10) set calibrated better unstable conditions, suggesting a relation of these results with the mean eddy size for each stability condition (see section 5.4.1 for a discussion on this result).

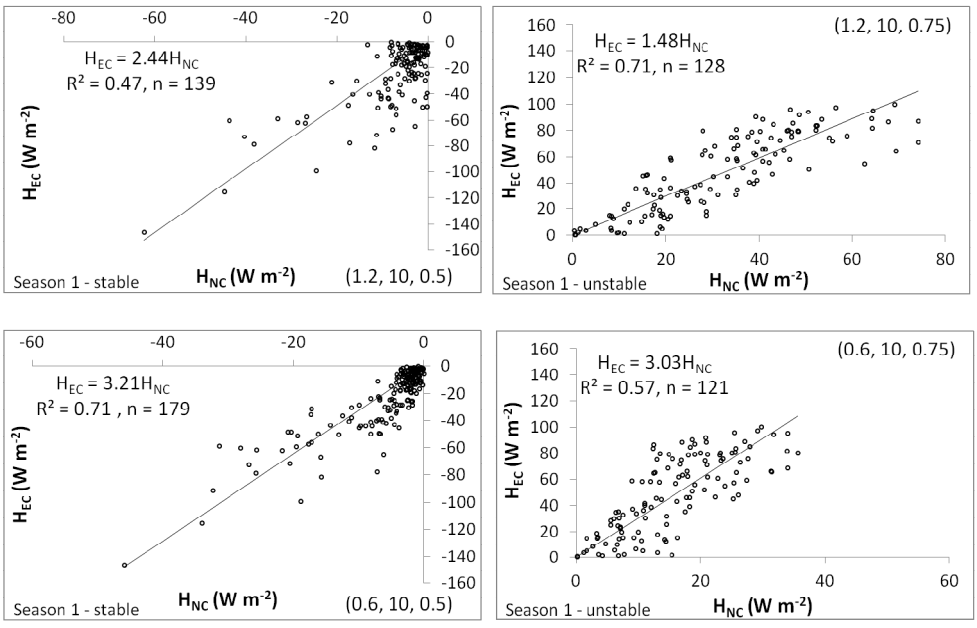

Figure 4.8 *– Two different calibrations in S1, between DOYs 225 and 231. The left and right plots represent the best calibration obtained for unstable and stable conditions respectively. The figures in parenthesis are the corresponding (z,f,r) set. All regressions were statistical significant at a 0.1%. Plant height was 0.6 m.*

Fig. 4.9 shows an example of the regressions during the calibration performed for period S2d. Best R^2 was obtained for the TC at z=2.4 m and stable conditions (see Fig. 4.7 for a typical daily curve of H in this period).

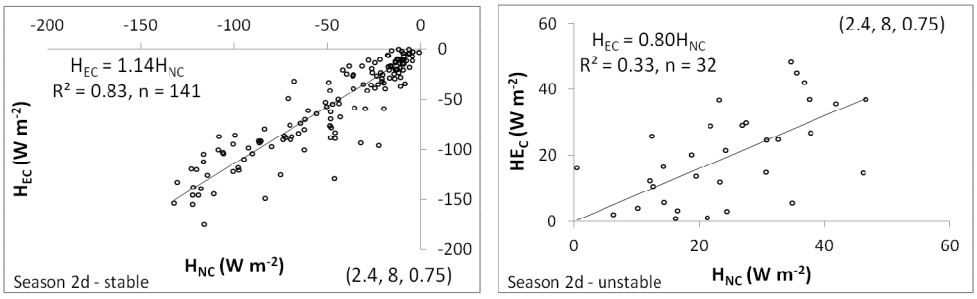

Figure 4.9 *– Calibration for period S2d, the figures in parenthesis are the corresponding (z,f,r) set. During this period plant height was 1.2 m. Both regressions were statistically significant at 0.01%.*

4.3.2.2. α and R^2

In order to analyze how the sampling rate and normalized measurement height affect the calibration results, the variations of R^2 and α with these variables were studied. The normalized measurement height is defined as zn=z/h. Figs. 4.10 and 4.11 show these relations for the best calibration results in S1 and S2d for stable and unstable conditions separately.

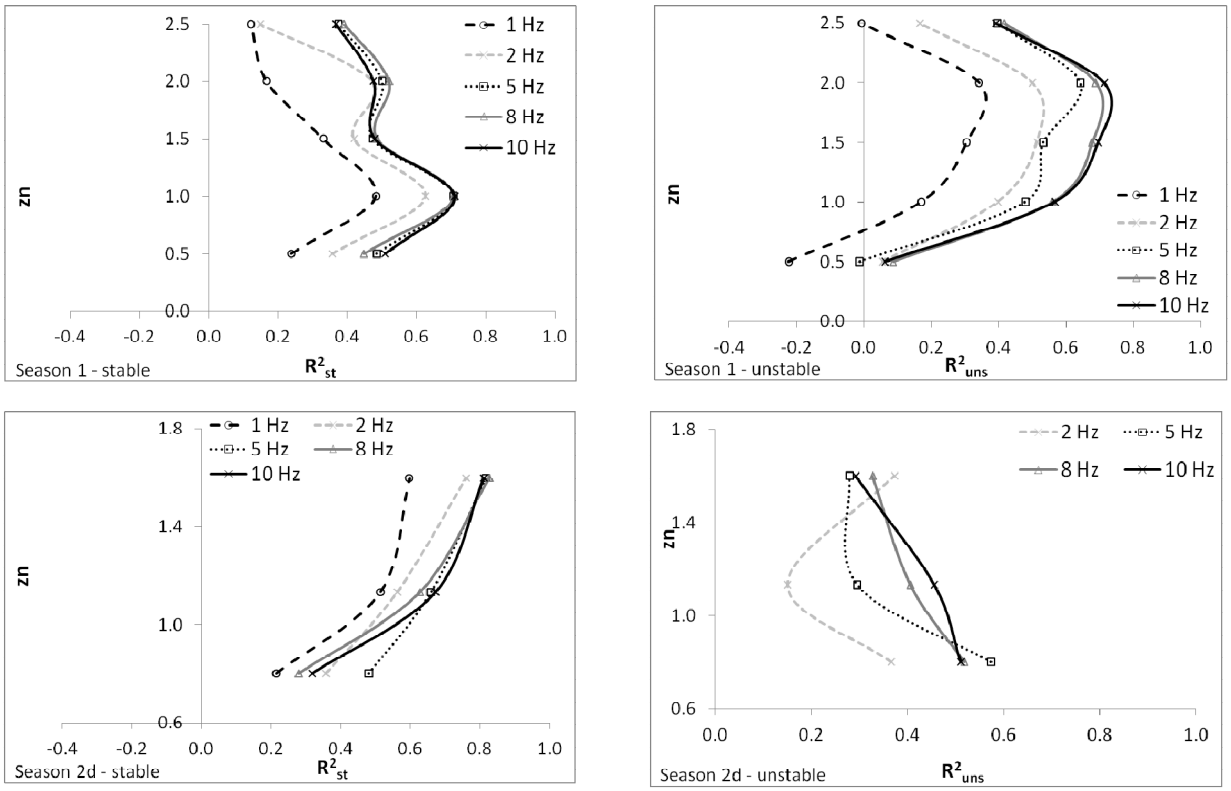

Figure 4.10 *– Best R^2 obtained for each sampling height at five different sampling rates. Negative values (unstable conditions) mean that a significant linear regression through the origin was not possible to perform for those conditions. Note the vertical axis in the S2d plots starting at zn=0.6 for a better visualization.*

Most of the results in these graphs show that highest R^2 and lowest α are obtained with the larger sampling rates as expected. In S2d measurements were performed at zn=1.0 and 1.07; however those measurements are not considered in this analysis since the results were not consistent, suggesting functioning errors in the TCs.

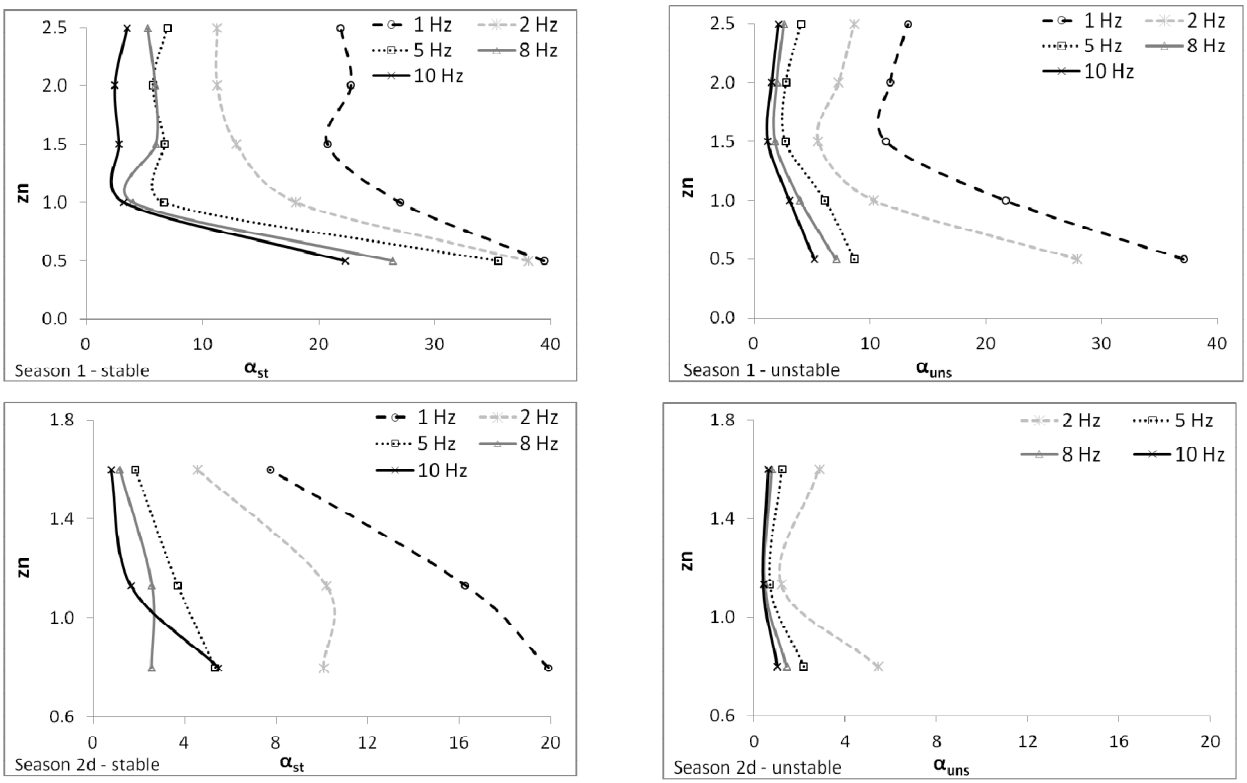

Figure 4.11 *– Curves showing α value obtained for the calibrations of the same sets presented in Fig. 4.10. Note the vertical axis in the S2d plots starting at zn=0.6 for a better visualization.*

4.3.2.3. Optimization

The criteria described in section 3.6.3.3 were applied to the data presented in the graphs showing the variation of R^2 with measuring height and sampling rate. Table 4.1 shows the optimization results corresponding to S1 and S2d. Since the same R^2 was found for two different zn in S1, the RMSE criterion was applied for choosing a single optimal level (see section 4.3.2.1). Therefore the R^2 presented in Table 4.1 for S1 and stable conditions is not the highest among all the possible combinations.S2d was chosen for optimization given that this was the period when the TC at z=2.4 m was working hence the *time lag in stability change* was not observed, making it possible to estimate LE_{SR}.

Season	Frequency (Hz)	1	2	5	8	10
S1	z (m)	1.20	1.20	1.20	1.20	1.20
	h (m)	0.60	0.60	0.60	0.60	0.60
	R^2_{st}	0.17	0.47	0.50	0.52	0.47
	$RMSE_{st}$ (W m^{-2})	33.18	32.75	31.17	30.93	25.06
	α_{st}	22.77	11.27	5.72	5.92	2.44
	r_{st} (s)	5.00	3.00	1.25	3.00	0.50
	R^2_{uns}	0.34	0.50	0.64	0.69	0.71
	$RMSE_{uns}$ (W m^{-2})	53.49	49.56	38.36	30.79	23.37
	α_{uns}	11.73	7.26	2.76	1.95	1.48
	r_{uns} (s)	3.00	5.00	0.75	1.00	0.75
S2d	z (m)	2.40	2.40	2.40	2.40	2.40
	h (m)	1.50	1.50	1.50	1.50	1.50
	R^2_{st}	0.60	0.76	0.82	0.83	0.81
	$RMSE_{st}$ (W m^{-2})	65.64	57.99	36.62	20.38	27.59
	α_{st}	7.74	4.55	1.85	1.14	0.78
	r_{st} (s)	5.00	5.00	1.00	0.75	0.25
	R^2_{uns}	-	0.37	0.28	0.33	0.28
	$RMSE_{uns}$ (W m^{-2})	-	17.75	12.29	12.56	16.79
	α_{uns}	-	2.86	1.22	0.80	0.64
	r_{uns} (s)	-	5.00	0.75	0.75	0.50

Table 4.1 *– Optimal (z,f,r) sets for S1 and S2d. All the regressions were statistically significant at 0.01% except of the case of f=1 Hz in S2d (p-value>0.05), hence this calibration is considered unacceptable and not presented here. Plant and measurement height are noted as h and z respectively.*

Table 4.1 shows that within each season the optimal measurement height was the same; zn=2 and 1.6 for S1 and S2d respectively for all frequencies. Overall, the higher R^2 were obtained for f=8 Hz for both seasons and all conditions with the exception of S1 unstable for which f=10 Hz was the best. There is a consistent decrease (increase) of R^2 (RMSE) as measuring sampling frequency decreases from 5 Hz downwards. The sets with either of the two higher applied *r* (i.e. 3 and 5 s) in the Structure Functions analysis resulted to be the optimal ones for frequencies of 2 and 1 Hz.

Regarding the obtained α coefficients, it is observed a consistent increase in their absolute value as measurement sampling frequency decreases for both stability conditions. Defining α_H as α obtained with f=10 Hz and α_M as α obtained with each frequency, the ratio α_M/α_H for each frequency was related with the ratio f_H/f_M, being f_H=10 Hz and f_M the corresponding frequency to each α_M (i.e. $\alpha_M=\alpha_H$ and $f_M=f_H$ for f=10 Hz). The proximity of the relations between both ratios to Line 1:1 (S1 and S2d stable) presented in Fig. 4.12 suggests that these ratios may be related in a very close manner.

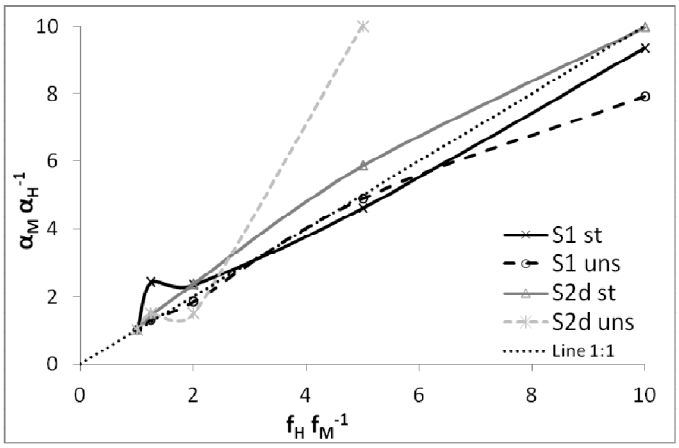

Figure 4.12 *– Ratios of α_M/α_H for each frequency related with the ratio f_H/f_M being α_M equal to α obtained with f=10 Hz and α_M equal to α obtained with each frequency and f_H =10 Hz and f_M the corresponding frequency to each α_M.*

4.3.3. Calibration depending on normalized measurement height

4.3.3.1. Considering different z/h

Period S2a is associated with the initial growth stage of the plants that grew from a height of 0.30 to 0.60 m in 14 days. This made possible to test how zn influences the results. During this period all the TCs were in a fixed position thus zn varied due to the growth of the plants. The objective of this particular analysis is to examine the effect of the normalized variable zn, regardless of the absolute values of either the TC height (z) or the plant height (h). Therefore groups of 3 days within S2a were chosen for each calibration, considering h as the average height for each 3 days and the calibration results were compared for pairs of equal zn (but different combinations of h and z), with equal sampling rates (f=10 Hz) and allowing the time lag (r) to be variable so as to return the highest R^2 (i.e. the best calibration) for the given zn and f. Because of the short period for each calibration (3 days) and the fact that most cases were unstable, for this particular analysis the calibrations were performed considering all data points for each 3 day period (i.e. stable and unstable together) hence obtaining one R^2, α, RMSE and p-value for each calibration. Results of this analysis are presented in Fig. 4.13, essentially showing that for zn > 1, the calibration results of R^2 and α are approximately consistent. Table 4.2 shows the results of all this analysis, including the (z,f,r) sets correspondent to each point presented in the plots, the calibration results and the days when the calibration was performed.

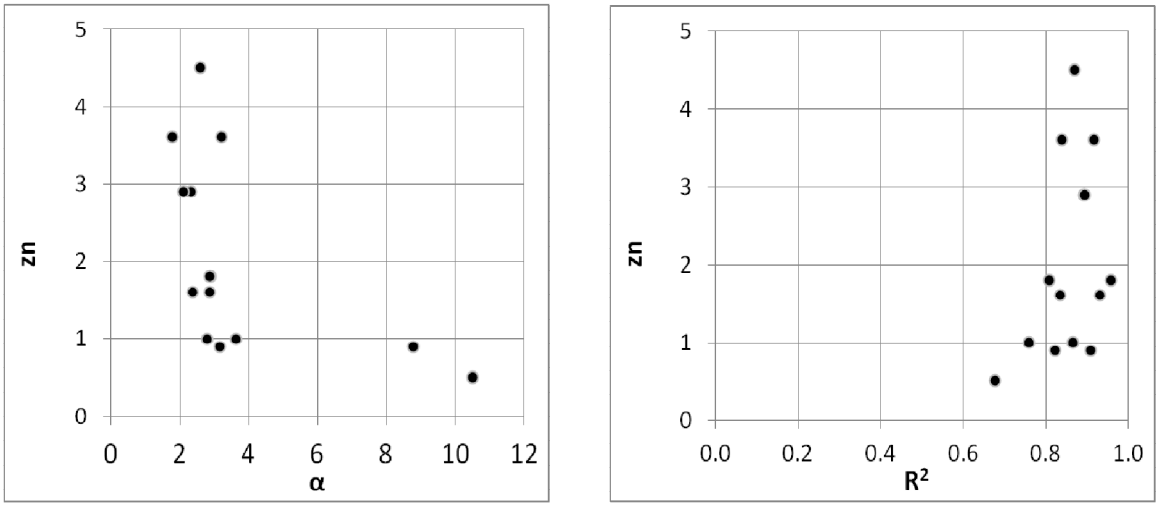

Figure 4.13 *– Analysis of the variation of the calibration results as a function of the normalized measurement height (zn).*

Table 4.2 *– Data points involved in the analysis presented in Fig.4.13. From and to DOY refer to the first and last day of calibration respectively.*

zn	0.5	0.9		1		1.6		1.8		2.9		3.6		4.5
z (m)	0.3	0.3	0.5	0.6	0.5	0.6	0.9	0.6	0.9	1.2	1.5	1.2	1.5	1.5
h (m)	0.57	0.33	0.55	0.57	0.5	0.38	0.57	0.33	0.5	0.42	0.53	0.33	0.42	0.33
R^2	0.68	0.91	0.82	0.86	0.76	0.93	0.84	0.96	0.81	0.89	0.89	0.92	0.84	0.87
α	10.49	8.79	3.15	2.80	3.63	2.85	2.37	2.88	2.87	2.32	2.11	3.21	1.79	2.59
p-value	0.000	0.000	0.000	0.000	0.000	0.000	0.000	0.000	0.000	0.000	0.000	0.000	0.000	0.000
RMSE ($W\ m^{-2}$)	43.72	105.71	35.67	35.69	39.50	63.75	33.52	78.79	36.39	55.76	33.18	84.30	48.95	78.50
r (s)	1.00	0.75	0.50	0.50	0.50	0.25	0.25	0.25	0.25	0.25	0.50	1.00	0.25	1.25
f (Hz)	10	10	10	10	10	10	10	10	10	10	10	10	10	10
From DOY	164	153	163	164	161	155	164	153	161	157	162	153	157	153
To DOY	166	155	165	166	163	157	166	155	163	159	164	155	159	155

4.3.4. The minimum calibration period required for obtaining a stationary α

Like any other calibration coefficient, the robustness and stationarity of α is of practical importance for the application of the SR technique. This was examined by estimating the minimum duration of calibration period needed to reach a constant alpha. The analysis was performed for period S2b, for fixed plant (h=1.5 m) and TC (z=1.5 m) heights and during a relative long period (17 calibration days). The approach used was to calculate α_{st} and α_{uns} for different number of calibration days. To test different combinations of days, this was done by starting from the beginning of S2b period, from the end and from the middle. For example, when starting from the beginning, an initial day was chosen (DOY 208) and α_{st} and α_{uns} were obtained for this single day. Then DOY 209 was added thus obtaining new α_{st} and α_{uns} for both days; and so on. Fig. 4.14 shows how α_{st} and α_{uns} reach an approximately stationary value after 5 days of calibration, for all the sampling rates, when starting from the beginning of period S2b. A

consistent difference in the absolute value of α between sampling rates is also observed. Moreover, for sampling rates ≥5 Hz, and unstable conditions, one day of calibration was sufficient to obtain an almost stationary value of alpha. Similar results were obtained when the analysis was started from the end and from the middle of S2b.

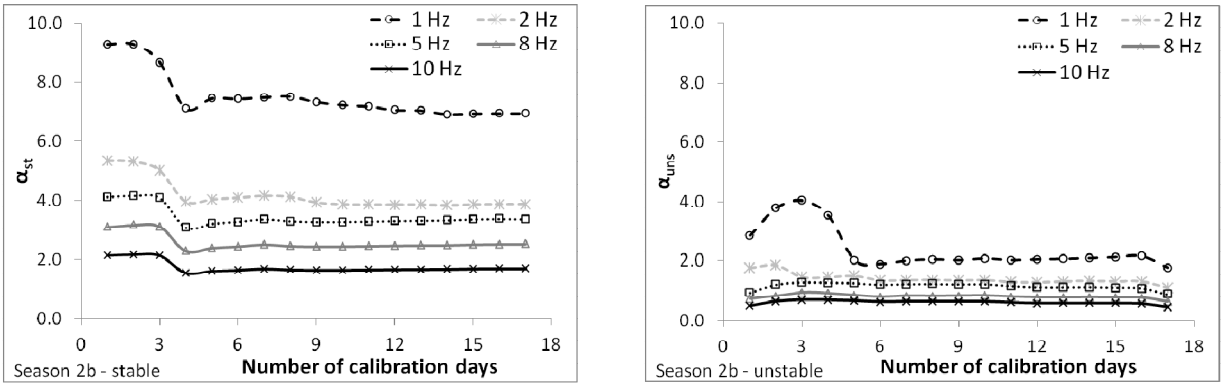

Figure 4.14 *– α_{st} and α_{uns} values depending on the duration (in days) of calibration. The minimum number of days resulted is five.*

4.3.5. The effect of the TC diameter on calibration

The SR technique is based on high frequency sampling of the air temperature with simple and cheap sensors, TCs in the case of this study. The diameter of the TCs junction pose a limit on the largest sampling frequency related to the response time of the sensor. Several applications of the SR technique have been reported in the literature using TCs built from 76 μm wire diameter, which are assumed to be capable of sampling at 10 Hz (Mengitsu and Savage, 2010). However the limitations of thicker TCs, although logical, have not been experimentally shown. Therefore a test was carried out for period S2c with the objective of studying these limitations. Three TCs were installed at the same height (z=1.5 m), each one with a different wire diameter, i.e. 76, 127 and 511 μm. Although the aim of using the 127 μm wire was to install an intermediate TC, measuring its junction diameter showed that it was indeed the thinnest one of the three. Therefore, considering their real junction size, the three TCs will be entitled hereafter as Thin, Intermediate and Thick (corresponding to junction diameter of 0.20, 0.25 and 0.92 mm respectively). The results from period S2c (Fig. 4.15) showed that for stable conditions a significant calibration at a 0.01% level was achieved for the three TCs with the exception of f=1 Hz for the Thick TC. For unstable conditions, a

reliable calibration was obtained only for the Thin TC hence suggesting being capable of correctly sampling at high rates.

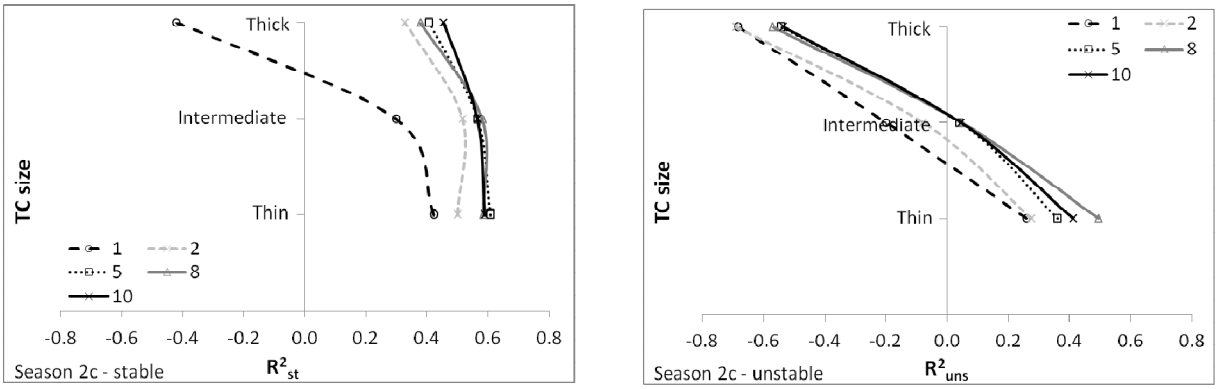

Figure 4.15 *– Test of the influence of TC junction size on the calibration results. Thin, Intermediate and Thick refer to approximately spherical TC junctions of 0.20, 0.25 and 0.92 mm diameter respectively.*

4.4. Validation of H

For validation, H_{SR} was estimated by multiplying H_{NC} by the corresponding α_{st} or α_{uns} (depending on which conditions H_{NC} corresponds to) as shown in Eq. 2.6. The R^2 and p-value of the regression between H_{EC} and H_{SR} are taken as the statistical measure for the validity of the estimations. The slope of the regression is interpreted as the average under- or overestimation of the H_{EC} flux by the H_{SR} flux.

Fig. 4.16 presents two examples of validations performed for the best calibrations corresponding to S1 and S2d. They showed that H_{SR} underestimated H_{EC} on an average of 19% and 21% for S1 and S2d, respectively. Note that in this case only one linear regression is used given that α_{st} and α_{uns} are already applied for estimating H_{SR}. Table 4.3 presents a summary of all optimal calibration and verification data obtained in this study.

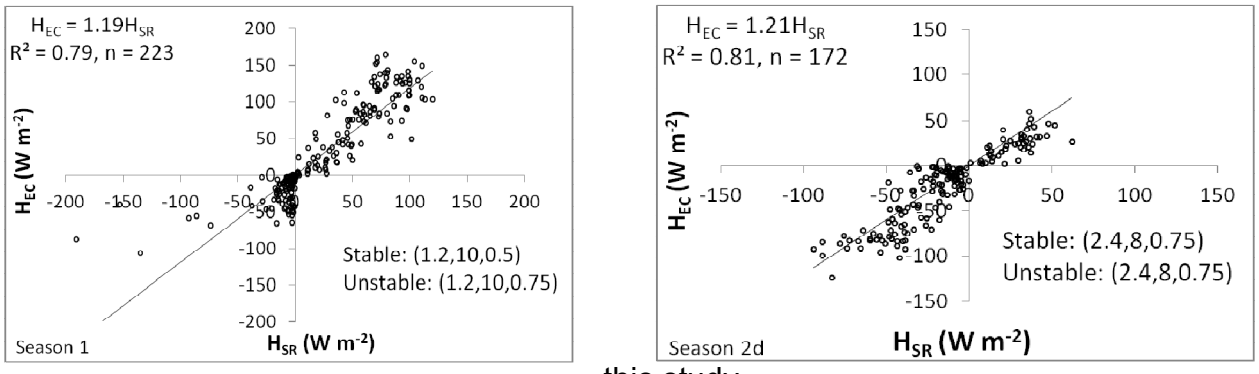

Figure 4.16 *– Two examples of data validation performed for S1 and S2d. These validations were done for data from DOY 232 to 237 for S1 and from DOY 238 to 241 for S2d. The regressions were statistically significant at 0.01% level.*

Season		Calibration		Validation
S1	From DOY	225		232
	To DOY	231		237
	z (m)	0.6		0.6
	h (m)	0.6		0.6
		Stable	Unstable	All data
	R^2	0.47	0.71	0.79
	RMSE (W m^{-2})	25.06	23.37	20.30
	α | slope	2.44	1.48	1.19
	f (Hz)	10		10
	r | r_{st} ; r_{uns} (s)	0.5	0.75	0.5 ; 0.75

Season		Calibration		Validation
S2b	From DOY	208		224
	To DOY	224		241
	z (m)	1.5		1.5
	h (m)	1.5		1.5
		Stable	Unstable	All data
	R^2	0.84	0.53	0.56
	RMSE (W m^{-2})	69.73	7.00	29.17
	α | slope	2.46	1.03	1.09
	f (Hz)	8		8
	r | r_{st} ; r_{uns} (s)	0.5	0.25	0.5 ; 0.25
S2c	From DOY	220		230
	To DOY	229		239
	z (m)	1.5		1.5
	h (m)	1.5		1.5
		Stable	Unstable	All data
	R^2	0.58	0.49	0.69
	RMSE (W m^{-2})	46.17	11.24	42.49
	α | slope	2.82	0.75	0.92
	f (Hz)	8		8
	r | r_{st} ; r_{uns} (s)	0.75	5	0.75 ; 5
S2d	From DOY	234		238
	To DOY	237		241
	z (m)	2.4		2.4
	h (m)	1.5		1.5
		Stable	Unstable	All data
	R^2	0.83	0.33	0.81
	RMSE (W m^{-2})	20.38	12.56	18.92
	α | slope	1.14	0.8	1.21
	f (Hz)	8		8
	r | r_{st} ; r_{uns} (s)	0.75	0.75	0.75 ; 0.75

Table 4.3 *– Optimal calibrations and corresponding validations obtained for part of the tests performed in the different periods. All the regressions were statistically significant at a 0.01% level. For S2b the considered α and R^2 are the values obtained at the fifth-day cumulative calibration. For S2c the calibration corresponds to the Thin TC and (f,r) that showed best performance.*

4.5. Daily ET estimation

The ultimate objective of applying the SR method is to estimate the daily ET (mm H_2O day^{-1}) of the crop of interest. This estimation is done by calculating LE_{SR} (Eq. 3.8) as the residual of the EB using H_{SR} as sensible heat flux. To calculate daily values of ET, the gaps in the half-hourly data of H_{SR} have to be fixed. The gaps are created by the H_{SR} data points which do not pass the filter imposed by the Structure Functions assumptions (see section 3.6.3.1); these points are less than 2% of the data and are not included in the calibration but must somehow be included when daily curves of H_{NC} or H_{SR} are sought. In this study the gaps were substituted by a linear average of the immediate previous and posterior data points. Another consideration related with S2 is the problem of the *time lag in stability change* which also caused some half-hourly points to be discarded when the calibration was performed. Discarding the points within the period of the day when this problem occurred meant not obtaining complete daily curves of H_{NC} during the calibration period. Therefore, only the S2d period was chosen for estimating total daily ET given that one of the TCs installed during this period (z=2.4 m) did not show the *time lag in stability change* problem. H_{SR} estimated with this TC showed a deviation of around 21% from the reference H_{EC} during validation; for the other sub-periods of S2 the deviations were lower than 10% thus the estimation of ET and the deviations from the reference for S2d give an idea of how an estimation of ET would be for the other periods. Fig. 4.17 presents the daily ET values for the five frequencies used for the SR data analysis in S1 and S2d, along with that deduced from the EC measurements, for both calibration and validation periods. For f=1 Hz in S2d the calibration was done with a single regression (i.e. for both stable and unstable conditions) in order to obtain a significant regression and include it in the results.

Fig. 4.17 shows that for each day, ET results are nearly the same for all frequencies. A quantitative assessment of the SR system performance at the different frequencies is presented in Table 4.4 where the mean daily ratio between SR and EC evapotranspiration values are presented, along with the corresponding estimation of RMSE (mm day^{-1}) on a daily basis (and considering the relatively small sample size for such a statistical estimate). Table 4.4 indicates that even at a frequency as low as 1 Hz the deviation is 8% at most implying on potential use of this technique using simple and low cost instrumentation with no need for high sampling rates and data storage.

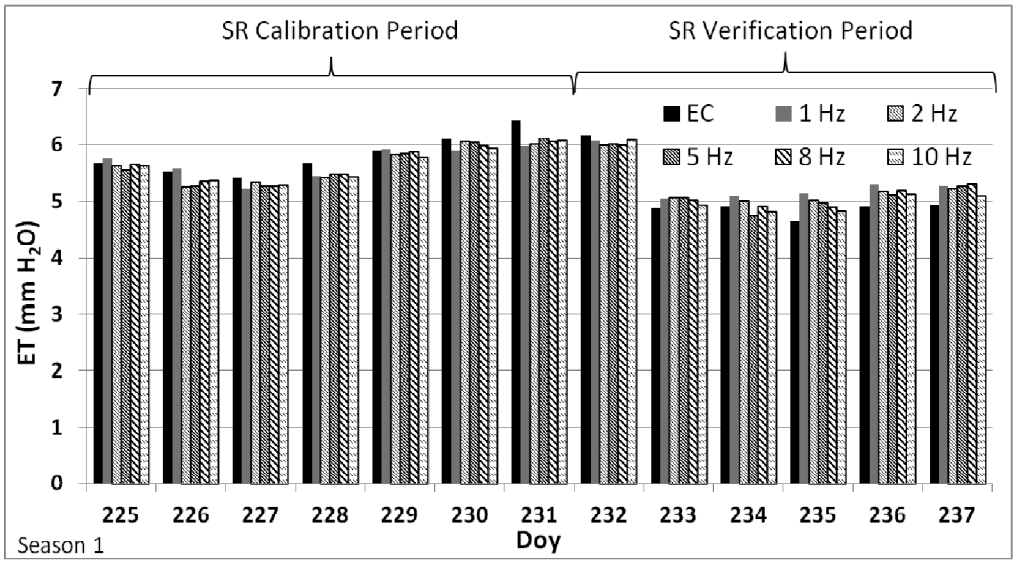

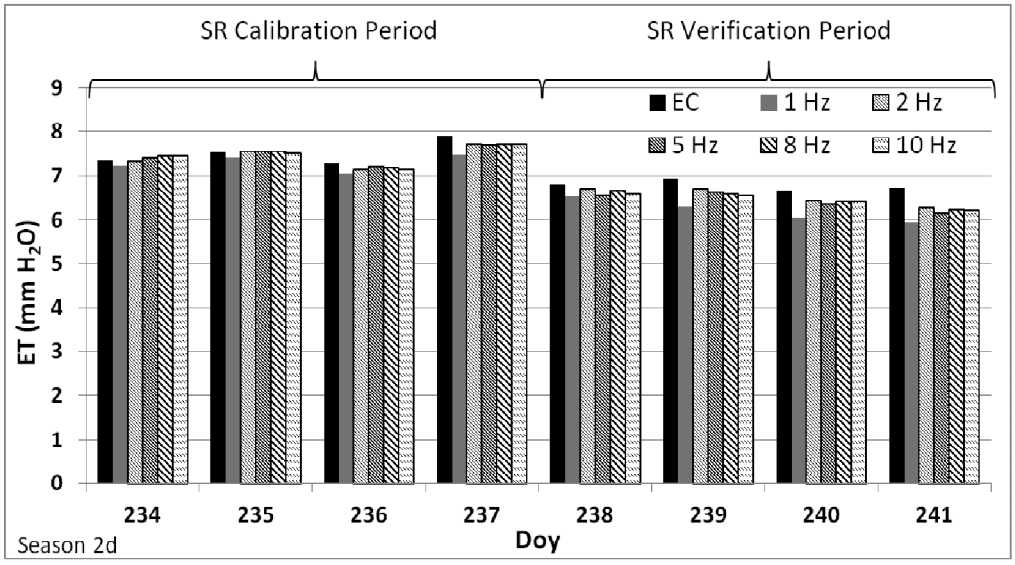

Figure 4.17 (up and center) *– Daily ET estimations for the studied agricultural stands in S1 and S2d. The estimations presented here correspond to the optimal calibrations and their validation period showed in Table 4.1.*

Table 4.4 (down) *– Statistics of the ET estimations performed. The ± figures correspond to the standard deviation of the mean daily ratios. In S1 calibration and validation were performed for 7 and 6 day respectively while in S2d they were both performed for 4 days (Table 4.3).*

Season	Period	Frequency	1 Hz	2 Hz	5 Hz	8 Hz	10 Hz
S1	Calibration	Mean daily ratio ET_{SR}/ET_{EC}	0.98 ± 0.03	0.97 ± 0.02	0.97 ± 0.02	0.97 ± 0.02	0.97 ± 0.02
		RMSE (mm H_2O day^{-1})	0.22	0.22	0.19	0.19	0.20
	Validation	Mean daily ratio ET_{SR}/ET_{EC}	1.05 ± 0.04	1.04 ± 0.04	1.03 ± 0.04	1.03 ± 0.04	1.02 ± 0.03
		RMSE (mm H_2O day^{-1})	0.31	0.25	0.24	0.23	0.14
S2d	Calibration	Mean daily ratio ET_{SR}/ET_{EC}	0.97 ± 0.02	0.99 ± 0.01	0.99 ± 0.02	0.99 ± 0.02	0.99 ± 0.02
		RMSE (mm H_2O day^{-1})	0.26	0.12	0.12	0.12	0.13
	Validation	Mean daily ratio ET_{SR}/ET_{EC}	0.92 ± 0.03	0.96 ± 0.02	0.95 ± 0.02	0.96 ± 0.02	0.95 ± 0.02
		RMSE (mm H_2O day^{-1})	0.60	0.28	0.37	0.33	0.35

4.6. SR analysis using sonic temperature measurements

The temperature measurements by the sonic anemometer have two main advantages over the TCs; (i) they are not affected by direct solar radiation and (ii) they are characterized by extremely small response time. Therefore, using the temperature signal obtained with the sonic anemometer for calculating the ramps characteristics and applying the SR method may be an approach for assessing the method's performance under almost ideal conditions. This test was carried out for S1 and S2d, when the sonic anemometer was at a height of 1.51 and 3.35 m respectively and plant height was 0.6 and 1.5 m respectively. Both calibration and validation of H were performed for the same days of those periods of the previous results using the TCs output. The complete results of calibration and validation for sonic temperature are presented in Table 4.5.

Season		Calibration		Validation
S1	From DOY	225		232
	To DOY	231		237
	z (m)	1.51		1.51
	h (m)	0.6		0.6
		Stable	Unstable	All data
	R^2	0.77	0.63	0.9
	RMSE (W m^{-2})	38.7	18.94	18.88
	α | slope	0.45	1.19	0.95
	f (Hz)	10		10
	r | r_{st} ; r_{uns} (s)	0.25	1.25	0.25 ; 1.25
S2d	From DOY	234		238
	To DOY	237		241
	z (m)	3.35		3.35
	h (m)	1.5		1.5
		Stable	Unstable	All data
	R^2	0.5	0.71	0.77
	RMSE (W m^{-2})	49.98	7.51	23.82
	α | slope	0.62	1.1	1.09
	f (Hz)	8		8
	r | r_{st} ; r_{uns} (s)	0.25	0.5	0.25 ; 0.50

Table 4.5 *– Optimal calibrations and correspondent validations obtained applying the SR method to the temperature signal measured with the sonic anemometer. All the regressions were statistically significant at a 0.01% level.*

5. Discussion

5.1. Measurement height

Both for S1 and S2 seasons the optimal measurement height resulted to be above the canopy top (zn=2 for S1 and zn=1.6 for S2). In S1 all measurement heights allowed an acceptable calibration of the SR method with different coefficient of determination (R^2) and root mean square error (RMSE). Although the results for S1 were in accordance with the assumption that the SR technique can be applied at any height close to the canopy top (Castellvi and Snyder, 2009b; Castellvi, 2012), that was not the case of S2. Once the plants were at maximum height (h=1.5 m) in S2, zn=1.6 was the optimal height and the only measurement height where it was possible to apply the SR technique without the limitation of the *time lag in stability change* (see section 4.3.1). At this height acceptable calibrations (p-value<0.001) were obtained for both stable and unstable conditions.

The relation between R^2 and zn (Fig. 4.10) in S1 suggests that there is a range (between zn=1 and 2) where R^2 is maximal hence measurements are better performed. The difference between stable and unstable conditions (i.e. R^2 being maximal at zn=1 and at zn=2 for stable and unstable conditions, respectively) suggests that measurements could be done at two heights simultaneously, one higher for sampling larger eddies (unstable) and one lower for smaller eddies (stable). This requires further research focused on a new calculation algorithm capable of merging results obtained at two levels into a single estimation of H_{SR}.

In S2d, R^2 was generally low and did not have clear patterns in relation with zn as in S1. The inconsistency of the observed patterns of R^2 and α in S2d (Figs. 4.10 and 4.11) suggests some limitation in the SR technique application for the tested measurement heights below zn=1.6 in the S2 experimental conditions. This limitation was associated with the observed *time lag in stability change* and deserves further study which should add temperature measurement at higher levels and an additional measurement of the turbulence characteristics at a lower level.

In S1 a general trend of asymptotically decreasing α with increasing measurement height (Fig. 4.11) was observed, in accordance to previously reported results (Spano et

al., 1997; Spano et al., 2000; Castellvi, 2004; Castellvi et al., 2012). Consistent trends of R^2 and α were also observed when testing their relation with zn in S2a (Fig. 4.13).

5.2. Measurement frequency

Measurement sampling rate affects the capacity of the sensor in identifying eddies of different size and frequency. As the sampling time interval is longer (i.e. lower frequency) higher frequency eddies may not be sampled by the sensor. It is considered that f=10 Hz is an acceptable frequency for the SR technique (Castellvi and Snyder, 2009b); implying that lower than f=10 Hz frequencies would not allow to correctly sample the temperature signal. However, following Paw U et al. (1995) suggestion about intermediate eddies being responsible for most of the energy exchange, and the assumption made regarding the simplified total derivative in Eq. 2.6 (Spano et al., 2000; Paw U and Brunet, 1991), it appears that measuring at f<10 Hz should be sufficient to correctly sample the larger coherent structures. The results obtained in this study showed that lower frequencies yielded lower and sometimes not acceptable R^2, and higher RMSE (Table 4.1). The optimal calibrations were obtained in all cases for the higher frequencies (Table 4.3). For a frequency f=8 Hz, the results were very close to those obtained at f=10 Hz and sometimes even better. This reinforces the assumption of the energy exchange performed mainly by intermediate eddies. When measurement sampling frequency was lower than f=8 Hz (f=5, 2 and 1 Hz) the decrease in R^2 was steeper (Fig. 4.11). These low values of R^2 showed to generate unacceptable calibrations in some cases, for example S2d under unstable conditions.

For some frequencies the calibration performance was reduced and deviation between H_{EC} and H_{SR} was around 20% in the validation period (Table 4.3). This did not impede the calculation of ET rates for all frequencies in S1 and S2d (Fig. 4.17). The results showed that the deviation between the reference ET and that calculated with the SR method were all within a small range of variability, being overestimated and underestimated in the validation periods of S1 and S2d, respectively. However, except for f=1 Hz estimation in S2d, these deviations never exceeded 5% (Table 4.4). This can be explained by the small absolute value of H in relation to LE under most conditions of this study, which resulted in a mean of $|H_{EC}/LE_{ECf}|$=0.26 and 0.06 between 8 and 18 h

during the validation periods of S1 and S2d, respectively. Under such conditions the effect of deviations in H on LE estimation as a residual of the EB equation is small.

5.3. Sensor diameter

When examining the influence of the sensor (TC) diameter (S2c), the thin TC clearly showed best performance (Fig. 4.15). The fact that small differences in TC diameters (~0.05 mm) caused large differences in the results suggests that this topic deserves to be treated in a deeper way. In the literature (Snyder et al., 1997; Simmons et al., 2007; Castellvi et al., 2012) wire diameter used for the TC, rather than the actual TC junction diameter is usually mentioned. These two dimensions are usually different, and the latter is the one which is relevant for the frequency response of the sensor (analysis not presented in this study). Our experience showed that a wider wire can result in a smaller sensing junction, due to the welding process of the junctions, in this study done manually in our lab.

A thicker TC junction is more influenced by direct solar radiation which varies during the day. Also, different shapes of the junction (ellipsoidal or spherical, incidentally obtained in the junction welding process) may cause the radiation influence to vary during the day. Radiation effects introduce noise to the sampled temperature signal by adding a heat source apart from the air temperature. The Thick TC showed a much worse performance for unstable conditions than for stable conditions. Unstable conditions are more associated with sunshine hours than stable conditions, suggesting that radiation, among other factors, could have influenced the results of the thick sensor.

5.4. α coefficient

5.4.1. Measurement height

The variation of α with measurement height is given by Eq. 2.6 and by the interpretation of α as a weighting factor accounting for the uneven cooling or heating of the eddy (Spano et al., 2000), which is expressed through the relative measurement position within an eddy. Two aspects of α are related with this approach: *(i)* α decreases with increasing measurement height and *(ii)* stability conditions are associated with different eddies size therefore α for each condition should be consistently different (Paw U et al., 1995; Castellvi, 2004). The results regarding the first aspect *(i)* were consistent with the

expected behavior of α (Figs. 4.11 and 4.13). Nevertheless, for the second aspect *(ii)* the obtained results were not coincident with the trends reported in the literature. In the present study, when using TCs as temperature sampling sensors, $\alpha_{st}>\alpha_{uns}$ (Table 4.3) was obtained for all cases; which is opposite to previous results (Paw U et al., 1995; Castellvi, 2004; Castellvi et al., 2008). However the SR application using sonic temperature measurements (Table 4.5) yielded $\alpha_{st}\sim0.5\alpha_{uns}$ in agreement with previous studies. Noting that (1) the same algorithm was used for the data processing of both the TC and sonic temperature signals and (2) that during S1 a TC showing $\alpha_{st}>\alpha_{uns}$, was placed at the same height as the sonic anemometer, we suggest that the difference in α behavior is associated with sampling limitations of the TCs. In this sense, because of their longer response time, not thin enough TCs would not be able to sample fast eddies thus bigger correction (calibration factor α) of the measurements may be needed in those cases.

Regarding the values of α (Table 4.3), they were generally in the upper range of the reported values in the literature. This was especially clear for S1 and S2a (Tables 4.1 and 4.2) suggesting that large α values are associated with short canopies and more cases with larger values of positive H during the day.

5.4.2. Measurement frequency

The increase in the value of α with decreasing frequency showed to have a consistent pattern (Fig. 4.12). This means that an additional role could be attributed to α: compensation for lower frequency measurements. In Fig. 4.12, the relations between the α_M/α_H and f_H/f_M are close to the 1:1 line suggesting that each frequency bandwidth of the spectrum of the eddies, equally contributes to the heat flux. This finding deserves further research by analyzing these relations for a wider database and different crops and climatic conditions.

5.4.3. α stationarity

One of the main discussions in the literature is the α value stationarity, i.e. what is the minimum calibration duration needed for obtaining a relatively constant α. This question is related to the application of the SR technique in different seasons or climatic conditions and the general desire for as short as possible calibration period. α is

supposed to be related to the mechanics of the ejections and sweeps process, and thus to the configuration of the canopy and the crop microclimate, the latter being influenced by measuring season or regional climatic conditions (Snyder et al., 2008; Mengitsu and Savage, 2010). In addition, reaching a stationary α coefficient allows the extrapolation of calibration results obtained in a given stand to different climatic conditions; which would be one of the main assumptions when pursuing a practical application of the technique. Results of the present study (Fig. 4.14) showed that under unstable conditions and high sampling frequencies, α appeared to be stationary after a single day of calibration whereas under stable conditions it required at least five days of calibration. There is a lack of agreement in the literature regarding this topic (Snyder et al., 2008; Mengitsu and Savage, 2010; Castellvi et al., 2012). Hence the results obtained in this study may contribute as an additional input to the data pool dealing with this question.

5.5. Time lag in stability change (S2)

Regarding the inter-daily variability of the *time lag in stability change,* it is observed that its length is not constant among days. Fig. 5.1 shows the lag between EC and TC at z=1.5 m for three different days, when EC system and plants were at constant height. It is observed that the lag length (the duration between the change in sign of H_{EC} and H_{SR} during daytime) is 6, 2.5 and 1 h for DOYs 237, 240 and 249 respectively. During S1 and S2a the *lag in stability change* was not observed and H measured with EC and SR showed a very coincident daily curve regarding stability, which supports the application of the SR technique.

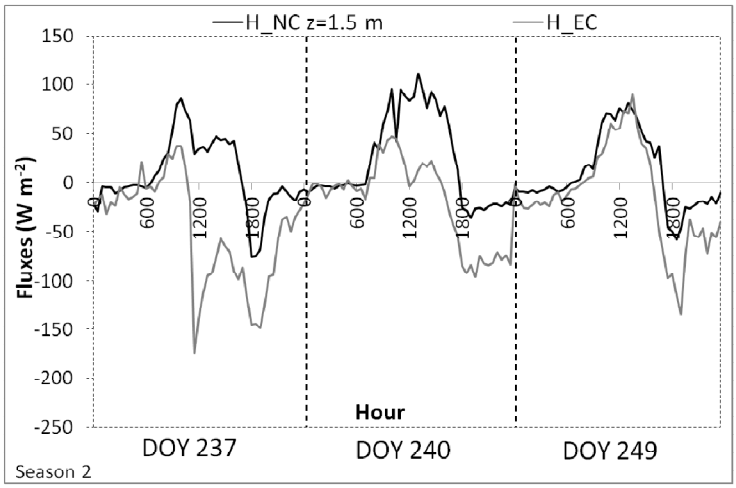

Figure 5.1 *– Three days of S2 showing the inter-daily variability of lag in stability change between H_{EC} and H_{NC} measured with TC at z=1.5 m. Lag length was 6, 2.5 and 1 h for DOYs 237, 240 and 249 respectively. EC system and plant height were 3.35 and 1.5 m respectively.*

The following presents an attempt to explain the origin of this undesired phenomenon. The time of the day at which the described time lag occurs (Fig. 4.7) suggests that it may be associated with strong winds while the fact that H_{EC} is negative associates its occurrence with high ET rates. An histogram showing the occurrence frequency of horizontal wind speed (u_h) values and the corresponding number of half hour points that showed opposite stability (sign of flux) between H_{EC} and H_{NC} ($H_{EC}/H_{NC}<0$) for two different TCs is shown in Fig. 5.2. The histogram was performed between DOYs 234 and 241, when the TC placed at z=2.4 m was operating. This analysis shows that for $u_h<3$ m s^{-1} the amount of half hour averages with opposite stability was almost the same for both TCs; however for $u_h\geq3$ m s^{-1} the number of points with $H_{EC}/H_{NC}<0$ splits sharply, being much larger for the TC at z=1.5 m. This analysis suggests that the *time lag in stability change* is associated with high wind speeds.

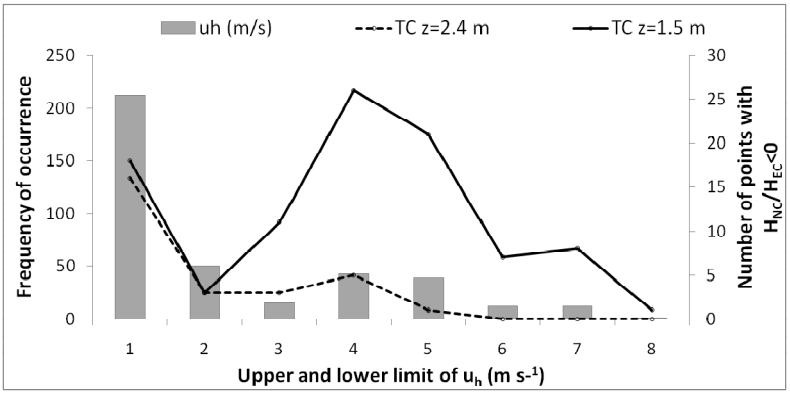

Fig. 5.2 *– Histogram showing the relation between wind speed and number of points with $H_{NC}/H_{EC}<0$ for two different TCs (right y-axis). The bars represent the frequency of occurrence (left y-axis) of half hour averages wind speed between the limits shown in the x-axis. The number below each bar represents the upper limit of each bin. EC system and plant height were 3.35 and 1.5 m respectively.*

Fig. 5.1 also suggests that this phenomenon is associated with high ET rates. To examine this we defined Net LE (MJ m^{-2}) as the sum of half hour averages of LE between 11:00 and 19:00 h. A significant correlation (p-value<0.001) was found between this magnitude and the length of the *time lag in stability change* for H_{NC} estimated with the TC at z=1.5 m, as shown in Fig. 5.3. Obviously, stronger winds induce higher ET rates and these two effects are not independent.

High mean wind shear may not allow clear ramp formation at the canopy top (Snyder et al., 1996). Spano et al. (1997) reported improvement in calibration associated with lower wind shear thus better defined ramps. For stronger winds acting over a stiff, well developed canopy (as cotton), this shear may have influenced negatively the ramp formation in S2 conditions. Mean daily wind shear between 11 and 19 h calculated at

the canopy top by $\frac{du_h}{dz} = \frac{u_*}{k}\frac{z_m}{z-d}$, where z_m (m) is the roughness length, in S1 and S2 (between DOYs 237 and 249) was 0.25 and 0.33 s^{-1} respectively. Slightly higher wind shear was obtained during S2 than S1, which may explain why ramp deterioration was only observed during S2. On the other hand, these values of wind shear are well below the threshold (~2 s^{-1}) suggested by Spano et al. (1997) to affect ramp formation. Moreover, a regression between mean wind shear (s^{-1}) at the canopy top and the length of the *time lag in stability change* for H_{NC} estimated with the TC at z=1.5 m (for the same conditions of Fig. 5.3), yielded a non-significant relation (p-value>0.05). Hence, the role of wind shear in inducing this phenomenon in the present study is not clear and requires further study (see below). This suggests that wind speed and its associated Net LE may be identified as principal reasons for this phenomenon, although, at the moment, we cannot identify a specific mechanism relating high ET rates and long time lags of stability change. Overall the hours of the day when the inconsistency between H_{EC} and H_{NC} appeared were not used in any data analysis in this study.

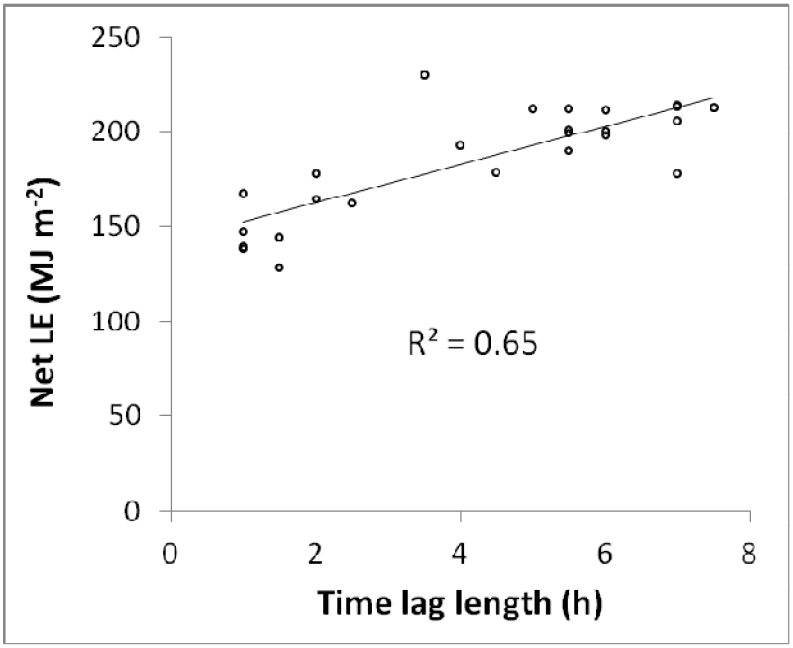

Figure 5.3 *– Relation between length of the time lag in stability change and Net LE, defined as the sum of half hourly averages of LE between 11:00 and 19:00 h. This relation was obtained between DOYs 225 and 249, with data of the TC at z=1.5 m, when the EC system and plant height were 3.35 and 1.5 m respectively.*

The problem of *time lag in stability change* requires further study. We plan an additional field campaign under similar conditions, namely, same region, same crop and same season. Our plan is to install another 3D-sonic anemometer near the canopy top, where this problem appeared in the present study. This will assist in better analysis of the flow structure and relation between turbulence characteristics at lower and higher levels above the canopy. However, this task is outside the scope of the present thesis.

6. Conclusions

Performance of the Surface Renewal technique was examined for two different crops in two different field campaigns in northern Israel. The study investigated the effect of temperature measurement height, sampling rate and sensor diameter on the SR performance. During calibration, the sensible heat flux estimated by the SR technique was regressed against reference data deduced from eddy covariance measurements. Evapotranspiration was extracted from the energy balance relation. The following major conclusions can be drawn from this field study:

- The SR technique is reliable in estimating whole canopy ET in processing tomato and cotton crops.
- Best calibration results were obtained for temperature measurements at 10 Hz sampling rate at zn=2, and at 8 Hz at zn=1.6 for processing tomato and cotton respectively.
- For the validation period, and for analysis frequencies equal to or larger than 2 Hz, daily ET values were almost insensitive to the measurement sampling rate.
- Best results were obtained for the TC with smallest diameter, as expected. Small influences in the TC diameter (~0.05 mm) had a large influence in the results.
- The possibility to reliably estimate ET using temperature signals acquired at low sampling rates is promising for the future development of a low-cost SR system which will be attainable for growers for day-to-day irrigation decisions.
- Further understanding of α coefficient is required in order to assess different experiment applications of the method in a better way.
- The particular result of the *time lag in stability change* could not be thoroughly explained by the data obtained in this research and may represent a limitation in the application of the SR which should be further researched.

Results are presented for two given crops at a specific climatic region. Extending this approach to different crops at other regions and over a wider range of crop development stages would be the next step of this research.

7. Bibliography

Allen, R.G, Pereira, L.S., Howell, T.A., Jensen, M.E., 2011a. Evapotranspiration information reporting: I. Factors governing measurement accuracy. *Agricultural water management*. 98, 899-920.

Anandakumar, K., 1999. Sensible heat flux over a wheat canopy: optical scintillometer measurements and surface renewal analysis estimations. *Agricultural and forest meteorology.* 96, 145-156.

Assouline,S., Mahrer,Y., 1993. Evaporation from lake kinneret: 1. Eddy correlation system measurements and energy budget estimates. *Water Resources Research*. 29(4), 901-910

Assouline, S., Tyler, S.W., Tanny, J., Cohen, S., Bou-Zeid, E., Parlange, M.B., Katul, G.G., 2008. Evaporation from three water bodies of different sizes and climates: Measurements and scaling analysis. *Advances in water resources.* 31, 160-172.

Baldocchi, D.D., 2003. Assessing the eddy covariance technique for evaluating carbon dioxide exchange rates of ecosystems: past, present and future. *Global change biology*. 9, 479-492.

Burba, G., Anderson, D., 2005. Introduction to the eddy covariance method: general guidelines and conventional workflow. *LI-COR Biosciences.* http://www.licor.com/.

Campbell Scientific Inc., 1998. Eddy covariance system—operator's manual, CA27 and KH20, Logan, Utah, USA.

Castellvi, F., 2004. Combining surface renewal analysis and similarity theory: a new approach for estimating sensible heat flux. *Water resources research*. 40, W05201.

Castellvi, F., Snyder, R.L., Baldocchi, D.D., 2008. Surface energy balance closure over rangeland grass using the eddy covariance and surface renewal analysis. *Agricultural and forest meteorology.* 148, 1147-1160.

Castellvi, F., Snyder, R.L., 2009a. On the performance of surface renewal analysis to estimate sensible heat flux over two growing rice fields under the influence of regional advection. *Journal of hydrology.* 375, 546-553.

Castellvi, F., Snyder, R.L., 2009b. Sensible heat flux estimates using surface renewal analysis. A study case over a peach orchard. *Agricultural and forest meteorology*. 149, 1397-1402.

Castellvi, F., Snyder, R.L., 2010. A new procedure based on surface renewal analysis to estimate sensible heat flux: a case study over grapevines. *Journal of hydrometeorology.* 11, 496-508.

Castellvi, F., 2012. Fetch requirements using surface renewal analysis for estimating scalar surface fluxes from measurements in the inertial sublayer. *Agricultural and forest meteorology*. 152, 233-239.

Castellvi, F., Consoli, S., Papa, R., 2012. Sensible heat flux estimates using two different methods based on surface renewal analysis. A study case over an orange orchard in Sicily. *Agricultural and forest meteorology.* 152, 58-64.

De Vries, D.A., 1963. Thermal properties of soils. *Physics of Plant Environment*. *North-Holland publishing company*. 210-235.

Finningan, J.J., 2000. Turbulence in plant canopies. *Annual review of fluid mechanics*. 32, 519-571.

Foken, T (2008). Micrometeorology. *Springer-Verlag Berlin Heidelberg*. p106.

Harman, I.N., Finningan, J.J., 2008. Scalara concentration profiles in the canopy and roughness sublayer. *Boundary later meteorology*. 129, 323-351.

Hendricks Franssen, H.J., Stocki, R., Lehner, I., Rotenberg, E., Seneviratne, S.I., 2010. Energy balance closure of eddy-covariance data: A multisite analysis for European FLUXNET stations. *Agricultural and forest meteorology*. 150, 1553-1567.

Horst, T.W., Weil, J.C., 1992. Footprint estimation for scalar flux measurements in the atmospheric surface layer. *Boundary layer meteorology.* 59, 279-296.

Horst, T.W., Weil, J.C., 1994. How far is far enough?: the fetch requirements for micrometeorological measurement of surface fluxes. *Journal of atmospheric and oceanic technology*. 11, 1018-1025.

Hsieh C.I., Katul G.G., Schieldge J., Sigmon J.T. and Knoerr, K., 1997. The lagrangian stochastic model for fetch and latent heat flux estimation above uniform and non uniform terrain. *Water Resources Research.* 33, 427-438.

Hsieh C.I., Katul G.G., Chi T.W., 2000. An approximate analytical model for footprint estimation of scalar fluxes in thermally stratified atmospheric flows. *Advances in Water Resources*. 23, 765-772.

Katul, G., Hsieh, C.I., Oren, R., Ellsworth, D., Phillips, N., 1996. Latent and sensible heat flux predictions from a uniform pine forest using surface renewal and flux variance methods. *Boundary layer meteorology*. 80, 249-282.

Kowalski, A.S., Anthoni, P.M., Vong, R.J., Delany, A.C., Maclean, G.D., 1996. Deployment and evaluation of a system for ground-based measurements of cloud liquid water turbulent fluxes. *Journal of atmospheric and oceanic technology.* 14, 468-479.

Mengitsu, M.G., Savage, M.J., 2010. Surface renewal method for estimating sensible heat flux. *Water SA*. 36 (1), 9-18.

Möller,M., Tanny, J., Li, J., Cohen, S., 2004. Measuring and predicting evapotranspiration in an insect-proof screenhouse. *Agricultural and forest meteorology.* 127, 35-51.

Moore, C.J., 1986. Frequency response corrections for eddy correlation systems. *Boundary later meteorology.* 37, 17-35.

Miyake, M., McBean, G., 1970. On the measurement of vertical humidity transport over land. *Boundary layer meteorology*. 1, 88–101.

Paw U, K.T, Brunet, Y., 1991. A surface renewal measure of Sensible heat flux density. *Proceedings of the 20th conference of agriculture and forest meteorology, Salt Lake City*. 52-53.

Paw U, K.T., Qiu, J., Su, H.B., Watanabe, T., Brunet, Y., 1995. Surface renewal analysis: a new method to obtain scalar fluxes. *Agricultural and forest meteorology.* 74, 119-137.

Paw U, K.T., Snyder, R.L., Spano, D., Su, H.B., 2009. Surface renewal estimates of scalar Exchange. *CA water plan update.* 4, 1-65.

Raupach, M.R., Thom, A.S., 1981. Turbulence in and above plant canopies. *Annual review of fluid mechanics.* 13, 97-129.

Raupach, M.R., Finningan, J.J., Brunet, Y., 1996. Coherent eddies and turbulence in vegetation canopies: the mixing layer analogy. *Boundary layer meteorology*. 78, 351-382.

Schmid H.P., 1997. Experimental design for flux measurements: matching scales of observations and fluxes. *Agricultural and Forest Meteorology*. 87, 179-200.

Simmons, L.J., Wang, J., Sammis, T.W., Miller, D.R., 2007. An evaluation of two inexpensive energy balance techniques for measuring water use in flood-irrigated pecans (Carya illinoinensis). *Agricultural water management*. 88, 181-191.

Singer, A., 2007. The soils of Israel. *Springer – Verlag Berlin Heidelberg.* 143-73.

Snyder, R.L., Spano, D., Paw U, K.T., 1996. Surface renewal analysis for sensible and latent heat flux density. *Boundary layer meteorology*. 77, 249-266.

Snyder, R.L., O'Connell, N.V., 2007. Crop coefficients for microsprinkler-irrigated, clean-cultivated, mature citrus in an arid climate. *Journal of irrigation and drainage engineering.* 133, 43-52.

Snyder, R.L., Spano, D., Duce, P., Paw U, K.T., Rivera, M., 2008. Surface renewal estimation of pasture evapotranspiration. *Journal of irrigation and drainage engineering*. 134, 716-721.

Spano, D., Snyder, R.L., Duce, P., Paw U, K.T., 1997. Surface renewal analysis for sensible heat flux using density structure functions. *Agricultural and forest meteorology.* 86, 259-271.

Spano, D., Snyder, R.L., Duce, P., Paw U, K.T., 2000. Estimating sensible and latent heat flux densities from grapevine canopies using surface renewal. *Agricultural and forest meteorology.* 104, 171-183.

Stanhill G., 1969. A simple instrument for the field measurement of turbulent diffusion flux. *Journal of Applied Meteorology*. 8, 509-513.

Stanhill, G., Rosa, R., 2011. On the inter-annual variation of rainfall in Israel since 1931: no change, much deviation, but with a useful signal. *Israel journal of earth science*. 58, 113-120.

Tanny, J., Haijun, L., Cohen, S., 2006. Airflow characteristics, energy balance and eddy covariance measurements in a banana screenhouse. *Agricultural and forest meteorology*. 139, 105-118.

Tanny, J., Cohen, S., Assouline, S., Lange, F., Grava, A., Berger, D., Teltch, B., Parlange, M.B., 2008. Evaporation from a small water reservoir: direct measurements and estimates. *Journal of hydrology*. 351, 218-229.

Tanny, J., Dicken, U., Cohen, S., 2010. Vertical variation in turbulence statistics and energy balance in a banana screenhouse. *Biosystems Engineering*. 106(2), 175-187.

Tanny, J., Cohen, S., Berger, D., Teltch, B., Mekhamandarov, Y., Bahar, M., Katul, G.G., Assouline, S., 2011. Evaporation from a reservoir with fluctuating water level: Correcting for limited fetch. *Journal of hidrology*. 404, 146-156.

Twine, T.E., Kustas, W.P., Norman, J.M., Cook, D.R., Houser, P.R., Meyers, T.P., Prueger, J.H., Starks, P.J., Wesely, M.L., 2000. Correcting eddy covariance flux underestimates over a grassland. *Agricultural and forest meteorology.* 103, 279-300.

Van Atta, C.W., 1977. Effect of coherent structures on structure functions of temperature in the atmospheric boundary layer. *Archives in Mechanics*. 29, 161–171.

Webb, E.K., Pearman, G.I., Leuning, R., 1980. Correction of flux measurements for density effects due to heat and water vapor transfer. *Quart.J.R.Met.Soc.* 106, 85-100.

Wilson, K.B., Hanson, P.J., Mulholland, P.J., Baldocchi, D.D., Wullschleger, S.D., 2001. A comparison of methods for determining forest evapotranspiration and its components: sap-flow, soil water budget, eddy covariance and catchment water balance. *Agricultural and forest meteorology.* 106, 153-168.

Wilson, K., Goldstein, A., Falge, E., Aubinet, M., Baldocchi, D., Berbigier, P., Bernhofer, C., Ceulemans, R., Dolman, H., Field, C., Grelle, A., Ibrom, A., Law, B.E., Kowalski, A., Meyers, T., Moncrieff, J., Monson, R., Oechel, W., Tenhunen, J., Valentini, R., Verma, S., 2002. Energy balance closure at FLUXNET sites. *Agricultural and forest meteorology*. 113, 223-243.

Zapata, N., Martinez-Cob, A., 2002. Evaluation of the surface renewal method to estimate wheat evapotranspiration. *Agricultural water management*. 55, 141-157.

Zion, N., 2006. The colonizatory project in the northern Hula valley 1934 – 1947. *Phd thesis, Hebrew University of Jerusalem.*

APPENDIX I – Structure Functions

The main idea of the mathematical analysis proposed by Van Atta (1977) is to decompose a temperature field into organized and turbulent contributions. For achieving this, he made the assumption of local isotropy of the turbulent part of a scalar θ (i.e. the *nth* moment of Δθ for odd values of *n* is null). Based on this assumption he modeled the organized part of the scalar field into a deterministic ramp model.

For this deterministic ramp model, an equation relates its characteristics (*a* and τ) with the variation of the coherent part of the scalar signal. This equation is possible to combine with the numerical calculation of the *nth* moment of Δθ (which requires the input of a time lag r (s)), obtaining a relation between the moment and the terms *a* and τ. By introducing a much-shorter-than τ time lag (i.e. r<< τ), Van Atta managed to simplify the relations between the 2nd through 8th moments of Δθ and *a* and τ; calling the simplified moments Structure functions (S^n) (being *n* the order of the moment) and thus he obtained a relation between S^n and the terms *a* and τ. In the calculations presented in section 3.6.3.1 the equations (3.2) through (3.6) show how Van Atta managed to provide a good estimation of *a* and τ by using the simplification for the 2nd, 3rd and 5th moments. Note that in the equations the moments are shown as S^n although they are calculated as the real moments, the fact that r<<τ allows assuming Van Atta's simplification thus relating them with the ramps characteristics (Mekhmandarov, personal communication).

APPENDIX II – Table of applications

Surface	Canopy height (m)	Measurement height (m)	Measurement frequency (Hz)	Sensor size (µm)	α	Intercept (W m^{-2})	R^2	Error (W m^{-2})	Reference measurement	Stability	Method	Reference
Maize	2.6	2.6	10	12.5	2.5	-28	0.46	19	EC	Unstable	SR1	Paw U et al. (1995)
	2.6	2.6	10	12.5	0.99	7	0.87	11	EC	Stable	SR1	
Walnut	6	6.0	10	12.5	1.42	5.5	0.68	45	EC	Unstable	SR1	
	6	6.0	10	12.5	0.66	-0.1	0.66	16	EC	Stable	SR1	
Mixed deciduous	18	18.0	10	12.5	1.06	4.3	0.81	34	EC	Unstable	SR1	
forest	18	18.0	10	12.5	0.64	15.8	0.55	19	EC	Stable	SR1	
Pines forest	13	13.0	10	sonic	0.96	-0.00209 *	0.86	0.028 *	EC	All data	SR1	Katul et al. (1996)
	13	14.0	10	hygrometer	1.1 **	-0.011 +	0.77	0.016 +	EC	All data	SR1	
Grass (alta fescue)	0.1	0.6	8	76.2	1	-	-	15-20	EC	All data	SR1	Snyder et al. (1997)
Grass (alta fescue)	0.1	0.3	8	76.2	1.88	0	0.4	33	EC	All data	SR1	Spano et al. (1997)
	0.1	0.6	8	76.2	1.1	0	0.93	11	EC	All data	SR1	
Wheat	0.7	0.7	8	76.2	1.28	0	0.9	57	EC	All data	SR1	
	0.7	1.0	8	76.2	1.07	0	0.93	38	EC	All data	SR1	
Sorghum	0.7	0.7	8	76.2	0.87	0	0.9	33	EC	All data	SR1	
	0.7	1.0	8	76.2	0.66	0	0.93	83	EC	All data	SR1	
Wheat	0.9	1.4	16	25	1	-	-	-	Scintillometer	All data	SR1	Anandakumar (1999)
Grape	2	2.0	8	76.2	0.88	0	0.8	44	EC	All data	SR1	Spano et al. (2000)
(Cabernet	2	2.3	8	76.2	0.81	0	0.74	62	EC	All data	SR1	
Sauvignon)	2	2.9	8	76.2	0.66	0	0.81	111	EC	All data	SR1	
Grape	2.1	1.5	8	76.2	1.31	0	0.84	58	EC	All data	SR1	
	2.1	2.1	8	76.2	0.89	0	0.93	34	EC	All data	SR1	
(Pinot bianco)	2.1	2.7	8	76.2	0.77	0	0.91	60	EC	All data	SR1	
Wheat	0.8	1.5	4	76.2	1	-	-	29.6 **	Lysimetry	All data	SR1	Zapata and Martinez-Cob (2002)
Grass (alta fescue)	0.1	0.6	8	76.2	0.67	0	-	-	EC	Unstable	SR1	Castellvi (2004)
	0.1	1.5	8	76.2	0.53	0	-	-	EC	Unstable	SR1	
	0.1	1.5	8	76.2	0.21	0	-	-	EC	Stable	SR1	
	0.1	0.6	8	76.2	0.77	-	-	-	EC	Unstable	SR2	
	0.1	1.5	8	76.2	0.59	-	-	-	EC	Unstable	SR2	
	0.1	1.5	8	76.2	0.23	-	-	-	EC	Stable	SR2	
Wheat	0.7	0.7	8	76.2	0.95	0	-	-	EC	Unstable	SR1	
	0.7	1.0	8	76.2	0.74	0	-	-	EC	Unstable	SR1	
	0.7	1.3	8	76.2	0.65	0	-	-	EC	Unstable	SR1	
	0.7	0.7	8	76.2	0.95	-	-	-	EC	Unstable	SR2	
	0.7	1.0	8	76.2	0.72	-	-	-	EC	Unstable	SR2	
	0.7	1.3	8	76.2	0.62	-	-	-	EC	Unstable	SR2	
Pecan	12.8	12.8	4	75	1.07	0	0.62	-	EC	All data	SR1	Simmons et al. (2007)
	12.8	9.1	4	75	0.44	0	0.5	-	EC	All data	SR1	
Orange	4.5	4.5	4	76.2	0.23	0	0.97	-	EC	All data	SR1	Snyder and O'Connell (2007)
Rangeland grass	0.25	2.0	10	sonic	1	12	0.85	41	EC	Unstable	SR2	Castellvi et al. (2008)
	0.25	2.0	10	IRGA	1.07 **	11	0.87	34	EC	Unstable	SR2	
	0.25	2.0	10	IRGA	1.09 ***	-0.4 ****	0.93	3.3 ****	EC	Unstable	SR2	
	0.25	2.0	10	sonic	0.45	-6	0.3	11	EC	Stable	SR2	
	0.25	2.0	10	IRGA	0.57 **	0	0.4	3	EC	Stable	SR2	
	0.25	2.0	10	IRGA	0.81 ***	0.5 ****	0.7	1 ****	EC	Stable	SR2	
Pasture	0.15	0.6	4	76.2	1.12	0	-	-	EC	All data	SR1	Snyder et al. (2008)
Peach	3.95	5.5	10	sonic	-	-	0.92	22	EC	Unstable	SR2	Castellvi and Snyder (2009a)
	3.95	5.5	10	sonic	-	-	0.85	9	EC	Stable	SR2	
	3.95	5.5	10	sonic	-	-	0.95	16	EC	All data	SR2	
Rice	< 0.85	1.8	10	sonic	-	-	0.9	10	EC	Unstable	SR2	Castellvi and Snyder (2009b)
	< 0.85	1.8	10	sonic	-	-	0.92	6	EC	Stable	SR2	
	< 0.85	1.8	10	sonic	-	-	0.96	8	EC	All data	SR2	
	> 0.85	1.8	10	sonic	-	-	0.93	13	EC	Unstable	SR2	
	> 0.85	1.8	10	sonic	-	-	0.93	5	EC	Stable	SR2	
	> 0.85	1.8	10	sonic	-	-	0.96	10	EC	All data	SR2	
Grape	2.3	2.8	10	sonic	0.51 *****	-	0.95	7	EC	Unstable	SR2	Castellvi and Snyder (2010)
	2.3	2.8	10	sonic	0.51 *****	-	0.81	7	EC	Stable	SR2	
	2.3	2.8	10	sonic	0.51 *****	-	0.97	10	EC	All data	SR2	
Orange	3.75	4.0	10	76.2	0.66	0	0.78	56	EC	Unstable	SR1	Castellvi et al. (2012)
	3.75	4.0	10	76.2	0.32	0	0.51	19	EC	Stable	SR1	
	3.75	8.0	10	76.2	0.64	0	0.65	72	EC	Unstable	SR1	
	3.75	8.0	10	76.2	0.17	0	0.47	19	EC	Stable	SR1	
	3.75	4.0	10	76.2	-	-	0.87	39	EC	Unstable	SR2	
	3.75	4.0	10	76.2	-	-	0.72	15	EC	Stable	SR2	

Table II.1 *– Summary of reviewed agricultural applications of the SR technique. References: - = data not shown; 0 = regression through the origin; * = °C m s^{-1}; ** = estimation of LE; *** = estimation of Fc; **** = µmol m s^{-1}; ***** = average α; + = g Kg^{-1} m s^{-1}*

APPENDIX III – Julian calendar

The Julian calendar numerates the days with their correspondent day of the year (DOY) as follows:

	January	February	March	April	May	June	July	August	September	October	November	December
1	1	32	60	91	121	152	182	213	244	274	305	335
2	2	33	61	92	122	153	183	214	245	275	306	336
3	3	34	62	93	123	154	184	215	246	276	307	337
4	4	35	63	94	124	155	185	216	247	277	308	338
5	5	36	64	95	125	156	186	217	248	278	309	339
6	6	37	65	96	126	157	187	218	249	279	310	340
7	7	38	66	97	127	158	188	219	250	280	311	341
8	8	39	67	98	128	159	189	220	251	281	312	342
9	9	40	68	99	129	160	190	221	252	282	313	343
10	10	41	69	100	130	161	191	222	253	283	314	344
11	11	42	70	101	131	162	192	223	254	284	315	345
12	12	43	71	102	132	163	193	224	255	285	316	346
13	13	44	72	103	133	164	194	225	256	286	317	347
14	14	45	73	104	134	165	195	226	257	287	318	348
15	15	46	74	105	135	166	196	227	258	288	319	349
16	16	47	75	106	136	167	197	228	259	289	320	350
17	17	48	76	107	137	168	198	229	260	290	321	351
18	18	49	77	108	138	169	199	230	261	291	322	352
19	19	50	78	109	139	170	200	231	262	292	323	353
20	20	51	79	110	140	171	201	232	263	293	324	354
21	21	52	80	111	141	172	202	233	264	294	325	355
22	22	53	81	112	142	173	203	234	265	295	326	356
23	23	54	82	113	143	174	204	235	266	296	327	357
24	24	55	83	114	144	175	205	236	267	297	328	358
25	25	56	84	115	145	176	206	237	268	298	329	359
26	26	57	85	116	146	177	207	238	269	299	330	360
27	27	58	86	117	147	178	208	239	270	300	331	361
28	28	59	87	118	148	179	209	240	271	301	332	362
29	29		88	119	149	180	210	241	272	302	333	363
30	30		89	120	150	181	211	242	273	303	334	364
31	31		90		151		212	243		304		365

Table III.1 *– Days numerated with their correspondent day of the year (DOY).*

APPENDIX IV – Historical background of the agricultural Zionist settlement at the Hula Valley

At the beginning of the 1930's, the area was sparsely settled by Falachim (traditional Arab farmers) and Bedouins living in 23 villages (Zion, 2006). The residents of the Hula Valley were in very poor health, and malaria was a determining factor in their lives. The only Jewish settlements in the region until 1939 were Metulla, which was established in 1896, and Kibbutz Kfar Giladi which was established in 1916. In 1934 the settlement enterprise in the area began and was on the focus of attention of the Zionist movement between the late thirties and early forties. Within eight years from 1939, sixteen agricultural settlements (thirteen kibbutzim and three moshavim) joined the two existing Jewish establishments, mainly in lands owned by the Jewish National Fund (KKL).

Although the general belief was that the land was fertile with abundant water, the fact was that weeds and malaria made the agricultural practice a tough activity in the area. However, agriculture was from the beginning the central activity of the Jewish settlement and contributed to reinforcing the settlements economically during the Second World War, when agricultural produce demand by the British increased significantly (Zion, 2006). After the establishment of the state of Israel (1948) and during the fifties the drainage of the swamps in the valley was a significant project carried out by the KKL and in 1963 the first nature reserve in Israel was created in a small portion of recovered swamps. Nowadays agriculture is still one of the main activities in the area and two experimental farms are located in the northern part of the valley, near the city of Kyriat Shmona. One of these farms (Field crops farm) was the location of the experiments of the current study.

APPENDIX V – Measurement devices calibration

During March 2011 a measurement devices calibration test was performed at the Soil and Water Science building, Volcani Center, Bet Dagan. The aim of this calibration test was to check the well functioning and calibration coefficients for the radiation sensors to be used in the S2 experiments. An additional check that was done in this period was verifying the calibration of some devices used in S1 which have been stored from the end of the experiment until that date. Therefore two installations were built at the roof of the building; one for calibrating radiation sensors (i.e. pyranometers, net radiometers and quantum sensors) and a second one for testing the EC system.

In the case of the radiation measurement devices, a brand new reference pyranometer (Kipp & Zonen, CMP6) was installed on a horizontal structure together with four other pyranometers. Additionally, four net radiometers and four quantum sensors were installed. All data were collected to a CR10X data logger (Campbell Sci., Logan, UT, USA). For the pyranometers the calibration was done by adjusting the calibration constants (in units of W m^{-2} mV^{-1}) for each device in order to fit the measurements with the reference device and obtaining a difference not bigger than 1% (tested with a linear regression) between the data from the different devices. For the net radiometers and quantum sensors, the factory calibration was tested by choosing the newest sensor as a reference and comparing the results between the different devices by linear regressions. It was arbitrarily fixed that a deviation not bigger than 5% constitutes an acceptable calibration. The net radiometers showed an acceptable calibration for three of the four cases including the one used in S1 in the positive results. The quantum sensors were all acceptably calibrated.

The EC system installation resembled the one that had been set during S1 and planned for S2. The main goal was to test the functioning of all devices and check the calibration of the infra red gas analyzer – IRGA (water vapor and carbon dioxide concentrations measurement). Therefore a complete EC system was installed, including the same 3-axis sonic anemometer and gas analyzer that had been used in S1 and an additional gas analyzer (same manufacturer and model). Together with this, all additional measurement devices that were intended to be installed at S2 were tested: soil heat flux plates, psychrometers, thermocouples, batteries and solar panels. All data were stored in CR3000 and CR23X data loggers (Campbell Sci., Logan, UT, USA). This installation allowed to test in a controlled environment all the devices and measurement procedures, and correct any

malfunctioning. In the case of the gas analyzers, formatting and zeroing were performed following the manufacturer's recommendations. The data obtained with the two devices differed in less than 5% for all day hours and climatic conditions (drier, more humid or rainy days). The sonic anemometer response was also tested by using the manufacturer's software.

Overall, the pyranometer, net radiometer, gas analyzer and sonic anemometer used during S1 experiment operated properly, thus they were chosen for S2 experiment. Regarding the difference between the two gas analyzers, it was approved by the manufacturer that the devices were correctly defined and that the measurements appeared to be logical.

APPENDIX VI – EC system position and maintenance

VI. EC system position and maintenance

VI.1. EC system position

Because they are the central measuring devices for covariance calculation, both sonic anemometer and IRGA have to be installed according to established guidelines. Nevertheless, also the net radiometer, the heat fluxes plates and the psychrometers installation need to follow certain criteria.

VI.1.1. EC system height

Three criteria were followed for positioning the EC system. First, the system should be higher than 2h, being h (m) the canopy height. According to Foken (2008), this is well above the roughness sublayer thus suitable for eddy covariance flux measurements. Secondly, the required fetch in all directions for an EC system should be between 50 and 100 times the system's height above the plant zero plane displacement height (Allen et al., 2011a). The plant zero-plane displacement is estimated following Stanhill (1969) and assuming neutral stability. This condition is not always possible to satisfy, as is the case of Israel, in small plots for all wind directions; therefore the criterion used is to install the system at a point which allows an acceptable (100:1) fetch/height ratio for the prevailing wind. The third criterion refers to the measurement frequency. A normalized frequency range of atmospheric turbulence is given by Miyake and McBean (1970) as:

$$0.001 \leq f(z-d){u_h}^{-1} \leq 10 \qquad \text{(VI.1)}$$

where f (Hz) is measurement frequency, z (m) is sensor height above the ground, d (m) is plant zero plane displacement and u_h (m s^{-1}) is mean horizontal wind speed at sensor height. To correctly capture the atmospheric turbulence, the measurement frequency should be larger than the upper limit of this range (Tanny et al., 2006).

VI.1.2. EC system direction and sensor separation

It is desirable to install the sonic anemometer's *x* axis facing the prevailing wind direction (i.e. stronger or daytime predominant winds). This direction is denominated as "*Anemometer azimuth*". The IRGA, position should not disturb the prevailing wind approaching the sonic anemometer. Regarding the location of the IRGA related to the sonic

anemometer, the azimuth of the direction IRGA – sonic anemometer (in that order) is also measured and denominated as "*IRGA – Anemometer azimuth*". Assuming that the middle point of the sonic anemometer's path and IRGA's path should be in the same horizontal plane; the distance between both devices (denominated as "*sensor separation*") is arbitrarily set to be between 10 and 15 cm. Although not critical, it is desirable that the IRGA will be in a vertical position since this is assumed in the frequency response corrections (see *Appendix VIII*).

VI.2. EC system maintenance

Regular maintenance needs to be performed on the EC system. For example, the net radiometer needs cleaning the dust that accumulates on its domes and checking its position to be horizontal. The sonic anemometer horizontal position and principal axis direction also need to be checked regularly together with cleaning the space between its measuring probes from spider web and dust. The IRGA needs its infra red lenses to be cleaned from dust. Regarding the electric power system, the solar panels need to be cleaned and their position corrected for heading south, while the batteries' charge needs to be monitored. Finally, psychrometers need to be filled with water regularly in order to maintain reliable wet bulb temperature measurement and the wooden box where the thermocouples are placed should be cleared from dead insects and spider webs.

APPENDIX VII – Matlab code related to the Structure Functions analysis

All data processing was done using Matlab (The Mathworks, Inc.) with a code specifically written for this project. This included the whole EC and the SR analysis. Following it is presented an example of the code used for performing the Structure Functions analysis. This was done using three functions, namely *SRsolutions.m*, *amplls.m* and *structfunc.m*

SRsolutions.m

```
% function
function
[aout,lsout,S2out,S3out,S5out]=SRsolutions(matrix,rvec,freqvec,int,TC,freqTC,zTC
,colTC)
lrvec=length(rvec);
lfreqvec=length(freqvec);
aout=[];
lsout=[];
S2out=[];
S3out=[];
S5out=[];
for i=1:lrvec
    r=rvec(i);
    j=1;
    while j<lfreqvec+1
             f=freqvec(j);
            [a,ls,S2,S3,S5]=amplls(matrix,r,f,int,TC,freqTC,zTC,colTC);
             aout=[aout a];
             lsout=[lsout ls];
             S2out=[S2out S2];
             S3out=[S3out S3];
             S5out=[S5out S5];
             j=j+1;
    end
end

%when this function finishes, there is, for each paramether, a matrix which
%has ONE day (no. of lines) and all the combinations of r and f (no.
%of columns. For ONE TC
%example: aout= | [     r1    ][    r2     ][     r3    ][    r4     ] |
%               | (f1 f2 f3 f4)(f1 f2 f3 f4)(f1 f2 f3 f4)(f1 f2 f3 f4) |
%               |                                                      |
```

---

amplls.m

```
%this function returns two matrixes with the values for amplitude and l+s (here
ls) using the structure
%functions calculated previously
function [a,ls,S2,S3,S5]=amplls(matrix,r,f,int,TC,freqTC,zTC,colTC)
S=structfunc(matrix,r,f,int,TC,freqTC,zTC,colTC);
B=size(S);
ar=zeros(3,B(1,2));
as=zeros(3,B(1,2));
for i=1:B(1,2)
```

```
    if abs(S(2,i))>0
       p = [1 0 ((10*S(1,i))-(S(3,i)/S(2,i))) 10*S(2,i)];
       ar(1:3,i)=roots(p);
    else ar(1:3,i)=0;
    end
    for k=1:3
        if imag(ar(k,i))==0
           as(k,i)=ar(k,i);
        end
        if sign(S(2,i))==-sign(as(k,i))
            amplis(1,i)=as(k,i);
        elseif sign(S(2,i))==0
            amplis(1,i)=0;
        end
    end
    lssl(1,i)=-((amplis(1,i)^3)*r)/(S(2,i));
end
a=amplis';
ls=lssl';
S22(1,1:B(1,2))=S(1,1:B(1,2));
S2=S22';
S33(1,1:B(1,2))=S(2,1:B(1,2));
S3=S33';
S55(1,1:B(1,2))=S(3,1:B(1,2));
S5=S55';
```

---

structfunc.m

```
%this function returns a matrix containing the values of S2,S3 & S5,
%structure functions. The matrix is called S and has 3 lines (S2,S3&S5
%respectively) and a number of columns equal to the number of intervals
%that fit in the time specified for calculation
%These values are used afterward for finding amplitude (a) and l+s
%r is the time lag (in sec), f is the frequency (in hz) and int is the interval
(in min.)
%for which the structure functions will be calculated
%hour1 and hour2 are the range for which we want to calculate the structure
%function. TC is which thermocouple we want to calculate

function S=structfunc(matrix,r,f,int,TC,freqTC,zTC,colTC)
m=int*60*f;
j=r*f;
jround=round(j);%round j for using it as an index for building S
fcounter=freqTC/f; %freqTC corresponds to frequency=20hz, which is the original
frequency
line1=1;
line2=(freqTC*60*60*24)-(fcounter-1); %freqTC corresponds to frequency=freqTChz,
which is the original frequency
ScolTC=size(colTC);
for i=1:ScolTC(1,2);
    if TC==colTC(1,i)
       TCcol=colTC(2,i);
    end
end
Scols1=24*60/int;
Scols=round(Scols1);
```

```
Tdif=matrix(line1+jround:fcounter:line2,TCcol)-matrix(line1:fcounter:line2-
jround,TCcol);
l=length(Tdif);
Tdif2=zeros(l,1);
Tdif3=zeros(l,1);
Tdif5=zeros(l,1);
for h=1:l
    Tdif2(h,1)=(Tdif(h))^2;   %S2
    Tdif3(h,1)=(Tdif(h))^3;   %S3
    Tdif5(h,1)=(Tdif(h))^5;   %S5
end
c=1;
S=zeros(3,Scols);
for k=1:Scols
    S(1,k)=(1/(m-j))*(sum(Tdif2((c:c+m-jround-1),1)));   %S2
    S(2,k)=(1/(m-j))*(sum(Tdif3((c:c+m-jround-1),1)));   %S3
    S(3,k)=(1/(m-j))*(sum(Tdif5((c:c+m-jround-1),1)));   %S5
    c=c+m;
end
```

APPENDIX VIII – EC fluxes calculation and validation of the measurements

VIII. EC fluxes calculation and validation of the measurements

VIII.1. Latent heat flux

Latent heat flux (W m^{-2}) was estimated by:

$$LE = L_v\overline{w'q'} \qquad \text{(VIII.1)}$$

where L_v (J g^{-1}) is the latent heat of vaporization and $\overline{w'q'}$ is the covariance between the fluctuations of vertical wind speed w (m s^{-1}) and vapor density q (g m^{-3}) averaged (represented by the horizontal overbar) over the desired measurement period (30 min in this study).

Raw data of LE is corrected for rotation, path averaging, sensor separation and density effects (see *Appendix IX*).

VIII.2. Sensible heat flux

Sensible heat flux (W m^{-2}) was estimated by:

$$H = \rho C_p\overline{w'T'} \qquad \text{(VIII.2)}$$

where ρ (kg m^{-3}) is the air density, C_p (J kg^{-1} °K^{-1}) is the air specific heat at constant pressure and $\overline{w'T'}$ is the covariance between the fluctuations of vertical wind speed w (m s^{-1}) and air temperature T (°K). The overbar represents time averaging over the desired measurement period (30 min in this study).

Fluctuations of air temperature are obtained from the sonic anemometer data. The sonic anemometer measures the so-called sonic temperature which is converted to air temperature using the air humidity as measured by the IRGA and the equation:

$$T = \frac{Ts}{1+0.51q} \qquad \text{(VIII.3)}$$

Where T (°K) is the air temperature, Ts (°K) is the sonic temperature and q is the vapor density (g m^{-3}).

Raw data of H is corrected for rotation and path averaging (see *Appendix IX*).

VIII.3. Friction velocity

Friction velocity u_* (m s^{-1}) is calculated as follows:

$$u_* = \left(\overline{u'w'}^2 + \overline{v'w'}^2\right)^{1/4} \qquad \text{(VIII.4)}$$

where $\overline{u'w'}$ and $\overline{v'w'}$ are the covariances between the fluctuations of vertical wind speed w (m s^{-1}) and horizontal wind components u and v (m s^{-1}), in x and y directions respectively, averaged (horizontal overbar) over the desired measurement period (30 min in this study).

Raw data of u_* should undergo rotation and path averaging corrections (see *Appendix IX*).

VIII.4. Energy balance

One method of independently validating the scalar flux measurements from EC is the energy balance (EB) closure (Wilson et al., 2002). The EB is posed between the ground and the canopy top level (Eq. 2.1 gives its analytical expression).

VIII.5. Footprint

An additional test of the reliability of the EC measurements is the footprint model by Hsieh et al. (2000), which was applied to the same periods when the EB closure was assessed for both seasons. This approximate analytical model estimates the scalar flux footprint in a thermally stratified atmospheric surface layer. The model relates atmospheric stability, measurement height, and surface roughness length to the footprint. Its inputs are friction velocity, sensible heat flux, air temperature, sensor's height above canopy and momentum roughness length.

APPENDIX IX – EC measurements rotation and corrections

Eddy covariance raw data should undergo a series of corrections: rotation, path averaging, sensor separation and density effects. The rotation correction accounts for either the sonic anemometer not being completely leveled or low winds associated with relatively large non-horizontal velocity components. The rotation scheme applied in this study corresponds to that proposed by Kowalski et al. (1996). Path averaging correction accounts for the fact that both the sonic anemometer and the IRGA measure a volume that is larger than part of the eddies to be captured. Sensor separation correction is needed since the distance between the two devices although small is likely to create a time or position lag for a given eddy that crosses the measurement paths. Density correction, accounts for the fact that any flux causes an expansion of the air and thus affects the scalar's density (Webb et al., 1980). In the present study path averaging and sensor separation corrections were performed by applying the frequency response corrections suggested by Moore (1986). The general approach of these corrections is to calculate a co-spectral transfer function which includes the effects that are intended to treat with the corrections (i.e. path averaging and sensor separation in the case of LE); these effects are included by calculating spectral transfer functions for each one of them and subsequently joining them with an arithmetical manipulation. After the spectrum has been built the corrections are applied by integrating it (i.e. considering all the frequency range and its effect) and relating them to the initial non-corrected flux. The density effects correction scheme applied in this study was that suggested by Webb et al. (1980) and considers the air humidity mixing ratio, the density of dry air and the molecular weights of dry air and water vapor for its calculations.

These corrections were applied with the iterative approach presented in Fig. IX.1 which follows the recommendations of Burba and Anderson (2005).

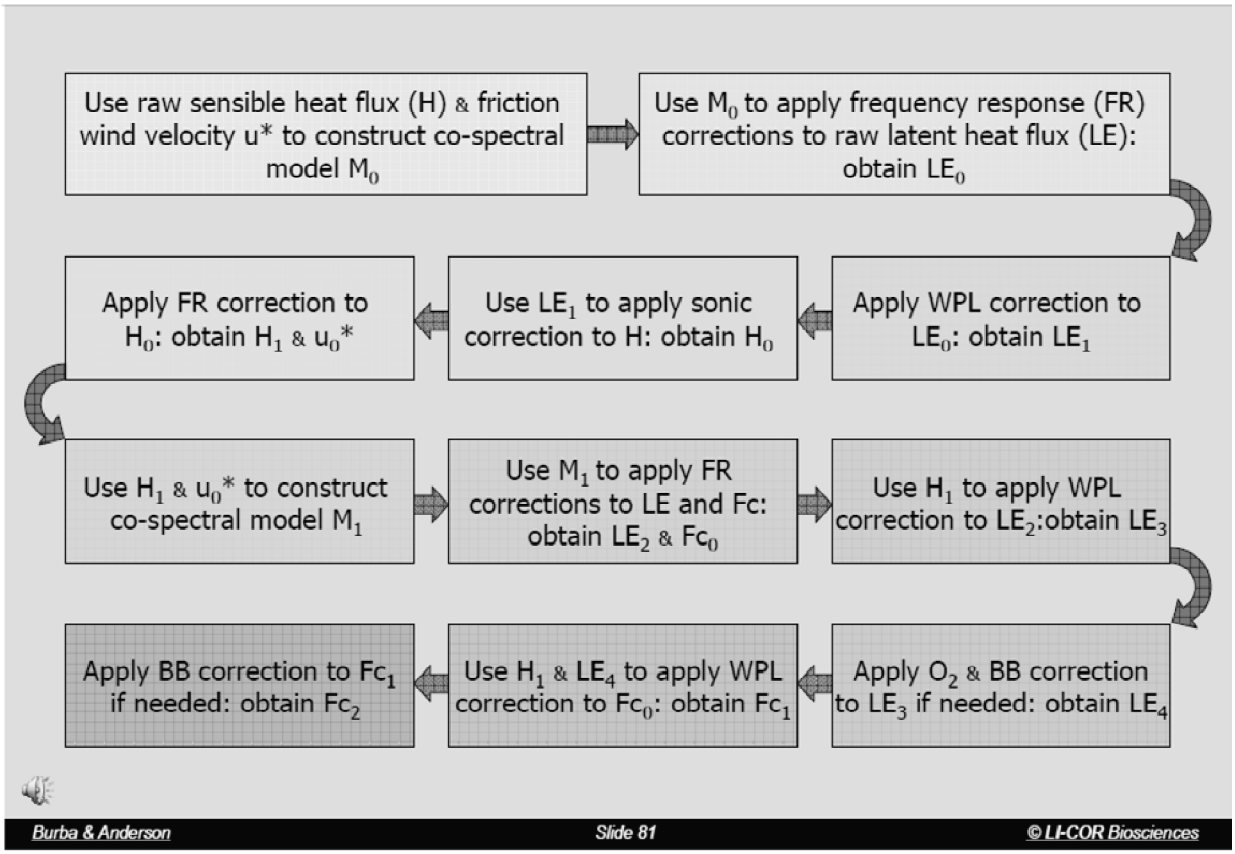

Figure IX.1 *– Diagram for applying corrections to flux measurements performed with the eddy covariance method (Burba and Anderson, 2005).*

APPENDIX X –Equations and data involved in soil heat flux calculation

The estimation of G is performed by considering the fraction of soil (F_{wet} and F_{dry} respectively) that each region represents:

$$G = G_{wet}F_{wet} + G_{dry}F_{dry} \quad \text{(X.1)}$$

G_{reg} (i.e. either G_{wet} or G_{dry}) (W m^{-2}) is estimated from the average flux measured by the heat flux plates ($G_{flux\text{-}reg}$) plus the energy stored in the layer above it (S_{reg}) following the recommendations of Hukseflux Company (*www.hukseflux.com*), and based on an energy balance of the layer from the soil surface down to the soil heat flux plates:

$$G_{reg} = G_{flux-reg} + S_{reg} \quad \text{(X.2)}$$

The storage term S_{reg} (W m^{-2}) is calculated as follows:

$$S_{reg} = (T_1 - T_2)C_V d_{hf}/(t_1 - t_2) \quad \text{(X.3)}$$

where $T_1 - T_2$ (°C) is the change with time of soil temperature within the layer, C_v (J m^{-3} °C^{-1}) the volumetric heat capacity of the soil, d_{hf} (m) the depth of the installation of the soil heat flux plates and $t_1 - t_2$ (s) is the measurement time interval. The volumetric heat capacity is calculated as:

$$C_V = r_d(C_d + q_m C_w)10^6 \quad \text{(X.4)}$$

where r_d (g cm^{-3}) is the soil bulk density, C_d (J g^{-1} °C^{-1}) is the dry soil heat capacity, C_w (J g^{-1} °C^{-1}) is the water heat capacity and q_m (g g^{-1}) is the soil water content. The bulk density (r_d) and soil water content (q_m) were estimated for S1 and S2 by sampling the soil in the experiment area and performing the relevant analysis. This included sampling three repetitions of a known volume of soil both for the dry and wet regions, weighting the samples, drying them at 105 °C during 24 hours and weighting them once more. The values for C_w and C_d were obtained from De Vries (1963); being C_w=4.18 J g^{-1} °C^{-1} and C_d calculated with the following approach:

$$C_d = f_{clay}C_{sclay} + f_{silt}C_{ssilt} + f_{sand}C_{ssand} \quad \text{(X.5)}$$

where f_{clay}, f_{silt} and f_{sand} are volumetric fractions of each of the granular components (Table 3.1) and C_s (J g^{-1} °C^{-1}) represent the specific heat values of each one according to De Vries (1963) and specified as follows:

	Sand	Silt	Clay
C_s (J g^{-1} C^{-1})	0.79	0.81	0.94

Table X.1 *– Specific heat values of sand, silt and clay (De Vries, 1963)*

APPENDIX XI – Summary of devices configuration

The following three tables show details of the instruments deployment during the two field campaigns.

Season	From DOY	Instrument	Height (m)
S1	146	Sonic anemometer	1.50
		IRGA	1.50
		Net radiometer	1.50
		Soil heat flux plates	-0.08
		Soil temperature 1	-0.06
		Soil temperature 2	-0.02
		Psychrometer 1	1.00
		Psychrometer 2	2.00
		Pyranometer	1.60
		Quantum sensor	1.60
S2	152	Sonic anemometer	1.50
		IRGA	1.50
		Psychrometer 1	0.90
		Psychrometer 2	1.90
		Net radiometer	2.00
		Soil heat flux plates	-0.08
		Soil temperature 1	-0.06
		Soil temperature 2	-0.02
		Pyranometer	1.50
		Quantum sensor	1.50
	191	Sonic anemometer	2.67
		IRGA	2.67
		Pyranometer	2.67
		Quantum sensor	2.67
	219	Sonic anemometer	3.35
		IRGA	3.35
		Psychrometer 1	1.60
		Psychrometer 2	2.70
		Pyranometer	3.35
		Quantum sensor	3.35

Table XI.1 (left) *– Summary of the devices and their position included in the flux measurement station.*

Table XI.2 (down) *– Summary of the EC systems position. The prevailing wind direction has an azimuth of 295°. "Anemometer azimuth" is the sonic anemometer's x axis direction. "IRGA – Anemometer azimuth" is the azimuth of the direction IRGA – sonic anemometer (in that order). "Sensor separation" is the distance between both devices, assuming that their middle point should be in the same horizontal plane.*

Season	From DOY	z (m)	Plant height (m)	d (m)	Anemometer azimuth (°)	IRGA - Anemometer azimuth (°)	Sensor separation (m)	Fetch from main wind direcion (m)
S1	225	1.50	0.60	0.39	288	75	0.12	199
S2	152	1.50	0.60	0.39	320	40	0.12	367
	191	2.67	1.15	0.73	320	60	0.13	367
	219	3.35	1.50	0.95	294	25	0.11	367

Season	From DOY	Plant height (m)	Sensor number	z (m)	Wire diameter (µm)	Working? (Y/N)
S1	225	0.60	1	0.3	76	Y
			2	0.6	76	Y
			3	0.9	76	Y
			4	1.2	76	Y
			5	1.5	76	Y
S2	153	0.30	1	0.3	76	Y
			2	0.6	76	Y
			3	0.9	76	Y
			4	1.2	76	Y
			5	1.5	76	Y
			6	0.3	76	N
			7	0.3	511	Y
	160	0.46	6	0.5	76	Y
			7	0.5	511	Y
	200	1.32	1	0.3	76	N
			2	0.6	76	N
			3	1.6	76	N
			4	1.2	76	N
			5	1.5	76	Y
			6	1.4	76	N
			7	1.4	511	Y
	207	1.47	1	0.3	76	N
			2	1.2	76	Y
			3	1.6	76	Y
			4	1.2	76	N
			5	1.5	76	Y
			6	1.4	76	N
			7	1.4	511	Y
	219	1.50	1	1.2	76	Y
			2	1.2	76	N
			3	1.6	76	Y
			4	1.7	76	Y
			5	1.5	76	Y
			6	1.5	127	Y
			7	1.5	511	Y
	223	1.50	1	1.2	76	Y
			2	2.4	76	N
			3	1.6	76	Y
			4	1.7	76	Y
			5	1.5	76	Y
			6	1.5	127	Y
			7	1.5	511	Y
	233	1.50	1	1.2	76	Y
			2	2.4	76	Y
			3	1.6	76	Y
			4	1.7	76	Y
			5	1.5	76	Y
			6	1.5	127	Y
			7	1.5	511	Y
	242	1.50	1	1.2	76	N
			2	1.2	76	N
			3	1.6	76	N
			4	1.7	76	Y
			5	1.5	76	Y
			6	1.5	127	N
			7	1.5	511	Y

Table XI.3 – *Summary of the TCs position, wire diameter and days of operation*

תקציר

במטרה לשפר את יעילות ההשקיה חיוני לכמת בצורה נכונה את תצרוכת המים של גידולי שדה. הערכות אלו יכולות להתבצע על ידי מדידה של אוופוטרנספירציה (ET) בחלקות חקלאיות או ע"י חישוב ET באמצעות מודלים שונים. רוב השיטות הקיימות למדידת ET יקרות או מסובכות ליישום, או שניהם. שיטת חידוש פני השטח (SR – Surface Renewal), נושא התזה הזאת, יכולה להיות אלטרנטיבה אפשרית, פשוטה וזולה לביצוע הערכות של ET.

מחקר זה בחן את היישום של שיטת ה-SR עבור הערכת ET בשני גידולי שדה שונים, עגבניות לתעשייה וכותנה, בעמק החולה שבצפון ישראל. שיטת SR מבוססת על הדינאמיקה של סחיפה ופליטה (sweeps and ejections) של גושי אוויר המתרחשות בקרבת פני השטח של הנוף. ההנחה היא כי מנגנון זה אחראי על חילופי החום המוחשי (ומרכיבים אחרים) בין הנוף לבין האטמוספרה. באמצעות מדידות בתדר גבוה של טמפרטורת אוויר, תהליך הסחיפה והפליטה של גושי אוויר מתואר ע"י רמפות של סיגנל הטמפרטורה באמצעות ניתוח בשיטת Structure Functions. משרעת ותדירות הרמפות מאפשרים להעריך את החום המוחשי (H) המוחלף בין הנוף לבין האטמוספרה. מטרה ספציפית של המחקר הייתה לכייל את שיטת SR, באמצעות נתוני ייחוס מדודים ע"י שיטת קורלצית הערבולים (EC) וכן לייעל את הכיול על ידי התאמת שלושה פרמטרים: גובה מדידת טמפרטורה, תדר המדידה וקוטר חיישן הדגימה של מדידת הטמפרטורה.

מערכות SR ו-EC התקנו בו זמנית בשתי עונות ניסוי שונות, S1 ו - S2, אשר מתאימות ל- 13 ימים בחודש אוגוסט 2010 ו- 96 ימים בין יוני לספטמבר 2011, בהתאמה. הגידול היה עגבניות לתעשייה ב-S1 וכותנה עבור S2. התקופה S1 חולקה ל-7 ימים של כיול ו - 6 ימים של אימות הנתונים, לעומת S2 שהייתה מחולקת שונה בתקופות שונות כדי לבצע מגוון רחב של ניתוחים, בהתאם לשלב גידול הצמחים ופריסת החיישנים. מדידות הטמפרטורה עבור SR בוצעו בו זמנית בגבהים שונים ע"י תרמוקפלים (TC) מיניאטוריים (מיצרים מחוט בקוטר 76 מיקרומטר) בתדר דגימה f=20Hz ועיבוד הנתונים נערך בתדרים של 1, 2, 5, 8 ו-10 Hz. גובה הצמח המקסימאלי היה 0.6 מ' ו- 1.5 מ' עבור העגבניות (S1) והכותנה (S2) בהתאמה.

סיגנל הטמפרטורה המדודה נותח באמצעות Structure Functions. כלי מתמטי זה מפרק את סיגנל הטמפרטורה לרכיבים מאורגנים וטורבולנטיים על מנת להתאים את החלק המאורגן למודל של רמפה דטרמיניסטית, על כל פרק זמן (30 דקות במחקר זה). כל פרק זמן מאופיין ע"י אמפליטודה ממוצעת של הרמפה a (°C) ותדירות ממוצעת של הרמפה τ (שנ'). שני פרמטרים אלה יחד עם גובה המדידה z (מ') ומקדם כיול (α) משמשים לחישוב שטף החום המוחשי H_{SR}. לכל סיגנל טמפרטורה ערכי a ו-τ תלויים בגורם עיכוב זמן r (שנ') ותדירות - f, המשמשים בניתוח Structure Functions. לכן סדרה של פרמטרים הוגדרה

כשילוב של שלושת הפרמטרים (z, f, r). עבור כל זוג של *a* ו-τ , הקשורים עם סדרה של פרמטרים (z, f, r), חושב H לא מכויל לפי SR (H_{NC}). כיול נערך על ידי רגרסיה בין H_{NC} לבין מדידות H ע"י EC (H_{EC}) עבור תנאים יציבים ולא יציבים בנפרד וכך נתקבלו שני ערכים של α (α_{st} ו-α_{uns}) שהוא שיפוע הרגרסיות, שני ערכי R^2, שני ערכי RMSE ושני ערכי p-values. לבסוף, השטף של החום הכמוס (LE) מחושב בשיטת SR (LE_{SR}) כשארית של משוואת מאזן האנרגיה (EB) בעזרת מדידות נוספות של קרינה נטו (Rn) ושטף החום בקרקע (G).

שיטת SR כוילה בהצלחה (p-value<0.001) עבור רוב גבהי המדידה ותדרי המדידה, עם מגמות ברורות של α ו-R^2 כתלות ב- z ו-f. החידוש העיקרי של מחקר זה הוא ניתוח המגמות של המקדמים R^2 ו-α עם התדר f. השוואה בין התוצאות שהתקבלו עם אלו המדווחות בספרות הראו הסכמה עם מגמת השינוי של α ביחס ל- z. עבור S1 (עגבניות לתעשייה) כיול אופטימאלי בין כל סדרות המדידה הושג בגובה מנורמל zn=z/h=2 (כאשר h הוא גובה הנוף) ב-f=10 Hz , עם α_{st}=2.44 ו- α_{uns}=1.48, R^2_{st}=0.47 ו- R^2_{uns}=0.71 עבור תנאים יציבים ולא יציבים, בהתאמה. עבור $RMSE_{st}$=25.06 W m^{-2}, ו- $RMSE_{uns}$=23.37 W m^{-2} S2d (כותנה) ,שהוגדר בתקופה שבין אוגוסט 22 ו-25, 2011, כיול אופטימאלי הושג בגובה מנורמל zn=1.6 בתדר f=8 Hz, עם α_{st}=1.14 ו- α_{uns}=0.8, R^2_{st}=0.83 ו- R^2_{uns}=0.33, $RMSE_{st}$=20.38 W m^{-2} ו- $RMSE_{uns}$=12.56 W m^{-2} עבור תנאים יציבים ולא יציבים, בהתאמה. כיולים אלה גרמו להערכה נמוכה ב- 20% בממוצע של H_{EC} על ידי H_{SR} בתקופות האימות של S1 ו-S2d. LE_{SR} שימש להערכת ET בתקופות S1 ו-S2d, תוך יישום של הכיולים האופטימאליים עבור כל תדר נבדק. האומדנים של ET יומי על ידי SR שבוצעו בתדרים 1, 2, 5 ו-10 Hz, היו בטווח קטן של השתנות, גבוה ונמוך ביחס ל- ET בתקופות אימות של S1 ו-S2d, בהתאמה. עם זאת, פרט להערכה ב-f=1 Hz ב-S2d, סטיות אלו לא עלו על 5%. תוצאות אלו נותנות תקווה לפיתוח עתידי של מערכת SR בעלות נמוכה, שאינה מחייבת מדידה בתדרים גבוהים ונפחי אחסון נתונים גבוהים, ולכן עשויה להיות ברת השגה ותפעול עבור המגדלים לניהול ההשקיה ברמה יומיומית. לגבי קוטר ה-TC, מחקר זה מציג את הצורך להעריך נכון פרמטר זה ואת ההשפעה הגדולה שיכולה להיות לשינויים קטנים (~ 0.05 מ"מ) בקוטר של החיישן על התוצאות.

בין התוצאות שהתקבלו בניסוי בכותנה (S2) נמצא כי עבור ה-TCs שהיו סמוכים לנוף, ובימים מסוימים, היה ל-H_{NC} סימן הפוך מ-H_{EC} במהלך כמה שעות ביממה. המהלך של תופעה זו יצר פיגור זמן בשינוי היציבות (*time lag in stability change*) כי כאשר מצב זה התרחש, H_{EC} (שנמדד בגובה 3.35 מ') הפך לשלילי (יציב) כמה שעות לפני H_{NC}. בדיקות שונות שבוצעו על הנתונים הקיימים, בניסיון להסביר תופעה זו, הראו קשר בין אורכו (בשעות) של פיגור זמן זה, עם שיעורי ET גבוהים ומהירות רוח גבוהה. עם זאת לא ניתן היה לזהות מנגנון ספציפי המייחס שיעורי ET גבוהים לפיגור הזמן בשינוי היציבות. המופע של פיגור זמן זה מייצג מגבלה ביישום של SR בגידול כותנה עם חיישני טמפרטורה הסמוכים מאד לנוף.

לסיכום, שיטת SR נמצאה אמינה בהערכת ET בגידולי עגבניות לתעשייה וכותנה. התוצאות של מחקר זה מציגות שני גידולים באזור אקלימי מסוים. כדי לפתח שיטה זו לכדי כלי יישומי לחקלאי, נדרשת הרחבת גישה זו לגידולים שונים באזורים אחרים ועל פני טווח רחב יותר של שלבי התפתחות הצמח.

ישום שיטת חידוש פני השטח לערכות של אוופורנספירציה בגידולי שדה

עבודת-גמר מוגשת לפקולטה לחקלאות, מזון וסביבה על שם רוברט ה. סמית של האוניברסיטה העברית בירושלים לשם קבלת תואר מוסמך למדעי החקלאות

רפאל רוסה

25 מרץ, 2012